論文 / 著書情報
Article / Book Information

題目(和文)	
Title(English)	Study on the effect of geometry of SCP improvement for mitigating liquefaction-induced embankment settlement
著者(和文)	李楊
Author(English)	Yang Li
出典(和文)	学位:博士（工学）, 学位授与機関:東京工業大学, 報告番号:甲第12116号, 授与年月日:2021年9月24日, 学位の種別:課程博士, 審査員:北詰 昌樹,髙橋 章浩,岩波 光保,竹村 次朗,田村 修次
Citation(English)	Degree:Doctor (Engineering), Conferring organization: Tokyo Institute of Technology, Report number:甲第12116号, Conferred date:2021/9/24, Degree Type:Course doctor, Examiner:,,,,
学位種別(和文)	博士論文
Type(English)	Doctoral Thesis

Study on the effect of geometry of SCP improvement for mitigating liquefaction-induced embankment settlement

Yang Li

Tokyo Institute of Technology

2021

Study on the effect of geometry of SCP improvement for mitigating liquefaction-induced embankment settlement

Yang Li

DISSERTATION

submitted in partial fulfillment of the requirements for the degree of

DOCTOR OF PHILOSOPHY

at

TOKYO INSTITUTE OF TECHNOLOGY

2021

Acknowledgements

My deepest gratitude goes first and foremost to Professor Masaki Kitazume, my supervisor, for his continuous support and adroit guidance during the study in Tokyo Institute of Technology. The role he played in this thesis work could never be overemphasized, and I must say that I could not have finish it without his support.

Second, I am grateful to Prof. Akihiro Takahashi for his valuable suggestions and guidance on my research. His advice on how to do a meaningful research greatly improved the quality of this dissertation.

I am also grateful to the committee members Asso. Prof. Jiro Takemura, Prof. Mitsuyasu Iwanami and Prof. Shuji Tamura, for their valuable comments and suggestions to enrich my dissertation.

I would like to extend my thanks to our lab technician, Mr. Sakae Seki for his support and help during experiments preparation. The successful completion of experiments would not have been possible without his support. I am also grateful to Dr. Kazuki Horikoshi for his support during this period.

I would like to thank Dr. Kenji Harada and Dr. Jun Ohbayashi, Fudo Tetra Corporation, who gave me a lot support and suggestions throughout this thesis work.

I am thankful to all my lab mates of the Geotechnical Engineering Group at Tokyo Institute of Technology. Special gratitude goes to Dr. Mao Ouyang, Mr. Lihang Hu, Mr. Runxing Zhang and Mr. Xin Shi, thank you for spending countless nights together in the lab, facing challenges and encouraging each other.

Finally, no less gratitude should be given to my parents and family, Mr. Weiguang Li and Mrs. Jieling Yang for their constant overall support, encourage and love, without which I would fail in realizing my dream.

Abstract

From the 1964 Niigata earthquake, liquefaction has been recognized as a serious problem in geotechnical engineering. Liquefaction has usually caused severe damage to embankment structures such as levees, earth dams, levees and dykes, supported on a loose sandy ground. In order to mitigate the damage caused by liquefaction, the most effective way is to increase the density of ground. The Sand Compaction Pile (SCP) method is a typical densification countermeasure against liquefaction, whose main purpose is to prevent liquefaction occurrence or reduce settlement. Generally, when the SCP method is adopted for the foundation ground of an embankment structure, the foundation ground is improved to a target density before the embankment is constructed. However, the ground with an existing embankment cannot be improved by the SCP method with vertical sand piles. It was reported that the major cause of the embankment settlement and/or failure is the lateral deformation of liquefied foundation soil below the embankment towards the free field. In the current design guide of liquefaction countermeasure for existing embankment, the soil under embankment toes is improved by the SCP method or the deep mixing method, aim at mitigating crest settlement by providing containment for the deformation of the liquefiable foundation soils below the embankment. With advancements in machinery, a new type of SCP method has been recently developed, which enables the vertical installation of sand piles or the installation of sand piles at a specific angle into the ground. Thereby, compacted sand piles can be formed in any direction underneath an embankment. The geometric form of the improvement zones may affect the response and deformation behavior of the improved ground and embankment. However, these influences are not well investigated and incorporated into the current design precisely. Therefore, the main purpose of this study is to investigate the performance of an embankment improved by the SCP method with various geometric forms including the angle and the extent of the SCP improvement zone.

This study consists of three parts to achieve the purpose. In the beginning, a series of dynamic centrifuge experiments and finite element analyses are conducted to evaluate the effectiveness of SCP improved ground with various geometric improvement forms in terms of embankment settlement, and to investigate the effects of the geometry of the improved zone on the ground response and deformation mechanism of embankments and foundation ground. In the centrifuge test program, the focus is on the angle of the improvement zone, which is defined as the angle between the SCP improvement form and the ground base, in which the angle is 50, 60 and 90 degrees. It is found that the lateral displacement beneath the embankment toes is mitigated by the presence of the improvement zone installed in the foundation ground. In particular, the case with a 50°

improvement zone is more effective and contributes to the lower settlement of the embankment.

In order to evaluate the SCP improvement angle in a wide range as much as possible in practice, in the second part of this study, the deformation mechanism of embankments supported on a liquefiable ground improved by the SCP method with 30 to 90 degrees was investigated. Accordingly, the investigation of liquefaction induced deformation of embankment on various ground condition (i.e., various SCP improvement angle) was carried out by a series of finite element analyses. Effects of the SCP improvement angle on ground deformation and embankment settlement were compared and analyzed. It was found that by making the improvement angle smaller than 60 °, the excess pore water pressure in the foundation ground could be suppressed, and the amount of settlement is also reduced.

In the third part of this study, the effect of the extent of SCP improvement was investigated by a FEM analyses in chapter 6. In the design of the SCP method as a liquefaction countermeasure, in addition to the improvement angle, the improvement extent must also be determined. The extent of the SCP improvement must satisfy two main aspects: (a) Stability of slip failure of embankment and ground, and (b) the amount of settlement should be kept below an allowable value. In this study, the former condition (i.e., ensuring stability) was set to be satisfied in all cases, and then the focus is on the effect of the extent of the SCP improvement on the liquefaction-induced embankment settlement. It was found that as the extent of the SCP improvement increases, the excess pore water pressure ratio generated in the ground below the embankment tends to increase. Nevertheless, increasing the extent of the SCP improvement was very effective for reducing the lateral deformation of the foundation ground under the embankment, resulting in smaller embankment settlement.

Table of contents

List of figures

List of tables

Chapter 1

Introduction

1.1 Background and problem statement

During an earthquake, saturated loose sandy soil is characterized by a substantial rise in excess pore water pressure, leading to a dramatic loss of its strength and stiffness. When the excess pore water pressure reaches to the initial effective overburden stress, soil particles do not support each other and liquefaction takes place (Seed and Lee, 1966). Liquefaction usually causes severe damages, such as cracking, slumping, lateral spreading and settlement, to river dykes, levees and road embankments. For instance, many embankments and river dykes failed due to the liquefaction of foundation ground was reported during the 1964 Alaskan and Niigata earthquake (Kawakami and Asada, 1966; McCulloch and Bonilla, 1967), the 1983 Nipponkai-Chubu, Japan earthquake (Tani, 1991), the 1995 Hyogoken-Nanbu, Japan earthquake (Tani, 1996), among many others. During 2011 Great East Japan earthquake, more than 2000 locations of embankment suffered some level of damage, caused by liquefaction of foundation ground (Oka *et al.*, 2012). Liquefaction triggering mechanisms (Seed and Lee, 1966), potential evaluation criteria (Seed and Idriss, 1971; Robertson and Wride, 1997; Idriss and Boulanger, 2006; Ghafghazi, Dejong and Wilson, 2017), liquefaction-induced damage prediction(Ishihara and Yoshimine, 1992; Towhata *et al.*, 1992; Towhata, Orense and Toyota, 1999; Sharp, Dobry and Phillips, 2010; Montassar and de Buhan, 2013), and remediation countermeasure (Okamura and Matsuo 2002; Adalier, Elgamal, and Martin 1998; Okamura and Tamura 2004; Dashti et al. 2010; Adalier and Elgamal 2004), have been extensively studied in the past decades. It was reported that the major cause of the embankment settlement was the lateral deformation of liquefied soil beneath embankment away from the embankment center.

Efficient remediation of soils susceptible to liquefaction induced damage is one of the most challenging problems in geotechnical earthquake engineering. To date, many liquefaction countermeasures based on various principles have been developed (e.g., densification, reinforcement, drainage, etc.). To provide a countermeasure against the liquefaction hazard and its consequences, different ground improvement techniques have

been developed over the last 50 years. Overall, these methods aimed to increase soil's shear strength and stiffness, decrease the driving shear stresses, and/or reduce the development of excess pore water pressures during earthquakes (Baez and Martin 1993). Currently, the available remediation methodologies include densification, reinforcement, drainage, preloading, replacement, chemical stabilization, and thermal and biological treatment (Han 2015).

As is well known, a soil's resistance to liquefaction is largely a function of relative density (Dr). Therefore, improving relative density of soil can be achieved by a substantial number of ground improvement methods, such as vibro-compaction, dynamic compaction, sand compaction pile, etc. Densification is attractive because the methods are relatively simple and practical and improvement can be easily verified using in-situ *N* value. On the other hand, creating stiffer elements as shear reinforcement within a soil mass can reduce the cyclic shear stress ratio applied to liquefiable soil. There are several design patterns in this method: full soil treatment, cellular or panel reinforcement, or individual column elements. Design of reinforcement is mainly based on the principle of strain compatibility between reinforcing elements and the enclosed soil. Unlike densification methods for liquefaction mitigation, the quality of reinforcement cannot be verified based on post-treatment. Engineers must utilize theoretical analyses for their design and effectiveness verification. Another method based on a different principle is drainage. Generation of excess pore water pressure in liquefiable soil is the primary triggering mechanism leading to liquefaction. Hence, liquefaction can be mitigated and the reduction of effective stress in liquefiable soil under seismic excitation may be controlled if the development of high excess pore water pressure can be prevented through rapid drainage. Although drains can successfully mitigate liquefaction, the improvement of the ductility cannot be expected and the volume of water drained during seismic event is still approximately equal to the amount of deformation observed at the surface of drain treated ground. In addition, the effectiveness of drains cannot be verified through the conventional in-situ tests.

Among many liquefaction mitigation methods, the sand compaction pile (SCP) method is one of typical ground densification methods, which has been often applied to mitigate the liquefaction, to densify the ground by installing vertical compacted sand piles into the ground. The SCP method is considered can increase ground density and uniformity (Kitazume, 2005). The effectiveness of the SCP method as a countermeasure against liquefaction has been confirmed in past earthquakes, including the 1978 Miyagi-Oki earthquake (Ishihara, Kawase and Nakajima, 1980), showing that this method is one of the most reliable ground improvement methods in Japan (Harada and Ohbayashi, 2017). It is also expected to be applied to the ground improvement of civil engineering structures in the future.

On the other hand, there is remain numerous existing soil structures worldwide which were either constructed before the seismic design standard established or without it (Mitrani and Madabhushi, 2010). To prevent potential damage to these existing structures from liquefaction in future earthquakes, it may be necessary to remediate the foundation soil. However, the conventional SCP method constructing sand piles in vertical direction is not able to densify ground underneath an existing structure. As mentioned above, during earthquake loading, most of the structural settlements and deformations are caused by the lateral movement of liquefied soils under the structure. To apply the SCP method to existing embankment structures, countermeasures are designed so as to provide containment for deformation of liquefied foundation soils away from embankment centerline toward free field, for which the well compacted sand piles are constructed under embankment toes. It has reported that occurrence of excessive settlement associated with a large lateral deformation of liquefied foundation soils could be prevented effectively by this method, however, some embankment crest settlement was inevitable due to the deformation of liquefied sand under the embankment and volumetric strain with excess pore pressure dissipation under the embankment (Adalier, Elgamal and Martin, 1998; Elgamal *et al.*, 2002; Okamura and Matsuo, 2002; Okamura and Tamura, 2004).

With the development of technology, a new type of SCP method was recently developed, SAVE-SP method, which enables to install sand piles vertically or at a specific angle into the ground. As the machine for this method is small, the compacted sand piles enable to be formed at any direction underneath structure, which is expected to prevent liquefaction and associated settlement more effectively. The geometric form of the improvement zones may affect the response and deformation behavior of the improved ground. However, these influences are not well investigated and incorporated into the current design precisely. A reliable and performance-based design of the new SCP method for embankments requires a clear understanding of the effect of various parameter that influence performance. The results of the present study aim to contribute to a better understanding of using the new type SCP improvement for mitigating liquefiable foundation and to facilitate its practical application.

1.2 Objectives

To understand the effects of various geometry of SCP improvement as a countermeasure for mitigating liquefaction-induced damages, the centrifuge tests and numerical analyses were carried out in this study. The main objectives of this study are as follows:

1. To observe the performance of SCP improved ground with various geometry for mitigating embankment settlement.

2. To investigate the seismic deformation of SCP improved ground with various geometry and associated embankment deformation.

3. Enhance the understanding of the working mechanisms of the improvement by new type of SCP method, through divide the factors contributing to embankment settlement.

4. To explore the effects of SCP improvement geometry (i.e., angle of SCP improvement, extent of SCP improvement) on mitigating liquefaction-induced embankment settlement.

1.3 Outline of dissertation

This dissertation is composed of 6 additional chapters. Below is a brief description of the six chapters that encompass the main body of the research work.

Chapter 1: *Introduction* – includes the background, objectives of this study, and an organization of the dissertation.

Chapter 2: *Literature review* – presents the current research related to this study. At first, it provides a brief literature review on liquefaction triggering mechanisms, and performance (failure mechanisms) of embankment resting on liquefiable ground. And then, the emphasis is on the effectiveness and performance of the conversional SCP method applied to existing embankment.

Chapter 3: *Centrifuge tests on seismic response of embankment with various geometry improved form* – a series of dynamic centrifuge tests were conducted on 4 different foundation conditions, where the SCP improvement form is installed into the ground from the embankment toe over 50 to 90 degrees, as well as benchmark model without any improvement. The effects of the different geometric improvement form on the response of the embankment and ground are discussed.

Chapter 4: *Numerical modeling of embankment ground with various geometric improvement* – simulates centrifuge model tests to further investigate the working mechanism of SCP improvement with various geometric form, using finite element analyses. The numerical results are compared with experimental results for the validation of numerical model used.

Chapter 5: *Effect of improvement angle on deformation of embankment and ground* – presents the numerical results of embankments resting on liquefiable ground improved with various improvement angle. The improvement angle is changed from 30 to 90 degree based on the possibility in practice. The effects

of improvement angle on deformation of embankment and ground are discussed.

Chapter 6: *Effect of improvement width on deformation of embankment and ground* – presents the numerical results of parametric studies conducted to compare the deformation of embankment and ground improved by different width of SCP form. The width of improvement form is varied in order to explore the critical width for mitigating the performance.

Chapter 7: Conclusions and recommendations of this study are presented.

Chapter 2

Literature review

2.1 Liquefaction

Saturated granular materials, such as sands and silts, subjected to cyclic loading will show a tendency to compress, resulting in build-up of excess pore water pressure if the soil is under undrained condition. When the excess pore water pressure reaches a value equal to the initial effective overburden stress, soil particles do not support each other, referred as a zero effective stress condition that is a state of initial liquefaction (Seed and Lee, 1966; Seed and Idriss, 1971; Martin and Finn, 1975). Liquefaction, which involves substantial loss of strength and stiffness of saturated sandy soils, has been reported as a cause of severe damage to embankment, bridges and other structures during past major earthquakes. In most cases, large deformations occurred due to liquefaction of the supporting loose cohesionless foundation soil (Seed, 1968; Tani, 1996), resulting in cracking, settlement, lateral spreading and slumping (See Figs. 2.1.1 - 2.1.4). The consequences of liquefaction vary for level ground and slope. Level ground sites undergo ground oscillations accompanied by cracks and fissures and settlements.

The destructive effects of soil liquefaction cause loss of billions of dollars due to structural damage, yet the casualties of human live is immeasurable. The Niigata and Alaska earthquakes in 1964 are the events that focused world attention on the phenomenon of soil liquefaction, illustrating the significance and damage caused by the liquefaction (Kawakami and Asada, 1966; McCulloch and Bonilla, 1967). Significant number of researches have been conducted so far in understanding the liquefaction phenomenon since last five decades. Soil liquefaction is also a major design problem for large sand structures such as mine tailings, impoundments and earthen dams. Earthquake induced liquefaction has become a major problem to soil embankments such as rive dykes, levees, road embankments and earth dams, supported on a cohessionless foundation soil. About 1200 levees were distressed during 2011 Great East Japan Earthquake due to liquefaction of foundation ground.

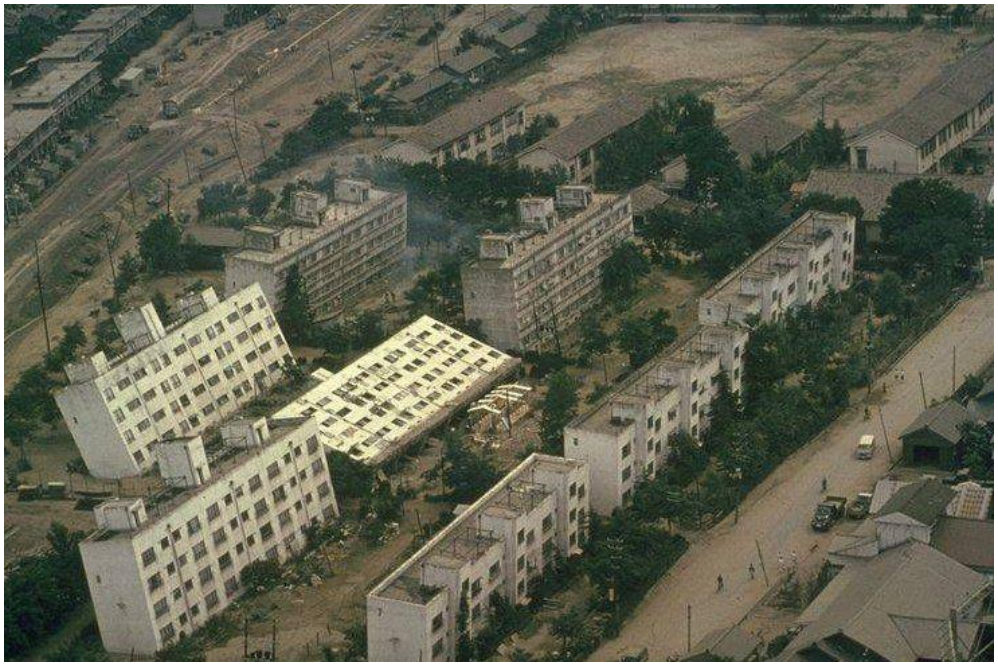

Figure 2.1.1 Collapse of buildings due to loss of bearing capacity during 1964 Niigata earthquake (University of Washington, 2000)

Figure 2.1.2 Embankment failure due to liquefaction on the Pan-American Highway during 2007 Peru earthquake (MCEER, 2007)

Figure 2.1.3 Lateral spreading at Raqui 2 bridge during 2010 Maule Earthquake in Chile (Yen et al, 2011)

Figure 2.1.4 Depression behind quay wall at Kashima port (EERI, 2011)

2.2 Case histories associated with foundation liquefaction

2.2.1 Embankment damaged during the 1964 Niigata Earthquake

A great earthquake occurred at Niigata, Japan in 1964, having a magnitude of 7.5 in the moment magnitude scale. The earthquake caused extensive damages to Niigata city in spite of the epicenter being located far from it. Investigation on the damages during the 1964 Niigata earthquake reveals that the adverse influence of poor sub-soil. In fact, the damages were more due to the movement of the foundation soil than the direct effect of ground shaking itself (Hamada *et al.*, 1986).

Two kinds of damage to earth structures by the Niigata Earthquake were found, namely damage due to the vibration of structures themselves and that due to the liquefaction of sandy ground. Among them, much damage to earth structures owing to the liquefaction of the ground, such as slides, settlements and heave on toes of embankments were found in the Niigata and Shonai Plains of alluvial deposit (Kawakami and Asada, 1966; Yamada, 1966).

Appearance of the damage on embankments due to the earthquake is shown in Figure 2.2.1 and Figure 2.2.2. Many cracks occurred on the crest of the embankment accompany with severe settlement. It is considered due to the lateral spreading of the foundation soil blow the embankment because the liquefaction occurred.

Figure 2.2.1 Damage to road embankment during the 1964 Niigata Earthquake (Hamada *et al.*, 1986)

Figure 2.2.2 Failure of embankment during the Niigata earthquake (Hamada *et al.*, 1986)

2.2.2 River dike failure during the 1993 Hokkaido Earthquake

Hokkaido, the northern island of Japan, encountered with earthquakes of magnitude 7.8 twice in January and July in 1993. The first on is named the Kushiro-Oki Earthquake. The epicenter is located 15-20 km south of Kushiro city. The second earthquake is the Hokkaido Nansei-Oki Earthquake and the epicenter is located 70 km northward of Okushiri island. These earthquakes brought disasters on kinds of infrastructures such as roads, railways, harbors, river levees and lifelines. Damage of river dikes caused by the Kushiro-Oki Earthquake reached the total length of 26,306 m through 52 sections. Damage of bank protection was 1,260 m at 11 sections. Damage of river dikes caused by the Hokkaido Nansei-Oki Earthquake was 8,915 m through 24 sections and that of bank protection was 3,511 m at 20 sections (Kaneko *et al.*, 1995; Sasaki and Tamura, 2007)

Dike material below the ground surface was submerged underground water and was potentially liquefied by earthquake. Surface of dike and marsh plane beside levee was frozen to the depth of 50-70 km and was effective to resist against sand eruption through peat bed from sand layer below through peat bed. Figure 2.2.4 shows a sketch of failure of the Kushiro River dike.

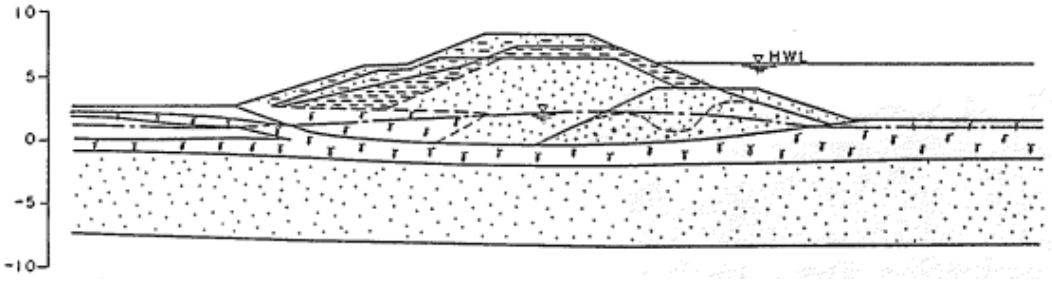

Figure 2.2.3 Geological cross-section of the embankment at the retarding basin of the Kushiro River (Kaneko *et al.*, 1995)

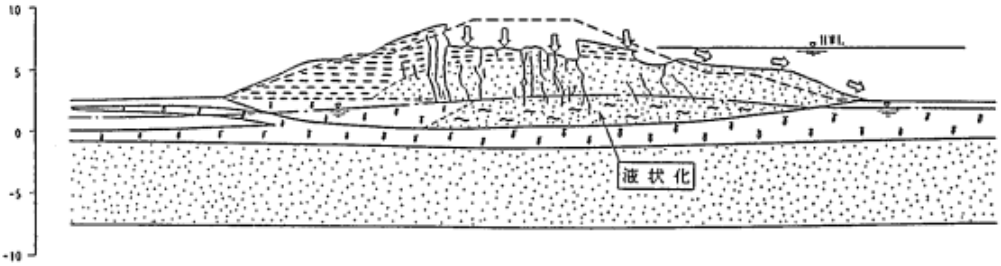

Figure 2.2.4 Mechanism of the embankment collapse due to the Kushiro-Oki Earthquake (Kaneko *et al.*, 1995)

2.3 Seismic response of embankment supported on liquefiable ground

Many earth embankments worldwide are located in seismically active areas, which were either constructed before the seismic design standard established or without it (Mitrani and Madabhushi, 2010). Many of these embankments may have the potential hazardous impact during earthquakes. The past major seismic events such as the Hyogoken-Nanbu 1995, the Great East Japan 2010 earthquakes continued to demonstrate the associated deformations and damaging effects of embankments. Earthquake induced liquefaction has become a major problem to soil embankments such as river dykes, levees, road embankments and earth dams, supported on a cohesionless foundation soil. Previous studies have shown that the widespread damage to such embankments occurred mainly due to the liquefaction of foundation soil, resulting in cracking, settlement, slumping and lateral spreading (Seed, 1968; Koga and Matsuo, 1990; Matsuo, 1996). Several experimental studies and numerical analyses have been conducted previously to examine the behavior of embankments resting on uniform clean cohesionless soil during earthquakes (Koga and Matsuo, 1990; Dobry and Liu, 1994; Ghosh and Madabhushi, 2007; Xia *et al.*, 2010; Wang, Wei and Liu, 2015). In this section, the review of literature

related to the mechanism of embankment failure due to foundation ground liquefaction and the main factors of embankment settlement is introduced.

2.3.1 Mechanism of embankment failure due to ground liquefaction

Koga and Matsuo (1990) carried out a series of shaking table tests on earthen embankment founded on saturated sand ground. They investigated the cyclic stress-strain behavior of soil in the ground by using the measurements. From the experiment results, it is found that the soil beneath the embankment does not reach zero effective stress state and keeps constant shear stress amplitude. However, the soil in the free field approaches the zero effective stress state and loses the shear stress amplitude. They concluded that the difference of the behavior between two locations was due to the spatial variation in stress condition.

Matsuo *et al.* (2000) conducted a series of 2D-FEM analysis of soil embankments resting on liquefiable sandy soils. In the numerical simulation, the cyclic behavior of the soil beneath the embankment was investigated and discussed. Figure 2.3.1 shows the effective stress path and stress-strain relations of the soil element beneath the embankment (at P4 in Figure 2.3.1). In Figure 2.3.1(a), the vertical axis denotes the deviatoric stress defined by $\sqrt{S_{ij} \cdot S_{ij}}$ where S_{ij} is the deviatoric stress tensor. In Figure 2.3.1(c), the vertical axis denotes the stress difference defined by $\sigma'_v - \sigma'_h$, and the horizontal axis denotes the strain difference defined by $\varepsilon_v - \varepsilon_h$. The weight of the embankment induced the large initial deviatoric stress and mean effective stress, and the initial stress state was very close to the failure state as shown in Figure 2.3.1(a). the deviatoric stress and the mean effective stress did not decrease down to the origin, and the stress path was traced along the failure line during shaking. The shear modulus did not decrease rapidly and the shear strain amplitude was not so large as the strain difference. On the other hand, the strain difference gradually increased toward the vertical compression side during shaking. The soil beneath the embankment behaves under the stress-constrained boundary condition, because the liquefied free ground cannot sustain the horizontal stress, which is generated from the embankment side. The excess pore water pressure beneath the embankment increased until the free ground liquefied, and then it remained almost constant. After the free ground liquefied, the deviatoric stress in the soil beneath the embankment remained, and led the soil state to failure as shown in Figure 2.3.1(a). As a result, the soil could not reach zero effective stress state. Thus, how the initial anisotropic stress varies spatially and when the free ground liquefied both affect the soil behavior in the ground beneath the embankment. If the stress state in the ground beneath the embankment was close to isotropic, the excess pore water pressure build-up would have been larger. Furthermore, under the stress condition in which the major principal stress is rotating around the vertical direction

during shaking, the soil beneath the embankment tends to soften and the plastic straining occurs predominantly in the vertical direction, as shown in Figure 2.3.1(d). the soil element spreads laterally accompanied by the settlement of embankment. Thus, the settlement of the embankment is affected by how the soil beneath the embankment deforms during shaking.

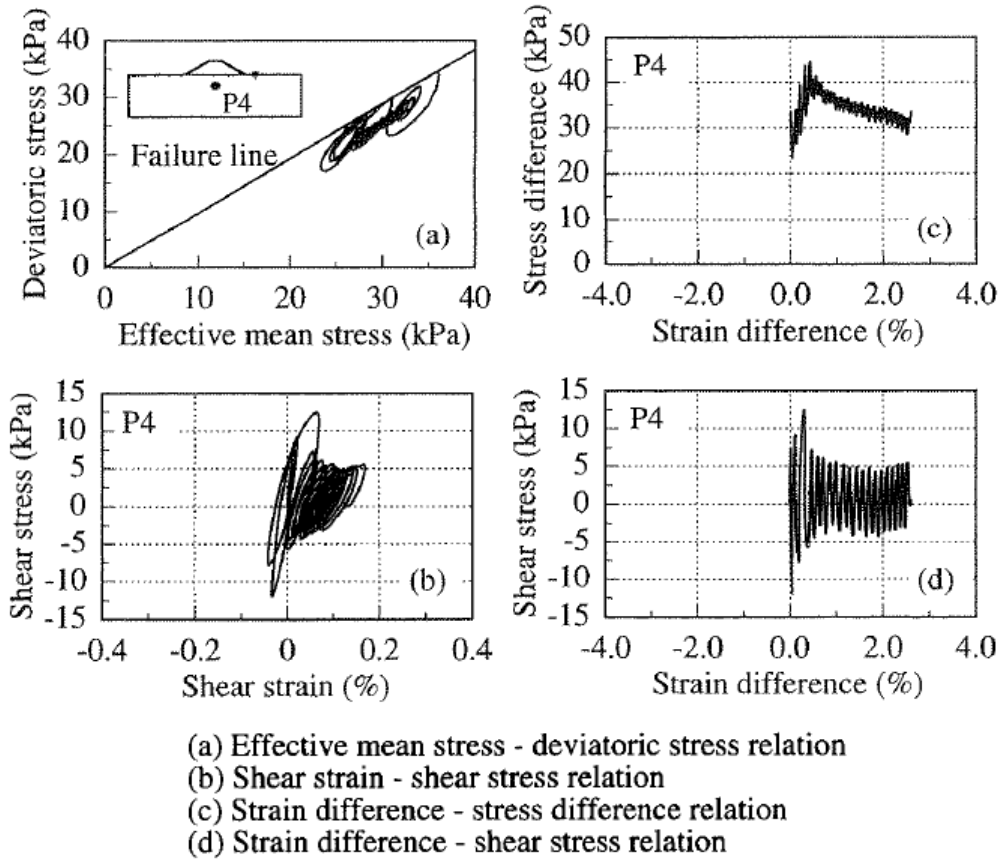

Figure 2.3.1 Stress-strain behavior in the ground beneath the embankment (Matsuo *et al.*, 2000)

The studies introduced in the preamble mainly discussed the seismic behavior of embankment resting on the liquefiable ground microscopically. Figure 2.3.2 and Figure 2.3.3 show a schematic diagram explaining the behavior during earthquake of the liquefiable ground and embankment divided into 5 stages (Sasaki, Moriwaki and Ohbayashi, 1997).

Stage 1: before the earthquake occurs, the foundation ground has sufficient bearing capacity for supporting the embankment. It is in a stable state as a whole.

Stage 2: since the earthquake induced cyclic shear stresses act on the embankment and ground, the excess pore water pressure starts to rise in the ground. Ultimately, when the excess pore water pressure rises to the value same as the initial overburden effective stress, liquefaction takes place, which leads to lose of the stiffness and strength of the ground.

Stage3: as the earthquake continues, the ground continues to be liquefied. Deformation of the bottom of the embankment progresses and a fracture zone occurs within the embankment.

Stage 4: as the plastic fracture zone develops, cracks occur in the embankment and liquefied layer undergoes lateral flow deformation.

Stage5: as excess pore water pressure dissipates after shaking, the pore water drains toward the ground surface, resulting in volume compression of ground.

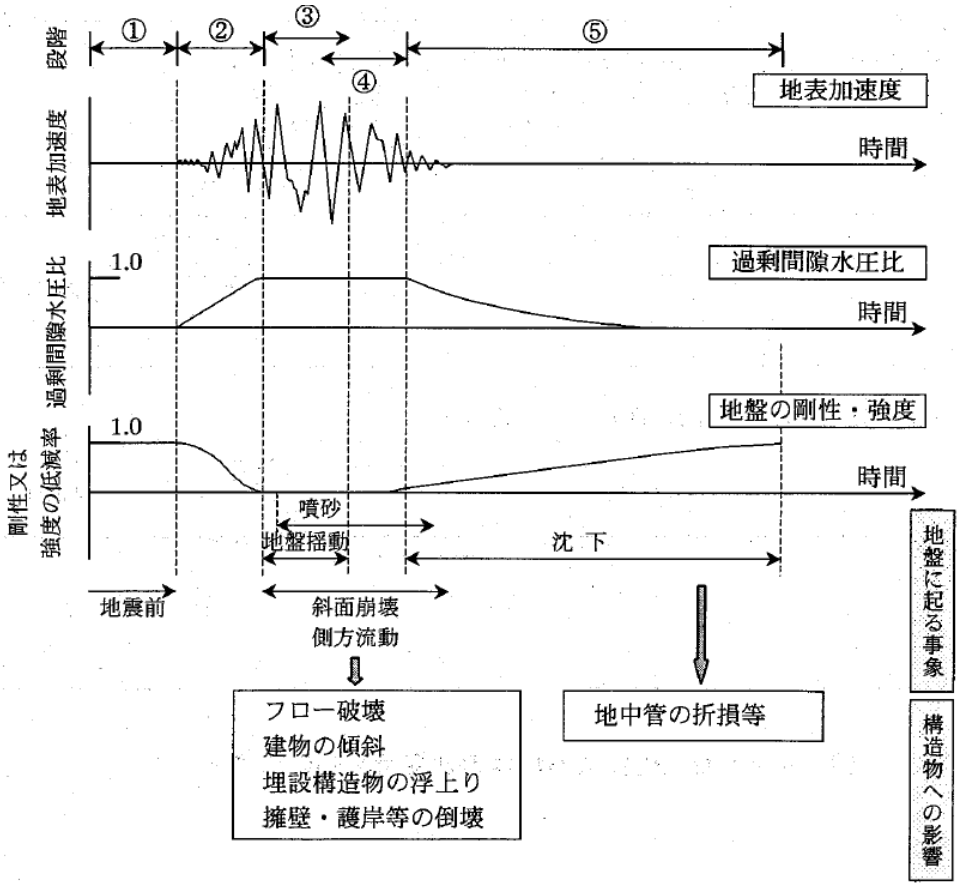

Figure 2.3.2 Conceptual diagram of ground behavior due to liquefaction during earthquake (Sasaki, Moriwaki and Ohbayashi, 1997)

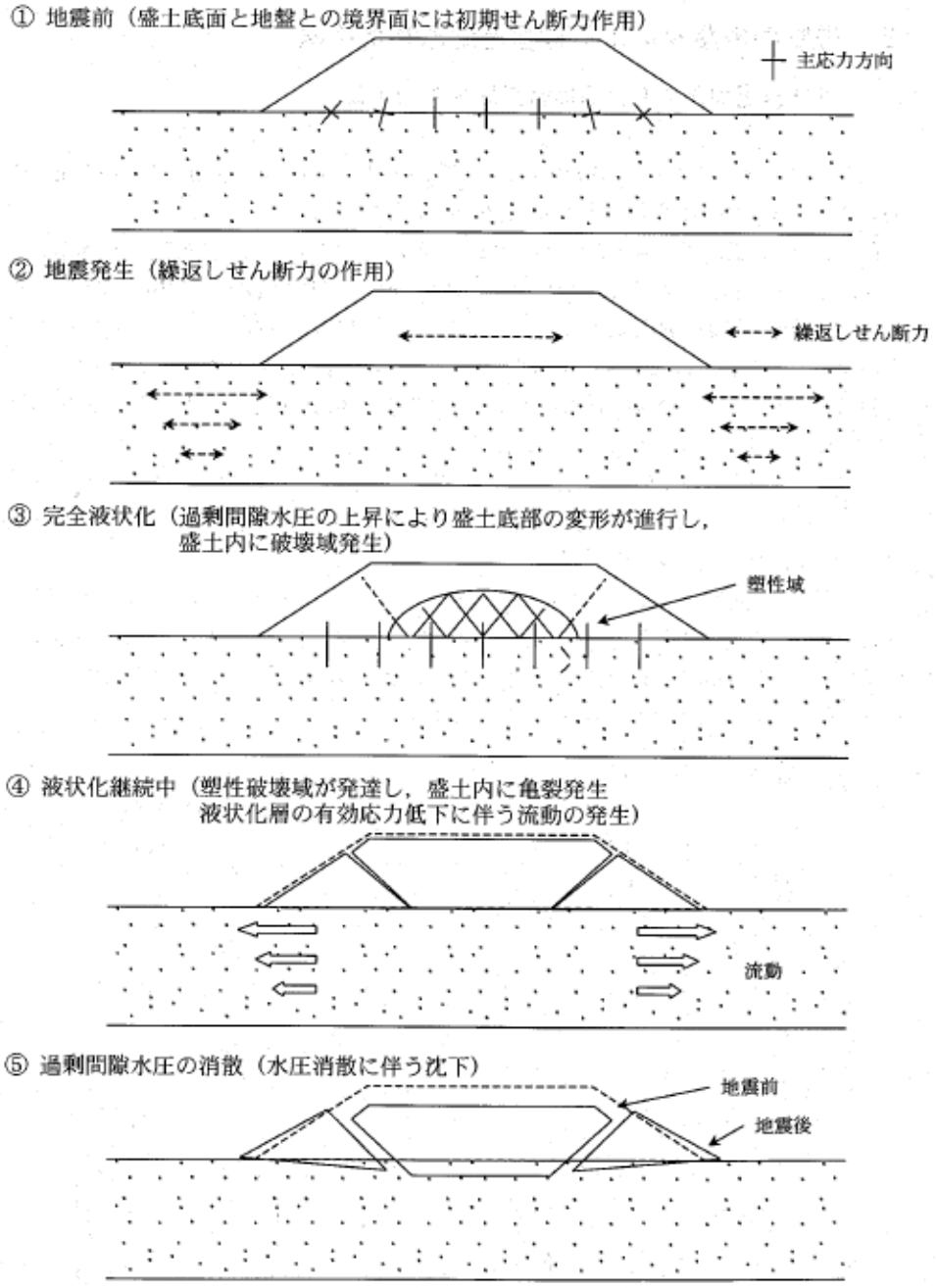

Figure 2.3.3 Conceptual diagram of embankment failure process resting on liquefiable ground (Sasaki, Moriwaki and Ohbayashi, 1997)

2.3.2 Main factors of embankment settlement

Several experimental studies and numerical analyses have been conducted previously to investigate the behavior of embankments resting on uniform clean cohesionless soil

during earthquakes (Koga and Matsuo, 1990; Adalier, Elgamal and Martin, 1998; Finn, 1998; Zhang, 1999; Matsuo *et al.*, 2000; Adalier and Aydingun, 2003; Okamura and Tamura, 2004; López-querol and Blázquez, 2006; Bhatnagar, Kumari and Sawant, 2016).

Koga and Matsuo (1990) conducted a series of shaking table tests on earthen embankment founded on saturated sand ground and found out that the ground beneath the embankment did not liquefy, whereas the ground in the free field liquefied and the slumping and cracking of embankment is due to the softening of the underlying ground associated with pore water pressure generation.

Adalier, Elgamal and Martin (1998) conducted a centrifuge-testing program to assess the earthquake performance of countermeasure techniques for a liquefiable foundation under an existing embankment. It was found that in unimproved case, near the embankment toe, a peculiar asymmetric response occurred with clear spikes during each cycle of excitation. Such asymmetric acceleration response was attributed to the occurrence of cyclic downslope deformations. The soil graually accumulates significant permanent strains for each additional cycle of loading. In this process, cyclic spikes appear to be associated with the tendency of the soil skeleton to dilate at large strains.

Matsuo *et al.* (2000) used a dynamic response finite element method to predict earthquake-induced deformation of soil embankment. From the results of analysis, it was found that the failed configuration of the embankment was affected by the behavior of the foundation ground, especially near the surface, beneath the embankment.

Okamura and Tamura (2004) conducted a series of dynamic centrifuge tests, in which it describes a practical prediction method for embankment settlement due to foundation liquefaction, which are remedied with the deep mixing method as Figure 2.3.5 shown. In this study, from observations of a series of centrifuge model tests on embankments underlain by loose saturated loose saturated sand with and without countermeasures, they clearly demonstrated the major factors that contributed the crest settlement.

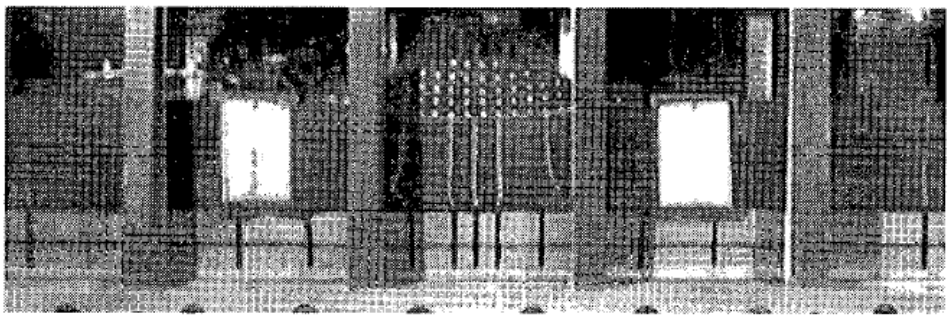

Figure 2.3.4 Deformation of model S1 after shaking event (Okamura and Tamura, 2004)

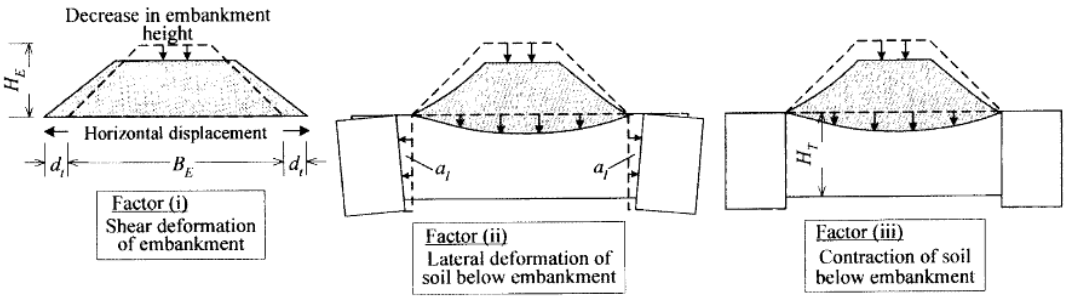

Figure 2.3.5 Three major factors contributing crest settlement (Okamura and Tamura, 2004)

Figure 2.3.4 shows a photograph of one of the models after shaking, in which lines in the foundation soil are dyed Silica sand put near the side glass of the container during model preparation so that ground deformation can be easily detected. From observations of the model deformation, it appeared that the following three major factors contributed the crest settlement; i) shear deformation of the embankment caused by horizontal deformation of the underlying liquefied sand, ii) lateral deformation of the liquefied loose sand layer and iii) contractive volume change of the sand under embankment. These factors are schematically illustrated in Figure 2.3.5. Assuming uniform settlement along the embankment base as well as uniform shear deformation of the embankment, the crest settlement, S_c, due to the embankment base settlement, S_1, and the change in embankment height, S_2, can be written as,

$$S_c = S_1 + S_2$$

$$S_1 = 2\frac{a_1}{B_E} + \varepsilon_v H_T$$

$$S_2 = \frac{2d_1 H_E}{B_E}$$

Where a_l=area of the lateral deformation of the block, ε_v=volumetric strain of the liquefied sand under the embankment, H_T=thickness of the liquefiable soil layer, d_l=lateral deformation at embankment toe, B_E=width of the embankment base and H_E=embankment height.

2.4 Previous research on the SCP improvement

The huge earthquakes which occurred in Alaska and Niigata in 1964 demonstrated the importance of soil dynamics and countermeasure of seismic disasters to geotechnical

engineers. Since then, liquefaction has been the main focus of geotechnical engineering (Kitazume and Okamura, 2010). The possibility of liquefaction used to be evaluated by the SPT N-value alone many years ago, and the main method used as a countermeasure to liquefaction was the densification of ground to increase the SPT N-value. The sand compaction pile (SCP) method is a method for improving soft grounds by means of installing well-compacted sand piles in the ground. In sandy grounds, the SCP method is mainly used as a countermeasure against liquefaction by increasing the N-value of the loose ground, and its effectiveness in preventing liquefaction has been confirmed through past large earthquakes. Figure 2.4.1 shows number of improved ground field case histories documented for each improvement method. It can be seen that the sand compaction pile method had well performance during past earthquakes compare to other improvement method, which demonstrates that SCP method is one of the most reliable ground improvement methods for mitigating liquefaction.

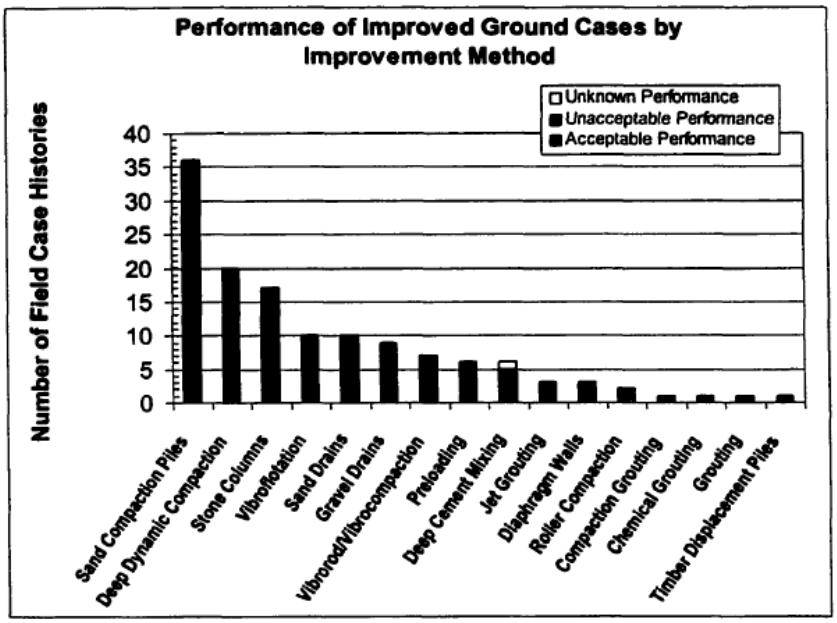

Figure 2.4.1 Number of improved ground field case histories documented for each improvement method (Hausler, 2002)

2.4.1 Introduction of the Sand Compaction Pile (SCP) method used as liquefaction countermeasure

The possibility of liquefaction during an earthquake is usually assessed by the following two steps: (1) particle size distribution and SPT N-value and (2) cyclic triaxial test. When a ground is considered to liquefy during an earthquake according to the above mentioned procedure, the density of ground should be increased to a certain level to prevent the

liquefaction of the ground. The main method used as a countermeasure to liquefaction is the densification of ground to increase the SPT N-value (Kitazume and Okamura, 2010).

The sand compaction pile (SCP) method is one of the densification methods. The principle of the SCP method for sandy grounds is primarily to decrease the void ratio of the ground and to densify the ground as a result of the sand pile installation, as shown in Figure 2.4.3 (Kitazume, 2005; Harada and Ohbayashi, 2017). Beside the direct measurement of ground density, the SPT N-value has been frequently used as an index to evaluate the property of improved ground. The void ratio of sandy ground is closely related to the SPT N-value. The initial and target void ratios are estimated by measured and target SPT N-value respectively. Then, the replacement area ratio of improvement for preventing liquefaction is calculated. Then the volume of sand to be installed and the arrangement of sand piles are determined according to the replacement area ratio.

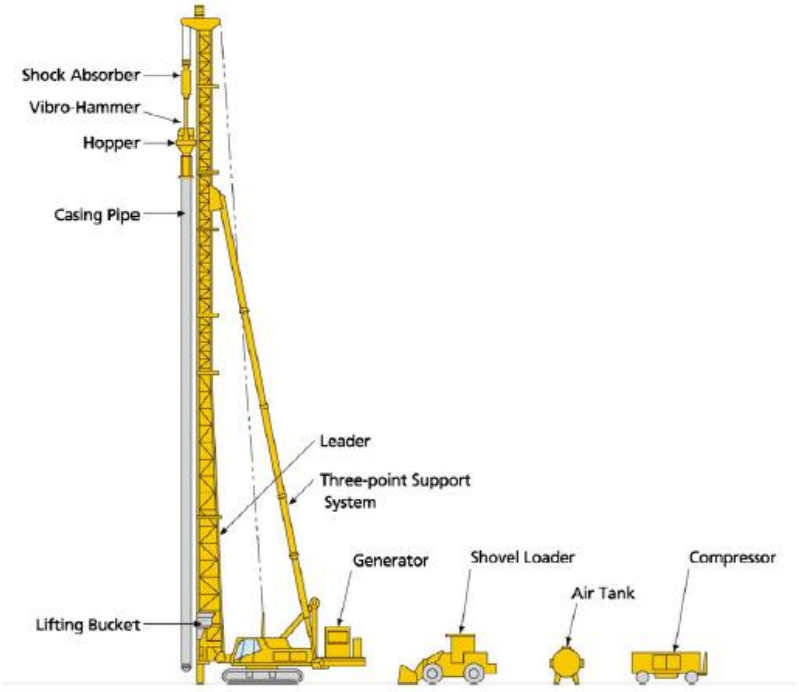

Figure 2.4.2 Vibratory SCP equipment

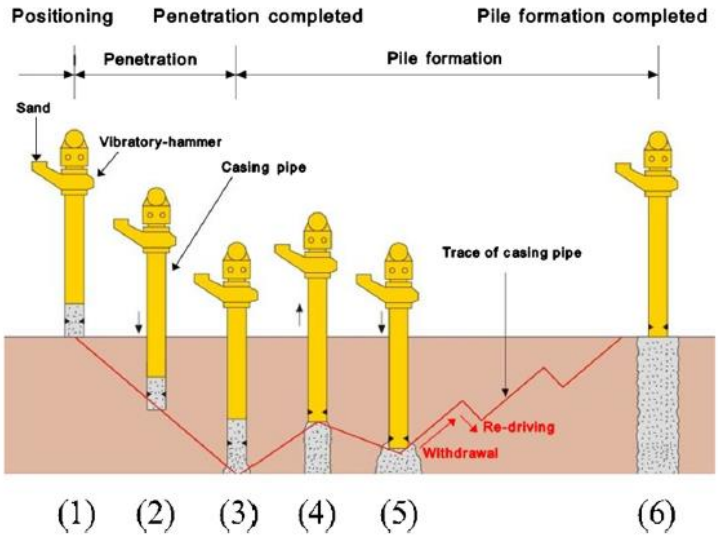

Figure 2.4.3 Installation procedure for vibratory SCP method

2.4.2 Existing embankment resting on liquefiable ground improved by SCP method

As is well known, a soil's resistance to liquefaction is largely a function of relative density (Dr). Thus, increasing cyclic resistance ratio can be achieved by a densification ground improvement method which can improving soil relative density (e.g. vibro-compaction, dynamic compaction, sand compaction pile, etc.). Through densification, liquefaction will not occur or the induced deformation may be controlled during earthquake. Densification method is attractive because the methods are relatively simple and practical and improvement quality can be easily verified using in-situ penetration techniques. The use of sand compaction piles to improve embankments supported on a liquefiable ground to increase the stability as well as to reduce the settlement has taken into account for the most popular application (Harada and Ohbayashi, 2017).

On the other hand, there are remain numerous existing soil structures worldwide which were either constructed before the seismic design standard established or without it (Marcuson and Silver, 1987). To prevent potential damage to these existing structures from liquefaction in future earthquakes, it may be necessary to remediate the foundation soil. However, the conventional SCP method constructing sand piles in vertical direction is not able to densify ground underneath an existing structure (e.g. road embankment, river dike and so on). Then, In Japan, it has usually applied the SCP improvement under existing embankment toes, aim at mitigating crest settlement by providing containment for the deformation of the liquefiable foundation soils.

There are various centrifuge tests and numerical analyses as well as shaking table tests at 1g on SCP improved ground supporting embankment to examine the performance of the improved ground and embankment under seismic loading.

2.4.2.1 Physical modeling tests

Adalier and others (1998) performed a series of four dynamic centrifuge models with different remediation techniques for foundation retrofit under an earthen embankment. The tested models included a benchmark model without any improvement, remediation with densification, solidification with cement, berm surcharge stabilization, and sheet pile enclosure as shown in Figure 2.4.4. It is found out from the experiment results that sand layers under lower overburden stress (e.g. free field and toe) are most vulnerable to liquefaction. Because a low resistance exit path is created, the foundation soil blow embankment is easy to move away from the embankment centerline, leading to a severe settlement of the embankment. Thus, the countermeasures are intended to (1) increase liquefaction resistance of the foundation soil; (2) improve the confinement of the foundation soil below the embankment, preventing lateral and vertical movement of soil toward the free surface; and (3) preserve the integrity of the embankment.

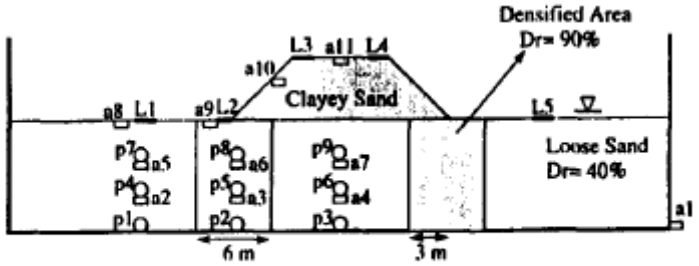

Model 2: Compaction

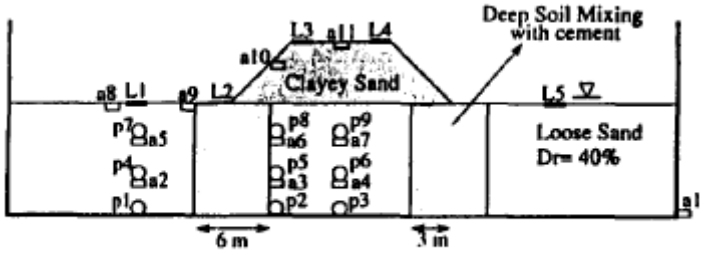

Model 3: Solidification

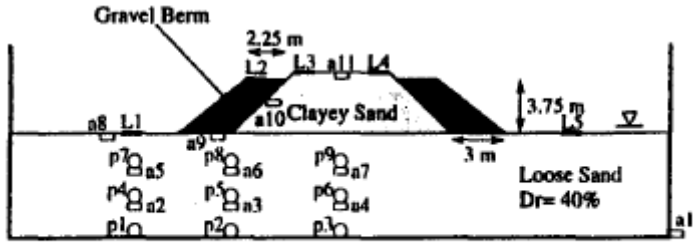

Model 4: Gravel Berm

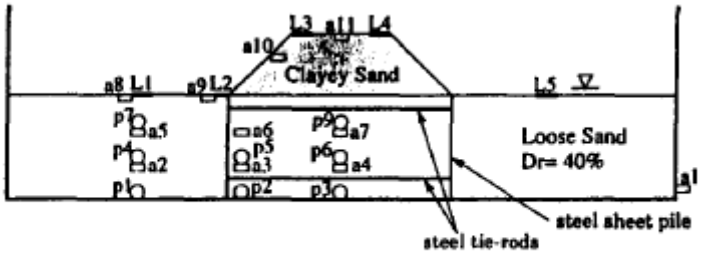

Model 5: Sheet Pile Enclosure

Figure 2.4.4 Model configuration (Adalier et al., 1998)

Okamura and Matsuo (2002) conducted a series of centrifuge tests to assess seismic performances of embankments with and without countermeasures, including three types of countermeasures used in the practice in Japan (the solidification by the deep mixing method, the densification by the sand compaction piles and the sheet pile enclosure). It was found from the results that, for the benchmark model without any improvement, the lateral deformation of liquefied sand and the shear deformation of the embankment were dominant. This might suggest effectiveness of countermeasure beneath toes, which provides containment to reduce both the lateral deformation and the lateral displacement of embankment toes. For cases with countermeasures constructed under toes, settlement due to the lateral deformation and shear deformation of the embankment decreased considerably. However, the crest settlement due to the volume change of loose sand under the embankment was larger in improvement cases.

Kogai *et al.* (2000) conducted 1G shaking table tests for a slope model consisted of saturated loose sand. The model slopes mitigated by a sheet pile and a wall of compacted sand were also tested to investigate the deformation characteristic of the slope and the effect of the improvement. Figure 2.4.5 illustrates the ultimate deformation of subsoils under three different test conditions; without any countermeasure, with a sheet pile and with a wall made of densified sand. The displacement of grids evidently indicates that both kinds of wall were able to reduce the magnitude of lateral displacement.

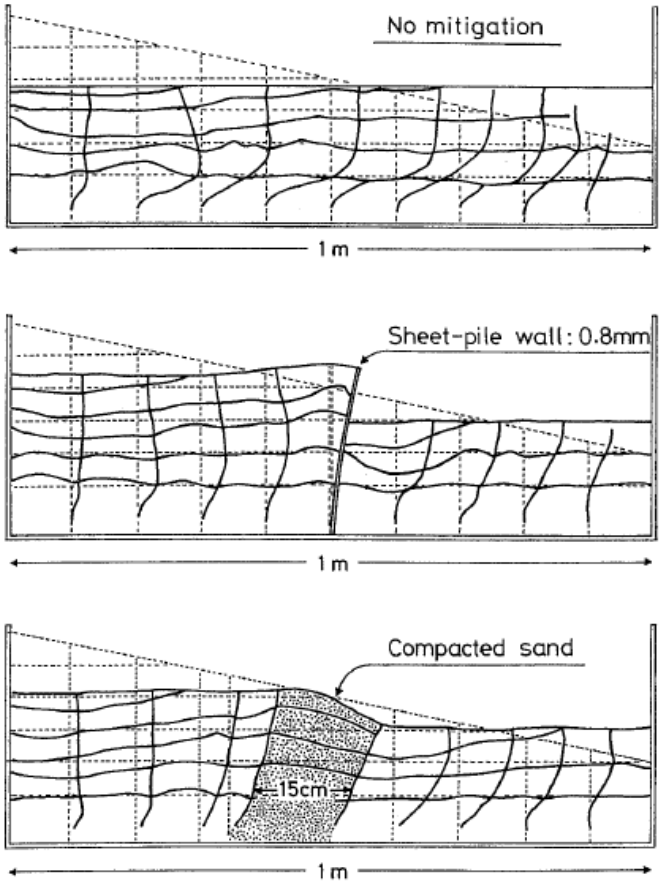

Figure 2.4.5 Deformation of model subsoil after shaking (Kogai *et al.*, 2000)

Furthermore, the ground surface in front of and behind the walls developed an elevation difference after deformation of the slopes. It is considered that the earth pressure difference between front and behind sides of the walls caused the deformation or bending of the walls.

Abe (1996) presented six 1G shaking table tests results conducted on an embankment resting on liquefiable ground and with different remediation applied under the toes, except for Case-2. The study tried to examine the dynamic behavior of earth-structure as a ground with embankment during liquefaction and assess the effectiveness of the liquefaction countermeasures. Figure 2.4.6 shows the input acceleration amplitude and the settlement of the embankment crest. It can be seen from this figure that in all experimental cases the amount of embankment crest settlement was found to increase with increase in the input acceleration amplitude. In the case improved by compaction method (Case-2), it was found that the amount of settlement of the embankment crest was significantly lower than for any of the other cases. However, in Case-2, the densified area was not only under the toes, but also the whole area below the embankment.

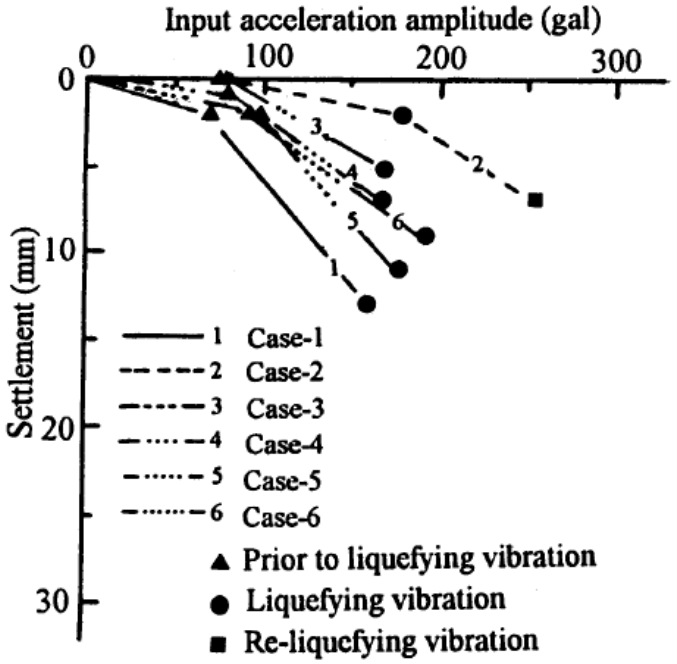

Figure 2.4.6 relation between settlement of embankment crest and input acceleration amplitude (Abe, 1996)

2.4.2.2 Numerical analysis

Adalier and Aydingun (2003) numerically simulated the seismic behavior of an earth embankment supported on liquefiable foundation ground, using an effective stress based, fully coupled, finite element code called DIANA-SWANDYNE II. In addition to the unimproved model, three models with remediation are analyzed, including densification of the sand under the toes, gravel berm surcharge, and sheet pile enclosure. The author point out that the deformation performance of an embankment supported on liquefiable soils will generally improve in relation to the degree of confinement provided by a given ground improvement method. The degree of confinement increases as the stiffness of the confining system increases. Confining systems installed at the toe of the embankment appear to be effective, provided the system is rigid and there is no opportunity for the liquefied soil to flow around the system. Embankment accelerations can be reduced if high excess pore water pressures develop in the foundation soil within the confining system, but this also results in larger consolidation settlements. Both experimental and computational data also indicate that (i) there may be a limit to the remedial effect that can be achieved, and (ii) a particular type of countermeasure may be effective for improving one type of ground response (i.e., deformation, acceleration, or pore pressures) but less effective for improving others.

Elgamal *et al.* (2002) investigate the dynamic response and deformation characteristics of the embankment-foundation system where SCP improvement and sheet pile were conducted under the toes. The finite element mesh used in the numerical analyses are shown in Figure 2.4.7. During the computational simulations, soil stress-strain responses were sampled at S1, S2 and S3 locations as shown in Figure 2.4.7. These locations were selected to represent zones of different response characteristics. The author pointed out several main findings from the results that, for no remediation case, higher effective confinement due to embankment weight appears to have sustained excess pore water pressure well below the level of liquefaction (see Figure 2.4.8). On the other hand, for the densification case, contractive response is seen to dominate below the embankment center, resulting in the typical pattern of cyclic loss of shear stiffness and effective confinement (see Figure 2.4.9).

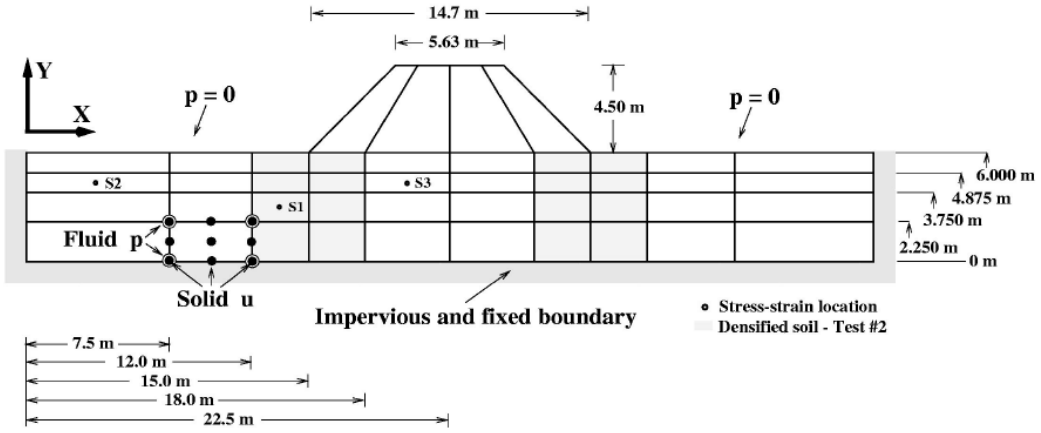

Figure 2.4.7 Finite element discretization and boundary conditions (Elgamal *et al.*, 2002).

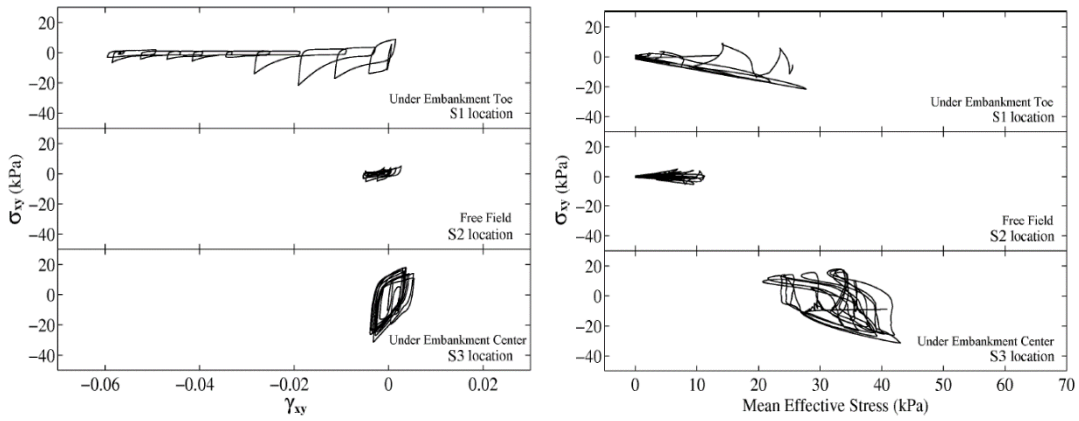

Figure 2.4.8 computed shear stress-strain and mean effective stress histories (no remediation)

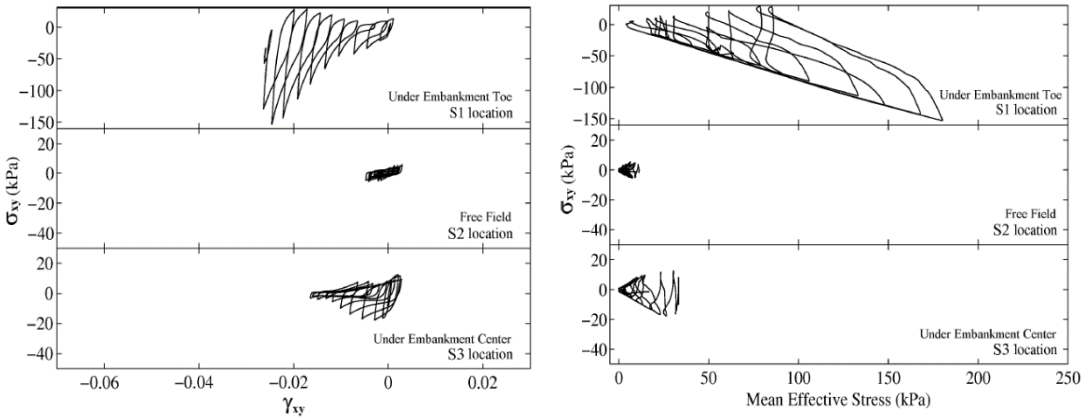

Figure 2.4.9 computed shear stress-strain and mean effective stress histories (remediation by densification)

Chapter 3

Centrifuge study on the effect of the SCP improvement geometry on the mitigation of liquefaction-induced embankment settlement

Liquefaction of foundation soil causes significant damage to infrastructures. The sand compaction pile (SCP) method is a countermeasure against liquefaction to densify the ground by installing dense sand piles. In recent years, an innovative method has been developed to install sand piles into the ground at any angle. In this study, a series of dynamic centrifuge tests are carried out to investigate the effects of the angle of the SCP improvement zone on mitigating the liquefaction-induced settlement of embankment crests. The lateral displacement beneath the embankment toes is mitigated by the presence of the improvement zone installed in the foundation ground. In particular, the case with a 50° improvement zone is the most effective in mitigating lateral displacement and contributes to the lower settlement of the embankment.

3.1 Introduction

Earthquake induced liquefaction has become a major problem to soil embankments such as river dykes, road embankments and earth dams, supported on a cohesionless foundation soil. Previous studies have shown that the widespread damage to such embankments occurred mainly due to the liquefaction of foundation soil, resulting in cracking, settlement, slumping and lateral spreading. Soil liquefaction and related damages to earthen structures have been extensively studied by many researchers in past decades (Seed, 1968; Sasaki *et al.*, 1992; Matsuo, 1996).

To date, many liquefaction countermeasures based on various principles have been developed (e.g., densification, deep mixing, drainage, etc.). Among them, sand compaction pile (SCP) method is one of typical ground densification methods, which has been often applied to mitigate the liquefaction, to densify the ground by installing vertical compacted sand piles into the ground. The SCP method is considered can increase ground density and uniformity (Kitazume, 2005). The effectiveness of the SCP method as a

countermeasure against liquefaction has been confirmed in past earthquakes, including the 1978 Miyagi-Oki earthquake (Ishihara, Kawase and Nakajima, 1980), showing that this method is one of the most reliable ground improvement methods in Japan (Harada and Ohbayashi, 2017). It is also expected to be applied to the ground improvement of civil engineering structures in the future. However, densification of a foundation soil can economically be done within a finite extent of improvement.

On the other hand, there are remain numerous existing soil structures worldwide which were either constructed before the seismic design standard established or without it. To prevent potential damage to these existing structures from liquefaction in future earthquakes, it may be necessary to remediate the foundation soil. However, the conventional SCP method constructing sand piles in vertical direction is not able to densify ground underneath an existing structure.

With advancements in machinery, a new type of SCP method was recently developed, SAVE-SP method, which enables the vertical installation of sand piles or the installation of sand piles at a specific angle into the ground. As the machine for this method is small, the compacted sand piles can be formed at any direction underneath structure, which is expected to prevent liquefaction and associated settlement more effectively (Kitazume *et al.*, 2016; Li *et al.*, 2019). In addition, in previous studies, Yoshida, Miyajima and Numata (2012) performed shaking table tests where the wooden sticks instead of sand piles, were installed into loose sand layer under residential houses at vertical and inclined angles. It was found that wooden sticks installed at an inclined angle were more effective than those installed at a vertical angle. Rasouli et al. (Rasouli, Towhata and Akima, 2016; Rasouli *et al.*, 2018) conducted 1 g model tests to evaluate the effect of sheet-pile walls as a countermeasure around the building's foundation and that combined with installing inclined drains under the structure. It was observed that the settlement and tilting of the building are reduced more significantly in combination with inclined drains under the structure due to the installation of drains providing an area of nonliquefied ground under the building edges.

The geometric form of the improvement zones may affect the response and deformation behavior of the improved ground. However, these influences are not well investigated and incorporated into the current design precisely. A reliable and performance-based design of the new SCP method for embankments requires a clear understanding of the effect of various parameter that influence performance. In this chapter, four dynamic centrifuge experiments are carried out to investigate the liquefaction induced deformation and response of the ground which is improved by SCP method with various geometric form. The effects of the different geometric improvement form on the responses of the ground are discussed.

3.2 Outline of new type sand compaction pile method

Sand Compaction Pile (SCP) method was first developed in 1956 and has been frequently applied to sandy ground and clay ground, where sand injected into a ground was compacted by a vibrator installed on the top of casing pipe (vibratory SCP method). In order to minimize adverse influence to surrounding caused by the vibrator, non-vibratory type SCP method was developed in 1995 (Silent, Advanced Vibration-Erasing Composer, SAVE method), where sand injected into a ground was statically compacted by the forced lifting/driving device instead of the vibrator. In recent years, it is required to prevent liquefaction of ground underneath existing structure such as building, river levee and airport runway. A sand injection type SCP method (SAVE-SP method) was developed for the requirement as shown in Figure 3.2.1. In the method, granular sand is fluidized by mixing with special agent and water, and is injected into ground through a small diameter pipe. The injected soil in the ground becomes granular state by a slow-acting retarding plasticizer to create compacted sands, as shown in Figure 3.2.2. On the basis of the principle that this method depends on the operation to inject sand into ground and to compact surrounding ground, the fluidized sand is required to have antipodal properties of the fluidity by keeping water-retainability to avoid pipe clogging and the modestly drainable characteristics to dissipate in order to obtain instantaneous high density of sand when pumped into the ground. Also, slow-acting retarding plasticizer is added to the fluidized sand to vanish the effect of fluidizing reagent after released into the ground.

Figure 3.2.1 SAVE-SP machine and mixing plant (Kitazume *et al.*, 2016).

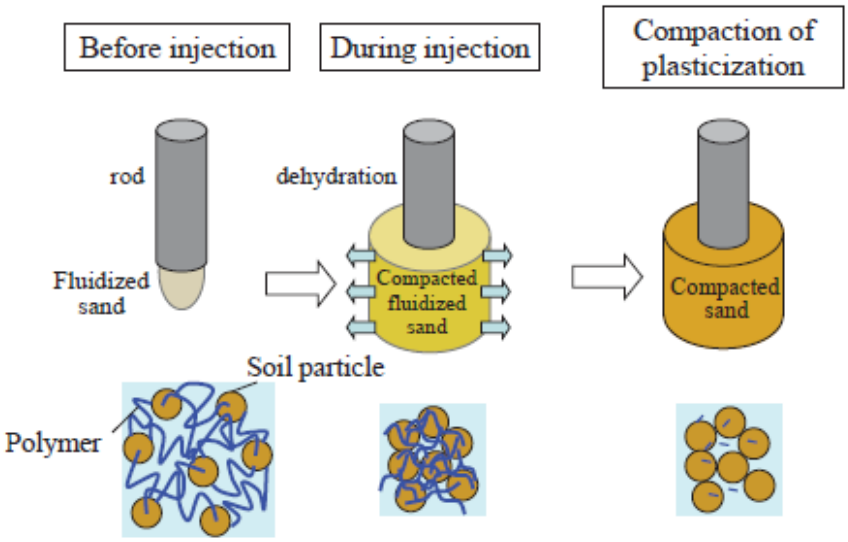

Figure 3.2.2 Schematic view of mechanism of the method (Kitazume *et al.*, 2016).

3.3 Scaling laws in centrifuge test

In geotechnical engineering, small-scale model experiments are usually carried out to study various problems, especially when complicated conditions are imposed. However, the behavior of the small-scale model, compared to a prototype model that may be N times larger than the small-scale model, will be completely different. This is because the stress-strain behavior of soil is known to be highly nonlinear. The main principle in centrifuge modeling is that a 1/N scale model placed at the end of a centrifuge arm subjected to a gravitational acceleration of N g will feel the same stresses as the prototype. The scaling laws described by (Schofield, 1981) for dynamic centrifuge modeling is summarized in Table 3.3.1. For instance, if a ground surface of 20 m depth has to be modeled the 0.4 m deep model container is filled with soil, placed on the end of a centrifuge and subject to a centrifugal acceleration of 50 g. The pressures and stresses are increased by a factor of 50. So, the vertical stress at the base of the model container is equivalent to the vertical stress at a depth of 20 m below the ground surface on earth. Thus the 0.4 m deep model represents 20 m of prototype soil. The reason for the centrifuge is to enable small scale models to feel the same stresses as a full-scale prototype. The stress would be 50 times smaller if it is measure under gravity. The scaling laws allow stresses and strains in model and prototype structures to be identical and hence true prototype behavior is observed in the model.

It should be noted that there is a discrepancy between static and dynamic scaling laws for time. The scaling law for time in static events scales as $1/N^2$ between the model and

prototype, while for dynamic events it scales as 1/N. One way to solve the discrepancy in a centrifuge is to use a viscous pore fluid.

Table 3.3.1 Scaling laws

Parameter	Ratio of model to prototype
Length	1/N
Area	$1/N^2$
Volume	$1/N^3$
Velocity	1
Acceleration	N
Frequency	N
Stress	1
Strain	1
Force	$1/N^2$
Time (dynamic)	1/N
Time (Consolidation)	$1/N^2$

3.4 The Tokyo Tech Mark III centrifuge

The Tokyo Tech Mark III centrifuge (Takemura et al., 1999) was used for all the tests. The centrifuge is a beam type centrifuge having a pair of parallel arms which holds platform on which the model container and a weight for counterbalance are mounted as shown in Figure 3.4.1. The radius of rotation is 2.45 m, which is the distance from the rotating shaft to the platform base. The surface of the swinging platform is always normal to the resultant of the centrifugal acceleration, and earth's gravity. Specifications of the centrifuge are summarized in Table 3.4.1.

For data acquisition, two types of signal transmission methods are used. One is classical electrical slip rings. Transducers are connected to the slip rings through a junction box and signals are transferred to amplifiers on the laboratory floor. The other type is an optical rotary joint. Transducers are connected to signal conditioners on the centrifuge.

Analog signals from the transducers are amplified there and then are converted to digital signals by A/D converters. Gains and the other conditions of the signal conditioners can be controlled by a PC on the lab floor. The digital signals are transferred to the PC on the lab floor through the optical rotary joint.

A hydraulic rotary joint with maximum pressure of 20.5MPa mounted on the centrifuge is used for charging and discharging oil to the centrifuge during spinning of the centrifuge. A big hydraulic accumulator is mounted on the centrifuge to satisfy the required flow rate of the pressurized oil for the high performance 1D shaker.

Table 3.4.1 Specifications of the Tokyo Tech Mark III Centrifuge

Radius	Platform radius	2.45 m
	Effective radius	2.0-2.2 m
Platform Dimensions	Width	0.9 m
	Depth	0.9 m
	Maximum height	0.97 m
Capacity	Maximum payload	50g.ton
	Maximum number of rotation	300 rpm
	Maximum payload at 80g	600 kg
Electrical slip rings	For instrumentation	72 channels
	For operation	20 channels
Rotary joint	Working pressure for air and water	1 Mpa
	Working pressure for oil	21 Mpa
	Wireless LAN	64 channels

Figure 3.4.1 Tokyo Tech Mark III Centrifuge

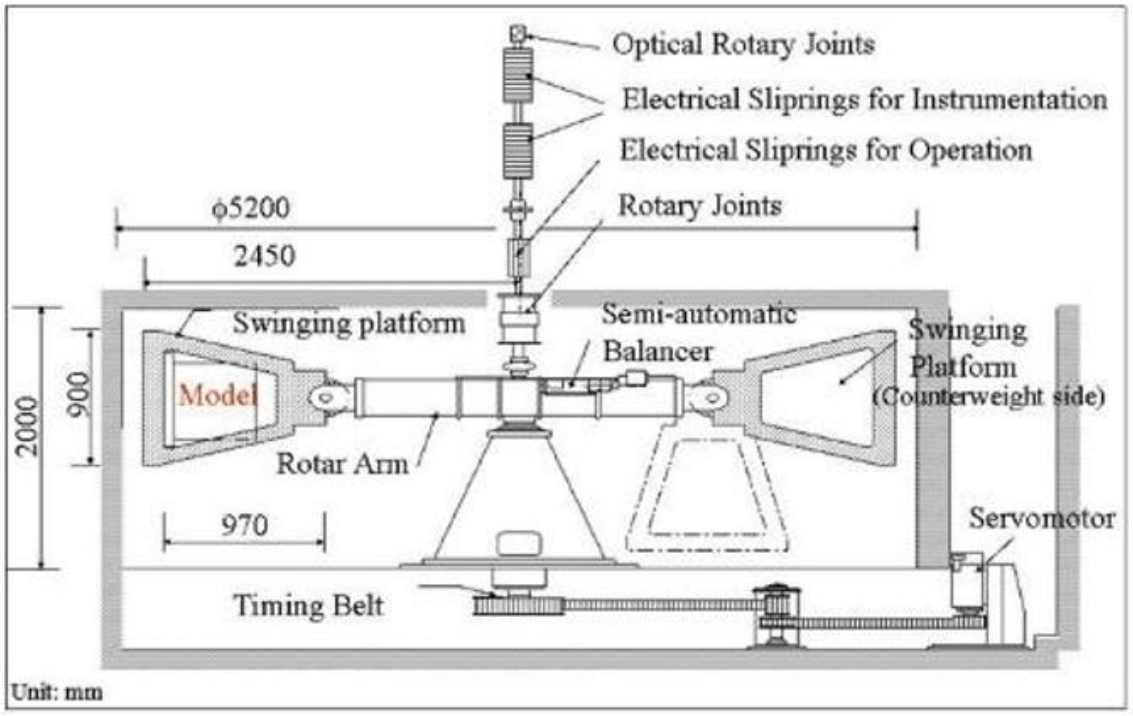

Figure 3.4.2 Sectional view of the Tokyo Tech Mark III Centrifuge

3.5 Centrifuge testing program

A series of dynamic centrifuge tests are conducted to evaluate the effectiveness of SCP-improved ground with various geometric improvement forms and to investigate the effects of the geometry of the improved zone on the ground response and deformation mechanism of embankments and foundation ground. In the centrifuge test program, the focus is on the angle of the improvement zone, which is defined as the angle between the SCP improvement form and the ground base, in which the angle is changed from 50 to 90 degrees. Dynamic centrifuge tests are carried out utilizing the Tokyo Tech Mark III centrifuge facility (Takemura *et al.*, 1999) with a radius of 2.45 m at a centrifugal acceleration of 50 g. The model configurations and the entire test results are presented in prototype scale units unless indicated otherwise.

3.5.1 Design and description of centrifuge models

Four dynamic centrifuge tests are conducted on three different angles of the improvement zone over 50 to 90 degrees, as well as the benchmark model without any improvement. The model configurations are shown in Figure 3.5.2 and Table 3.5.1. All tests simulate a prototype soil deposit of 7.5 m depth and an embankment of 2.5 m height with a 1:2 slope. Case 1 constitutes the benchmark model under the typical condition that an embankment is supported by saturated loose sandy ground without any ground improvement. In Case 2, the vertical SCP improvement zones are placed under the embankment toes, which represents a conventional liquefaction remediation design for the existing embankment. Cases 3 and 4 simulate the improved ground using the new type of SCP method, where the densified improvement zones are constructed at the angles of 60 and 50 degrees within the foundation ground. It should be noted here that the SCP improvement zone modeled in this study is not the same as the real condition of SCP improved ground. As shown in Figure 3.5.1, in the practical design of SCP-improved ground, the interval of SCPs is determined based on the targeted density of the ground, and the extent of SCP improvement will be determined to ensure the stability of the embankment (Harada and Ohbayashi, 2017). In practice, the SCP improvement zone is considered a composite ground consisting of dense SCPs and adjacent soil densified by SCPs. In this study, the SCP improvement zone is modeled by a uniform sand block with a relative density Dr = 90% for easy model preparation. To determine the extent of the SCP improvement zone in the centrifuge experiment, preliminary experiments were conducted. Since this study focuses on the effect of the angle of SCP on mitigating embankment settlement, the extent of the SCP improvement zone is set to be large (5 m at the proto scale) so that the obvious effect can be confirmed.

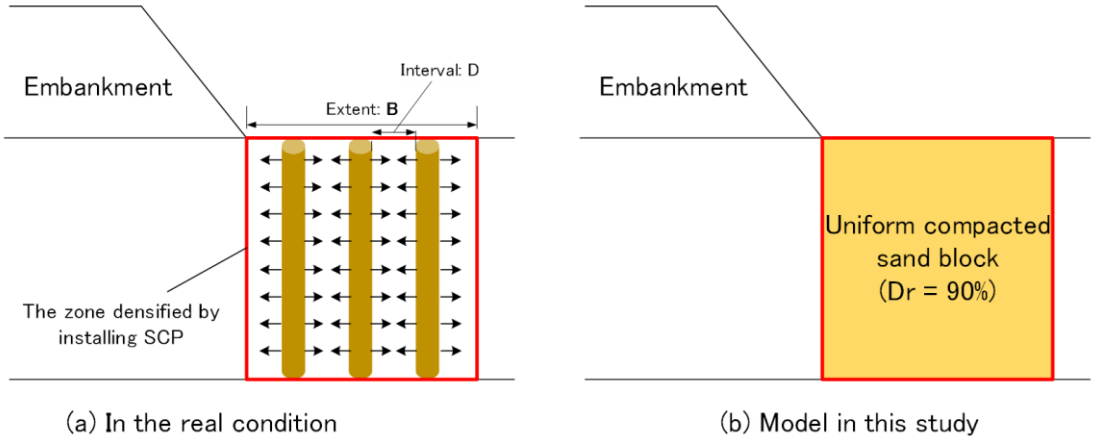

Figure 3.5.1 Simplification of the SCP improvement zone modeled in the centrifuge experiment

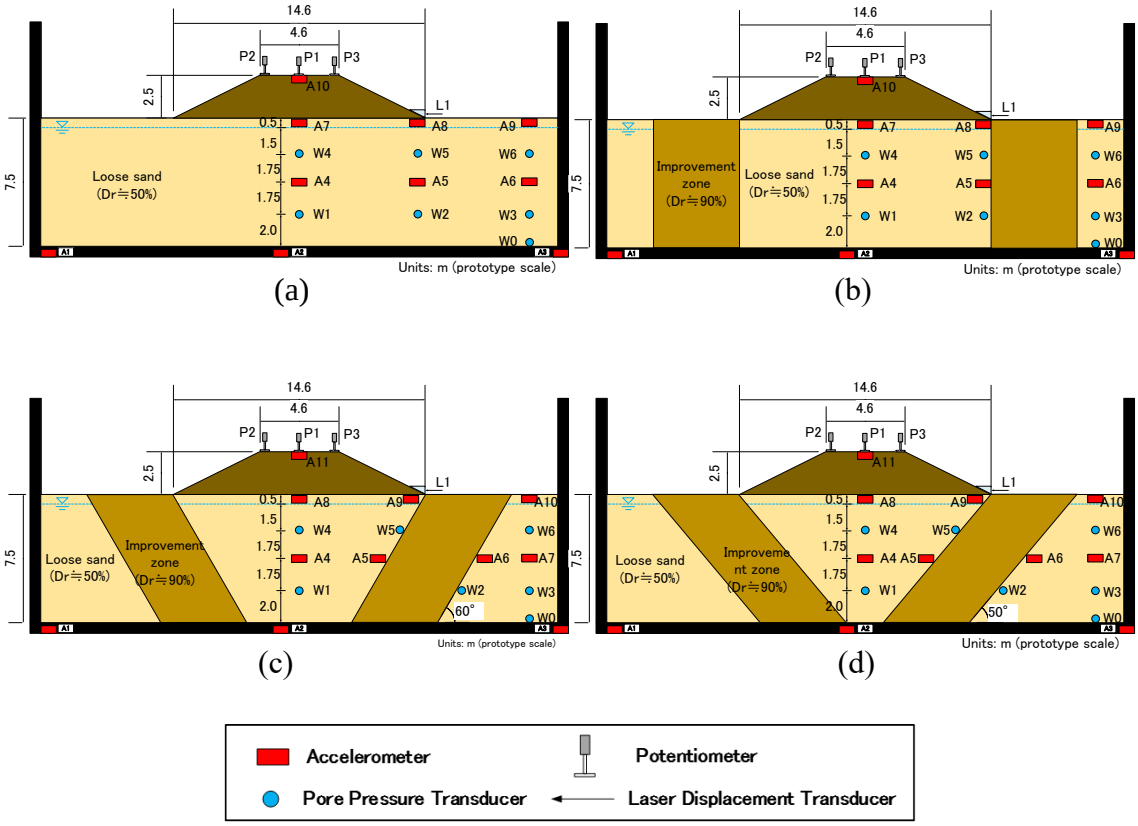

Figure 3.5.2 Model configurations, (a) Case1: unimproved ground, (b) Case2: 90° improvement, (c) Case3: 60° improvement, (d) Case4: 50° improvement

Table 3.5.1 Test condition

Test code	Model description	Relative density (%)		Peak acceleration of input motion (gal)	
		Liquefiable layer	Improvement zone	First shaking	Second shaking
Case1	unimprovement	46.5	-	150	220
Case2	90° improvement	45.3	88.5	140	210
Case3	60° improvement	48.5	88.3	140	220
Case4	50° improvement	49.6	89.2	140	240

3.5.2 Model preparation

A rigid container with inner dimensions of 600×150×400 mm was used in the tests. Front of the rigid container has a transparent window, which enable to observe the model ground in the container during the experiment. Toyoura sand was used in the tests for the foundation and the improvement zone, whose properties is shown in Table 3.5.2.

Table 3.5.2 Index properties of Toyoura sand.

Property	Value
Specific gravity, G_s	2.65
D_{50} (mm)	0.19
D_{10} (mm)	0.14
Maximum void ratio, e_{max}	0.973
Minimum void ratio, e_{min}	0.609
Permeability, k (m/s) at Dr=50%	2×10^{-4}
Permeability, k (m/s) at Dr=90%	1.5×10^{-5}

In Case1, the uniform sand ground was made by air pluviation to the relative density, Dr ≈ 50%. The sand was poured through air from a hopper, while the falling height was kept constant to obtain the desired relative density. In Case2, Case3 and Case4, the improvement zones were made by tamping with 10% water content to Dr ≈ 90% first and then frozen, which models the improvement zone by SCP method. The front window of the container was disassembled and the frozen soil block was placed at predetermined position as shown in Figure 3.5.3. The remained unimproved portions were filled with sand by the sand falling technique to the relative density, Dr ≈ 50%. DL clay, which consists of 90% silt and 10% clay, was mixed with 22% silicon oil by weight to build the embankments, having a unit weight of 18 kN/m3. After the foundation ground was constructed, the embankment was carefully placed on the foundation ground at the desired place. The model ground was saturated with a mixture of water and 2% Metolose (hydroxypropyl methylcellulose) by weight of water, to achieve a viscosity of about 50 times the viscosity of water. The purpose of using Metolose solution is to ensure the compatibility of prototype permeability of the soil and to set up the affinity between dynamic and diffusion scaling laws (Madabhushi, 2014). The de-aired Metolose solution was dripped slowly from the top of the container to the ground surface under vacuum condition, which is continued until the water table reaches up to the top surface of the foundation ground. This saturation process required approximately 48 hours. Refer to Figure 3.5.4 for the detailed preparation procedure for the model ground and embankment.

Accelerometers and pore pressure transducers were installed as shown in Figure 3.5.2, during model preparation to measure the accelerations and excess pore water pressure (△u) generated at three regions representing different stress states: (1) free field, defined as the region which unaffected by the embankment load; (2) under the embankment toe where static shear stress exists; and (3) under the center of embankment where large effective stress exists. Potentiometers were set at the embankment crest to measure the crest settlement during experiment and laser displacement transducer was placed at the embankment toe to measure the horizontal displacement of embankment toe. Spaghetti noodle sticks were installed at predetermined positions between the foundation ground and the glass window of the container. After model saturation, the noodles became soft and acted as markers that were used to map deformation patterns and magnitudes within the foundation ground.

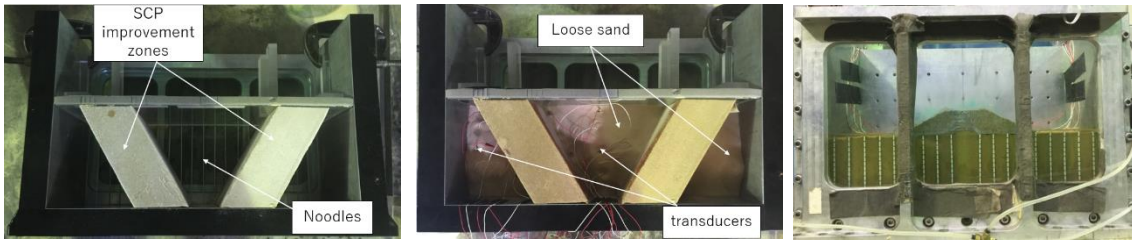

Figure 3.5.3 Photographs of model preparation

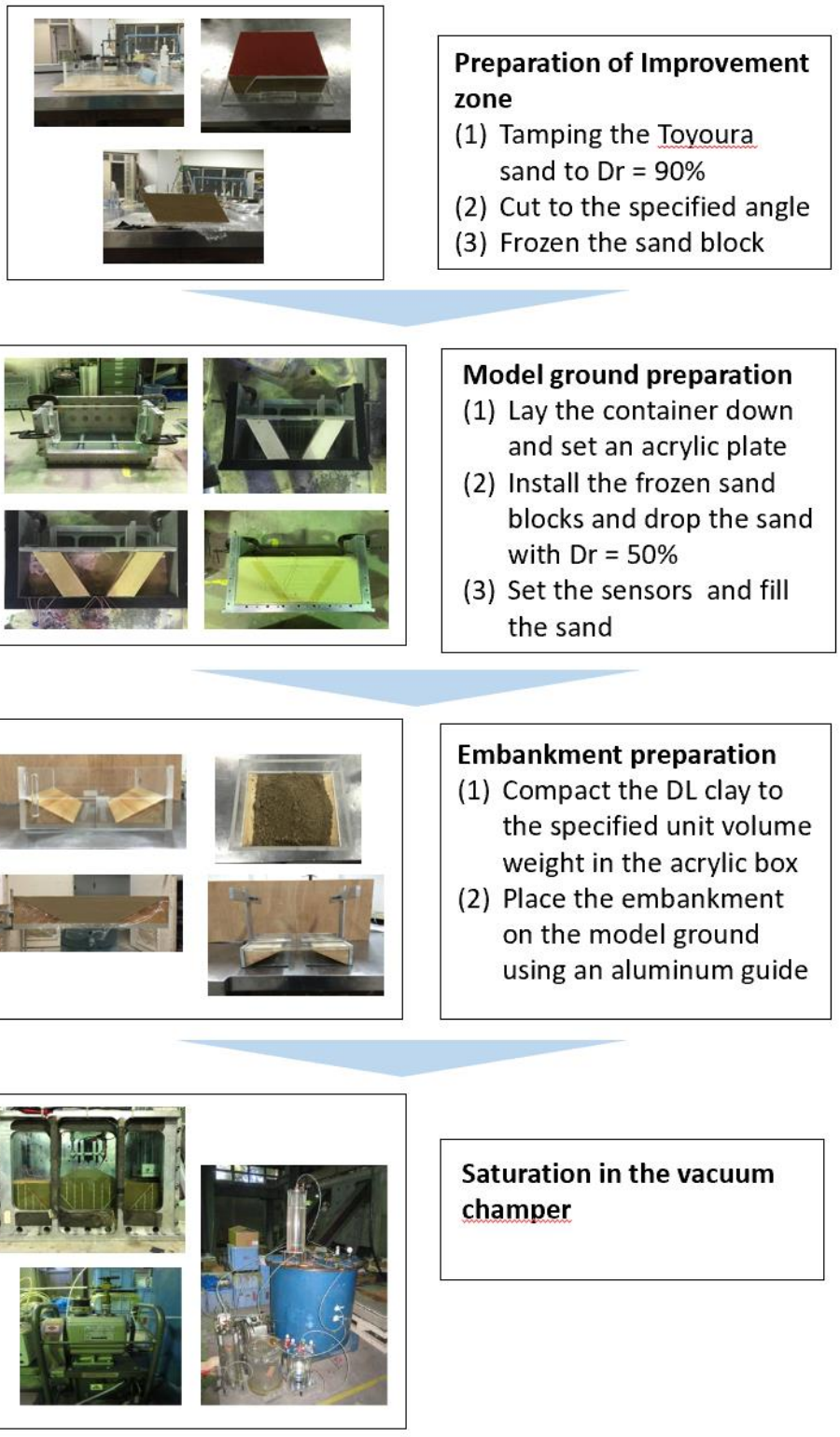

Figure 3.5.4 Procedures of model preparation

3.5.3 Input motions

All the models were subjected to the sinusoidal waves for 2 times with a dominant frequency of 1 Hz, where the acceleration amplitude of first shaking is about 150 gal and that of second one is about 220 gal. Figure 3.5.5 shows the acceleration time histories of input base motions for Case1 and Figure 3.5.6 arias intensities of input base shakings for all cases for comparison. It is recognized from the figures that there is no noticeable difference in input motions between each case. The second shaking was imparted after full dissipation of pore water pressure in the foundation ground. Table 3.5.1 summarizes the model ground conditions and the peak acceleration of input motions in each case. After completion of the tests, each model was carefully inspected to measure the final locations of noodles for mapping the deformed shape.

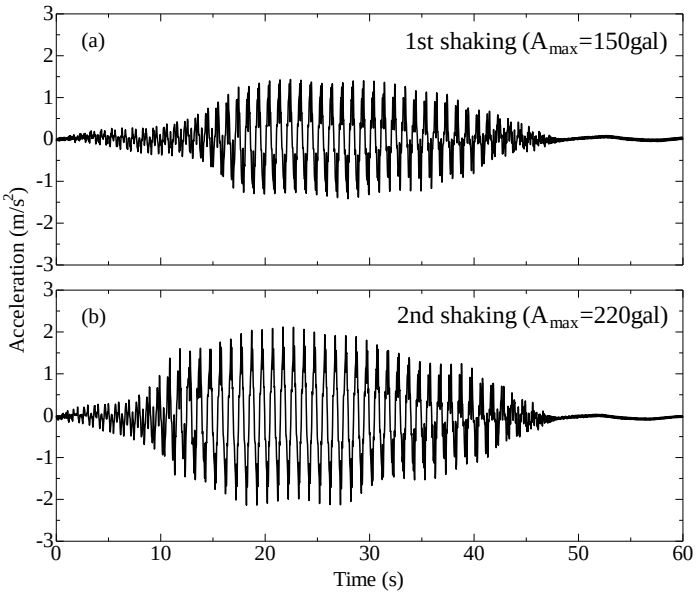

Figure 3.5.5 Acceleration time histories of input base motions for Case1

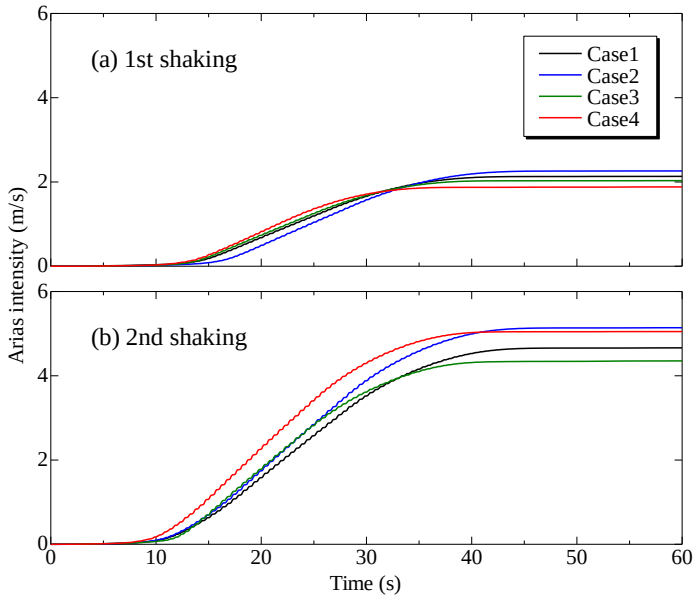

Figure 3.5.6 Arias intensities of input base shakings for all cases

3.6 Test results and discussions

The dynamic response of saturated ground predominantly depends on the generation of excess pore water pressure and the propagation of the seismic wave. In the following, the ground response to the seismic excitations is described and discussed.

3.6.1 Excess pore water pressure and settlement responses

This section presents time histories of the excess pore water pressures and settlement of embankment crest for four cases during the first and second shakings. All the test results shown in the following sections are in the prototype scale unless mentioned otherwise. Excess pore water pressure (EPWP) is measured at several desirable locations as shown in Figure 3.5.2. Evolution of EPWP plays a vital role in the understanding of the liquefaction phenomena. The initial effective vertical stress at the relevant location is plotted with a horizontal dashed line in the figure ($r_u = 1$ lines). The initial vertical effective stresses due to the embankment loading are calculated based on the influence values assuming the foundation ground to be elastic semi-infinite as proposed by Osterberg (1957). Soils at certain depth undergo liquefaction if the excess pore water pressure reaches the initial vertical effective stress ($r_u = 1$ line). The ends of the shakings are indicated with vertical dashed lines in the figures.

The EPWP time histories during the first shaking event of $A_{max} \approx 150$ gal are presented in Figure 3.6.1. In the free field of the benchmark model (Case1), the EPWP at W6 (at a

depth 2.0 m) attains the initial effective vertical stress indicated by r_u=1 line at 25 s after the base shaking starts and that at W3 (at a depth 5.5 m) reaches r_u=1 line at 30 s, corresponding to the condition of sand liquefaction at these regions. These demonstrate the fact that the liquefaction of the sand layer in the free field starting near the ground surface and propagating downward. Under the embankment toe, the EPWP at W5 reaches r_u=1 line at almost the same time with the same depth in the free field (W6). Unfortunately, the pore water pressure transducer W2 did not work correctly because of the EPWP beyond the measurable range from 25 s to 90 s, but it is presumed from measured data that the EPWP at W2 also reaches r_u=1 line at about 30 s, which means liquefaction also occurred under the embankment toes during the first shaking in Case1. Beneath the embankment center, low EPWP is observed at a depth of 2.0 m (W4), with a significant reduction behavior of EPWP during shaking (from about 25s). The EPWP at the deeper portion under the center of the embankment (W1), is generated to the value same as that in the free field at the same depth (W3), but the EPWP does not reach the r_u=1 line. Such lower EPWP values beneath the embankment were also reported by other centrifuge and 1g tests (Koga and Matsuo, 1990; Adalier, Elgamal and Martin, 1998; Mehrzad *et al.*, 2018). The deviatoric stress induced by the embankment surcharge is a beneficial component, which prevents the buildup of EPWP during shaking. Furthermore, the rapid liquefaction in the free field might have reduced the confinement (horizontal effective stress) of the soil below the embankment, leading to the soil below the embankment tends to move laterally away due to large induced shear stress. This mechanism dictates the soil to dilate, resulting in a reduction in the EPWP.

In Case2 improved by 90° angles improvement zones blow the embankment toes, unfortunately, the pore water pressure transducers W3 and W6 indicating the EPWP in the free field did not work correctly because of the EPWP beyond the measurable range from 25 s. However, it is presumed from the measured data that the situation of the free field in Case2 are similar to Case1 in term of liquefaction occurred in those regions. At W5 beneath the embankment toe, similar behavior of EPWP is observed to that in Case1, which indicates liquefaction also occurs below the embankment toes in Case2. Unfortunately, the pore water pressure transducer W2 in Case2 did not work because of some unforeseen reasons and hence are not shown in Figure 3.6.1. Under embankment centerline, the EPWP at deeper portion (W1) is very similar to that in Case1. Whereas, different behavior is observed at the shallower portion beneath the embankment center (W4) between Case2 and Case1. There is no reduction of EPWP at W4 in Case2 during the first shaking. This may be attributed to the smaller horizontal deformation beneath the embankment center due to the confinement of the improvement zones.

On the other hand, quite different responses of EPWP are observed in Case3 and Case4, compared to the above two cases. In Case3 having the inclined improvement zones with 60° angles under the embankment, even though there is no significant difference of the input acceleration between each case (see Figure 3.5.6), the EPWP at W6 in the free field

is generated fast at beginning of shaking, but decreases immediately, though the shaking continues. Similar responses of EPWP are also observed at the deeper portion in the free field (W3), below the embankment toe (W2 and W5) and under the embankment center (W1 and W4). It is not clear about this response of EPWP, but one possible reason is that the pore pressures propagates to the improvement zones very quickly due to large pressure difference between improvement zone and surrounding sand. In Case4, the EPWP at W6 is observed similar to Case1 during shaking, which indicates liquefaction occurred in the free field near the ground surface. Unfortunately, W3 did not work correctly from 25s. Under the embankment toe, at W5, the EPWP starts to increase at the beginning of shaking but decreases immediately as observed in Case3. However, at W2, the high EPWP is generated, which reaches the r_u=1 line, but dissipates immediately during shaking. The EPWP under the embankment center in Case4 is very similar to that observed in Case3.

Settlements measured at the embankment crest (P1, shown in Figure 3.5.2) during the first shaking are shown in Figure 3.6.2. In the benchmark model Case1, the settlement begins with the EPWP increasing within the foundation ground (10-25 s), and that increases rapidly when liquefaction occurs below the embankment toe and in the free field from 25 s (see Figure 3.6.1). A relatively large embankment crest settlement of about 0.38 m is measured. Essentially, almost all of this settlement takes place during shaking. The settlement response in Case2 is very similar to Case1 until 35s during the shaking, due to the similar EPWP responses in Case1 and Case2. In contrast, the settlement rate is decreased from 35 s during shaking, which is considered due to the effectiveness of the vertical improvement zones under the embankment toes for mitigation of lateral displacement of the ground below the embankment, which will be discussed in later section. On the other hand, a significantly small amount of settlements is observed in Case3 and Case4. It is considered that because of the significantly lower EPWP values below the embankment in these two cases, the stiffness of the ground below the embankment in Case3 and Case4 has not degraded significantly during the first shaking.

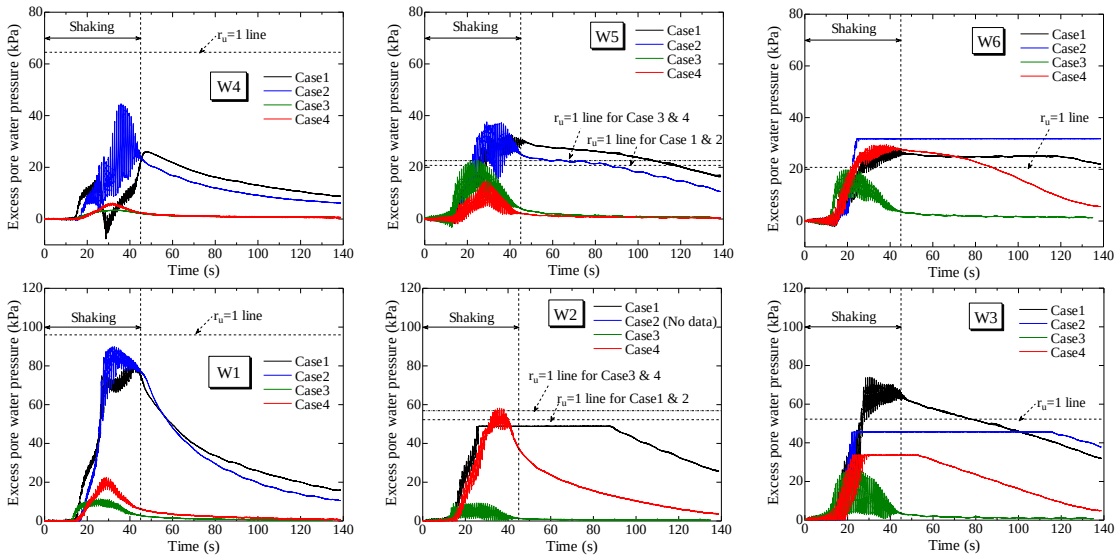

Figure 3.6.1 Excess pore water pressure time histories during first shaking

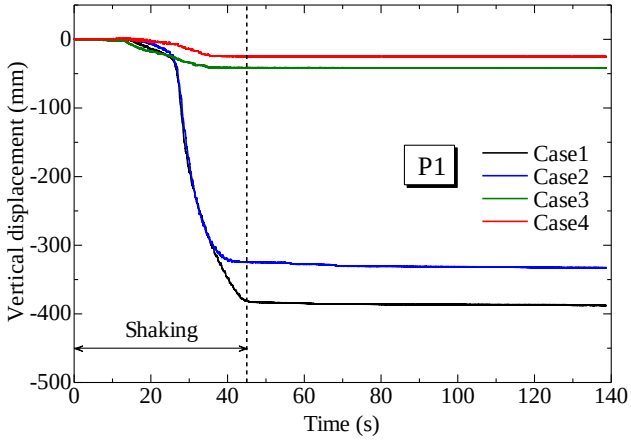

Figure 3.6.2 Settlement time histories of embankment crest during first shaking

Figure 3.6.3 shows the EPWP time histories during the second shaking event of Amax ≈ 220 gal. The responses of EPWP in Case1 and Case2 are almost the same as those during the first shaking, i.e. liquefaction occurs below the embankment toe and in the free field; whereas the soil under the center of the embankment does not reach liquefaction state, but high EPWP is generated at the deeper portion. During the second shaking, in Case3 and Case4, liquefaction occurs below the embankment toe and in the free field, caused by the large cyclic shear stress induced by the larger shaking. It is worth to note that the EPWPs at the deeper portion under the center of the embankment in Case3 and Case4, seem become larger compare to Case1 and Case2. Whereas, the EPWP values at the shallower portion (at W4) in Case3 and Case4 are smaller than those in Case1 and

Case2. It may be because the deeper portion is liquefied during the shaking period, and prevents the waves from propagating upward.

Figure 3.6.4 depicts the settlement time histories of the embankment crest during the second shaking. In herein, it should be noted that the ground conditions of cases are altered due to the first shaking. Particularly, in Case1 and Case2, the density of the soil below the embankment should have become denser in comparison with that before subjected to the first shaking, because of considerable settlement during the first shaking. Also, the gradients of embankment slope in Case1 and Case2 are less in comparison with that before the first shaking, which indicates a reduction in shear stress within the ground induced by the embankment. In Case1, excessive settlement is also observed during the second shaking. In Case2, the settlement starts with a smaller rate in comparison with Case1, when liquefaction occurs within the ground. In Case3 and Case4, less settlement is observed in comparison with Case1, and especially settlement ceases faster in Case4 compared to Case3, which suggests that 50° improvement (Case4) is more effective in mitigating the embankment settlement in comparison with 60° improvement (Case3).

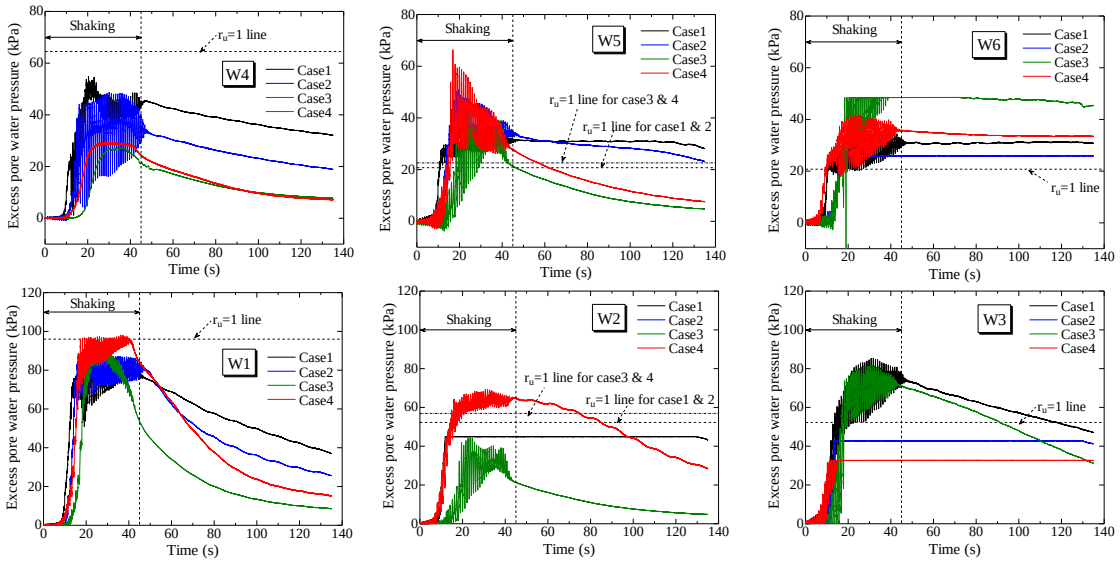

Figure 3.6.3 Excess pore water pressure time histories during second shaking

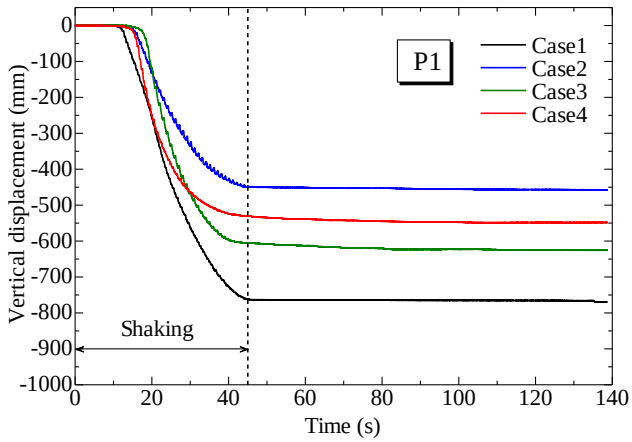

Figure 3.6.4 Settlement time histories of embankment crest during second shaking

3.6.2 Acceleration response

Figure 3.6.5-Figure 3.6.8 show the time history of the response acceleration at the center line of the embankment in each case. It can be seen from the figures that the response acceleration at the center of the ground (A4) and the surface of the ground (A7 or A8) attenuated from 20s. It is considered that this is because the excess pore water pressure in the deep part of the ground reached near the initial effective stress from 20s in all cases, the stiffness of the soil was greatly reduced, and the shaking wave was difficult to propagate upward. On the other hand, it can be seen that the acceleration at the crest of the embankment is amplified until 20s. The amount of amplification is observed to increase as the improvement angle decreases. It is considered that this is because the smaller the angle of the improved body, the larger the improvement rate in the ground below the center of the embankment, which makes it easier for the shaking waves to propagate upward.

Figure 3.6.9 show the maximum accelerations at the embankment crest compared with each case. It is clearly shown in the figure that, the maximum acceleration of embankment crest generated in the improved ground is larger than that in the unimproved ground. Besides, when the improvement angle changes from 90 ° to 60 °, the maximum acceleration at the crest of the embankment increases by about 25%.

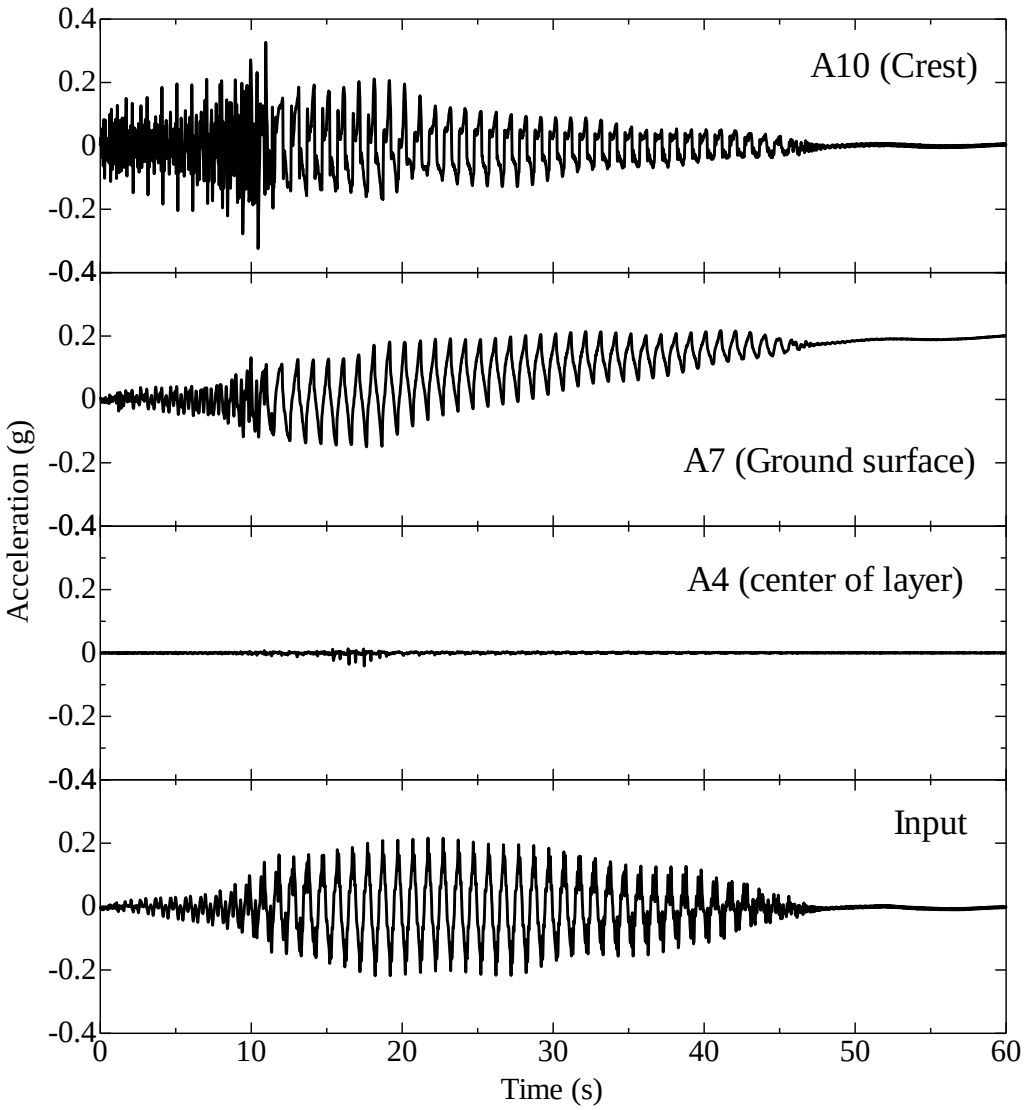

Figure 3.6.5 Acceleration responses in Non-improvement (Case 1)

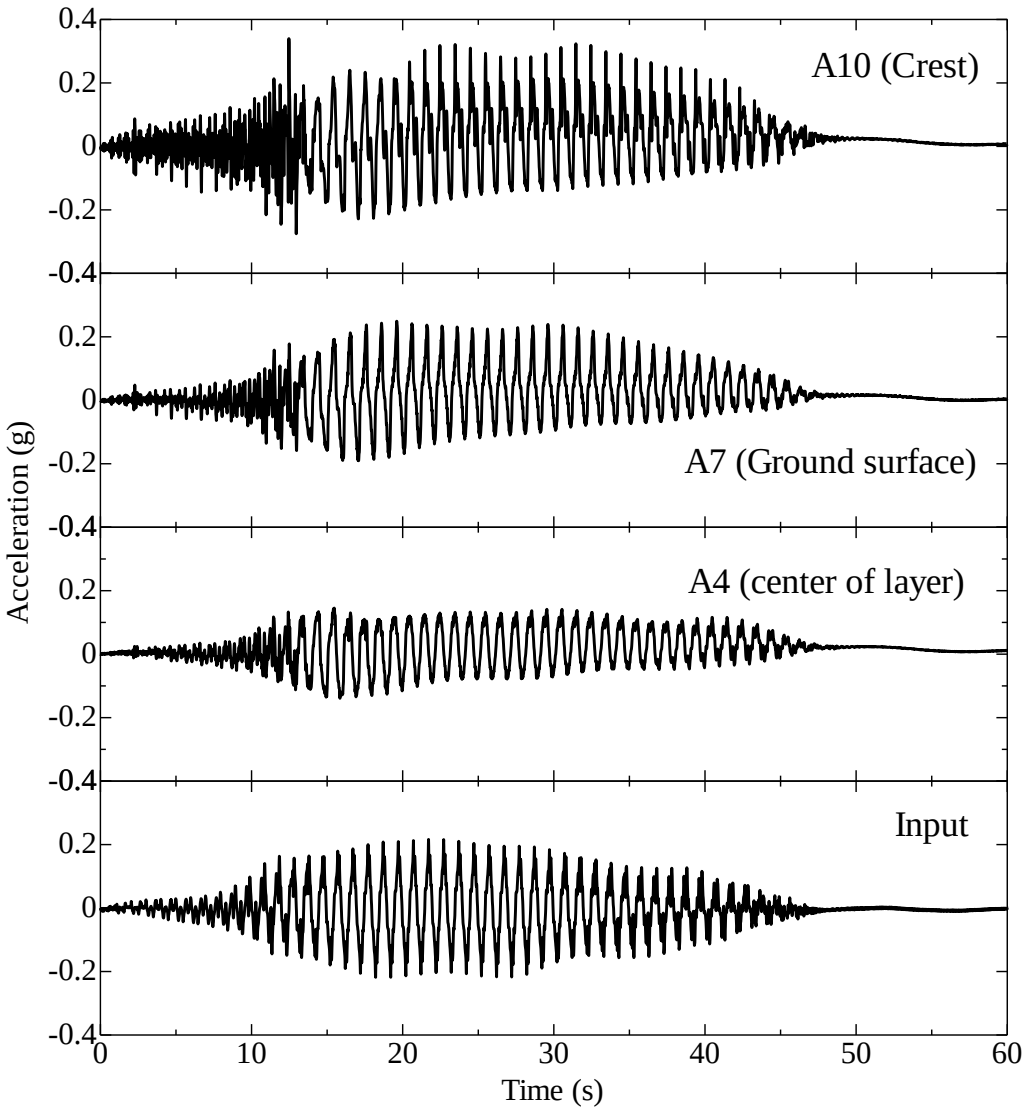

Figure 3.6.6 Acceleration responses in 90° improvement (Case 2)

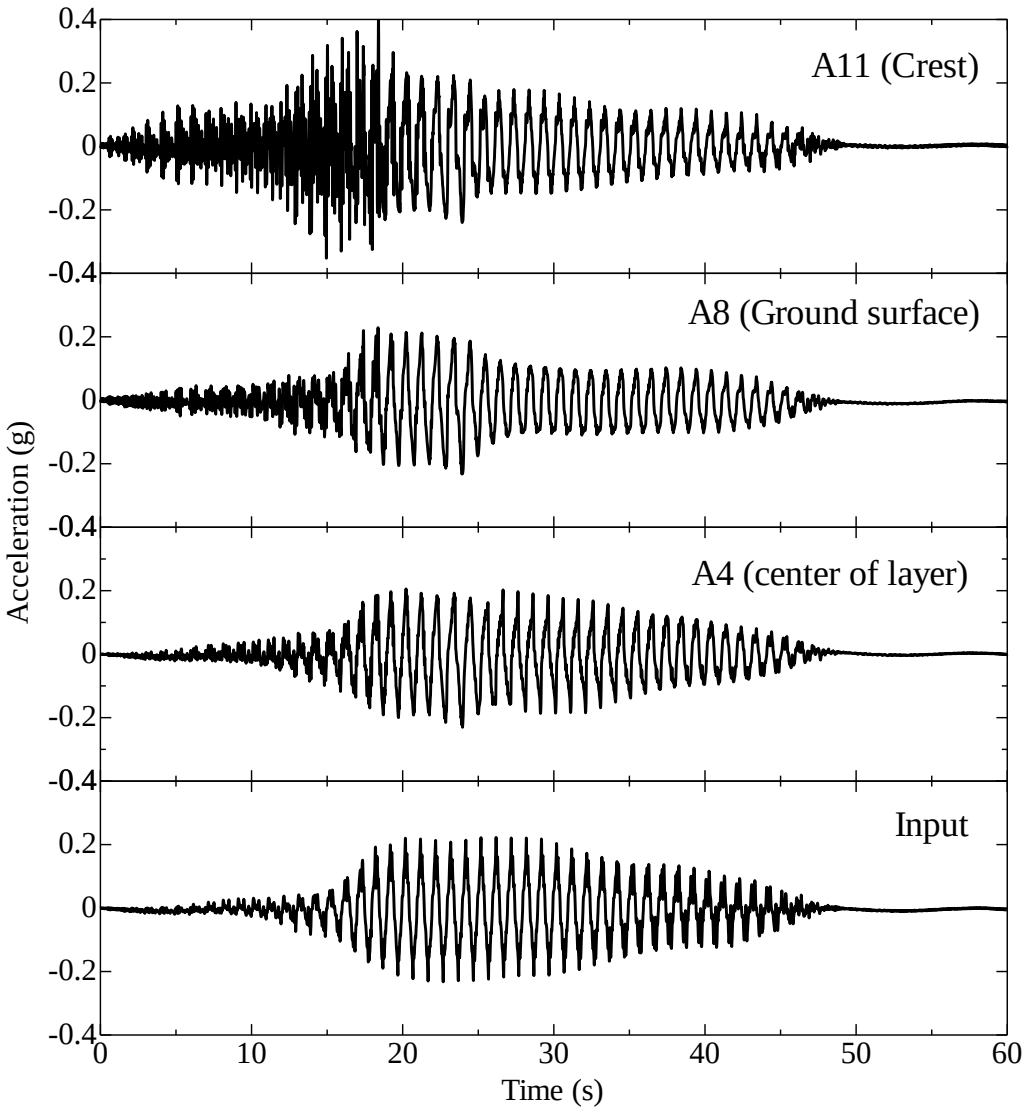

Figure 3.6.7 Acceleration responses in 60° improvement (Case 3)

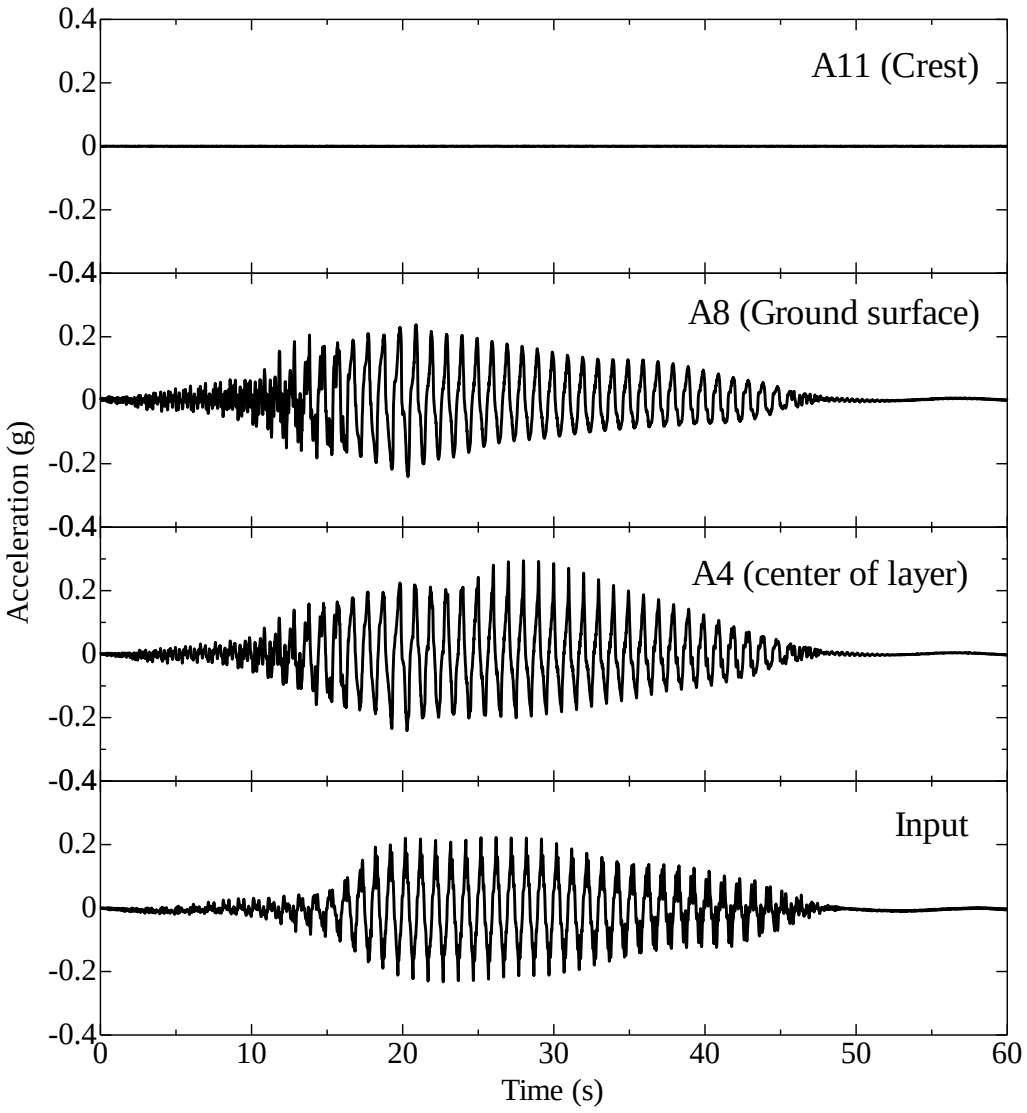

Figure 3.6.8 Acceleration responses in 50° improvement (Case 4)

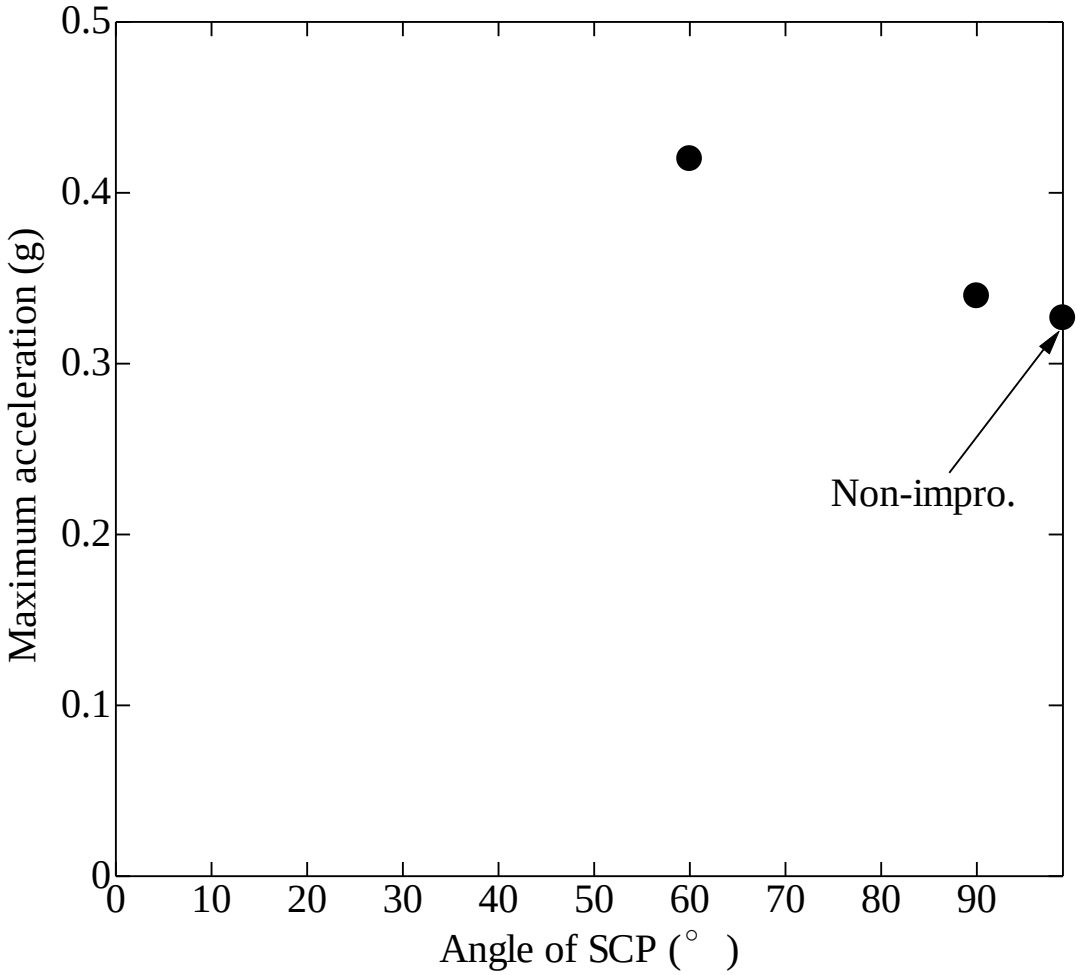

Figure 3.6.9 Maximum accelerations measured at the embankment crest

3.6.3 Distribution of maximum excess pore water pressures under the embankment

Figure 3.6.10 and Figure 3.6.11 illustrate the distribution of the maximum EPWP with depth under embankment center and toe subjected to the first and second shakings, respectively. It should be noted that the maximum EPWP values indicated in these figures, are the monotonic component picked up from the EPWP time histories. The dashed lines in the figure represent the initial vertical effective stress along the depth. These figures are plotted to clarify the extent of liquefaction in different cases during each shaking event. In the first shaking, as shown in Figure 3.6.10, the maximum EPWP values do not reach the initial vertical effective stress under the embankment center in all cases, which means the soil under embankment centerline is not liquefied even though the values of the maximum EPWP is different between each case. The effect of improvement angle on the amount of EPWP values will be discussed later. Beneath the embankment toe, at a depth 2.0 m, the maximum EPWP in Case1 and Case2 reaches the initial effective stress, indicating that liquefaction occurs beneath the toes in these two cases. At the same location, the maximum EPWP values in Case3 and Case4 are below the initial effective stress line, indicating the soils is not liquefied beneath the toes in these two cases during the first shaking.

Figure 3.6.11 shows the maximum EPWP distribution for all cases during the second shaking event (Amax≈220gal). Under the embankment center, the maximum EPWP at deeper portion (at a depth of 5.5 m) tends to be the similar value in all cases, among which the improved ground cases (i.e. Case2, Case3 and Case4) showed more higher EPWPs than the unimproved ground case. At shallower portion (at a depth of 2.0 m), the EPWPs in all cases stay at much lower values than the initial effective stress. Beneath the embankment toe, the soils are considered liquefied irrespective of the ground conditions, because the EPWPs in all cases at this location reaches the initial effective stress.

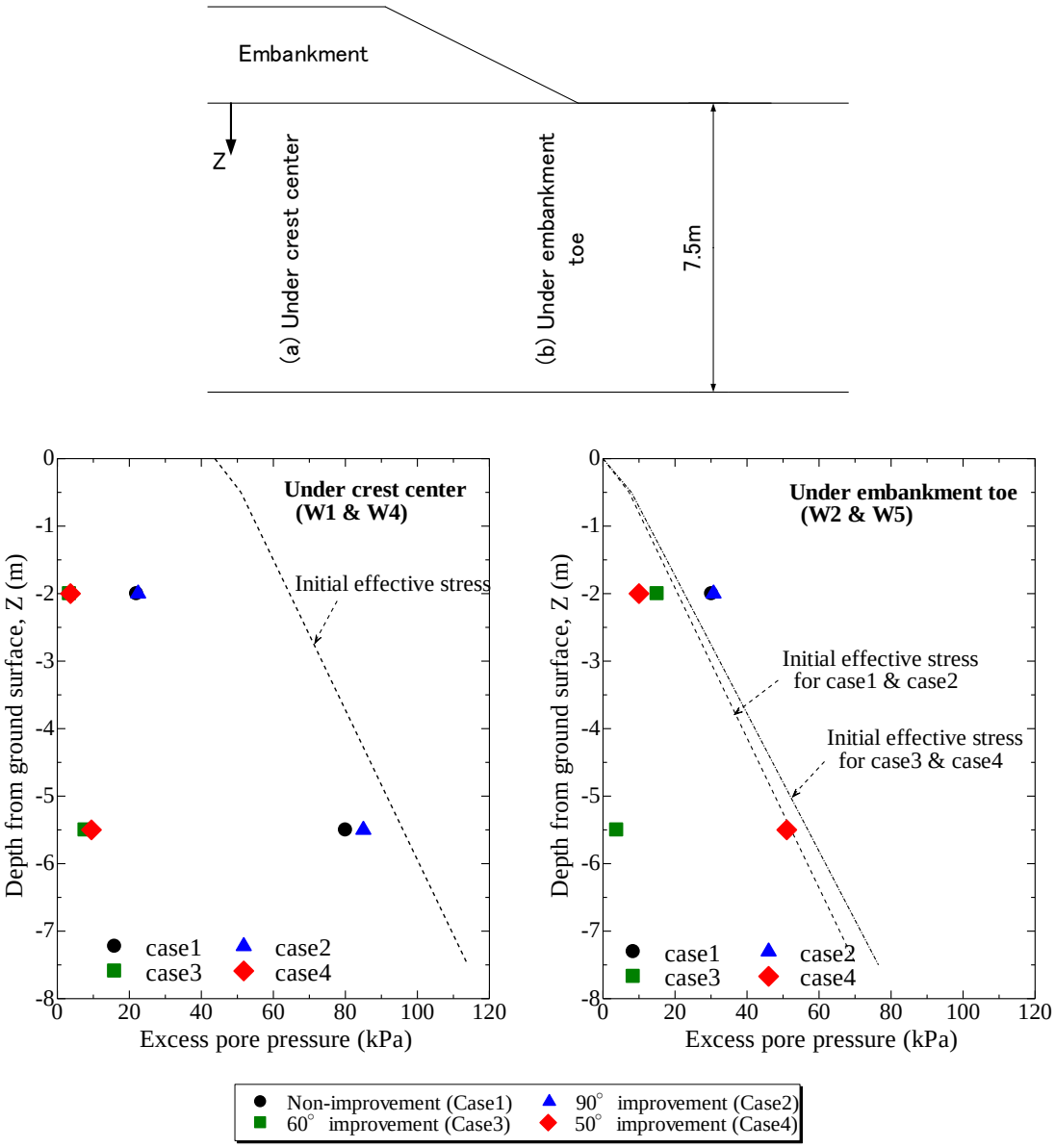

Figure 3.6.10 Maximum excess pore water pressure profiles during first shaking (A_{max}≈150)

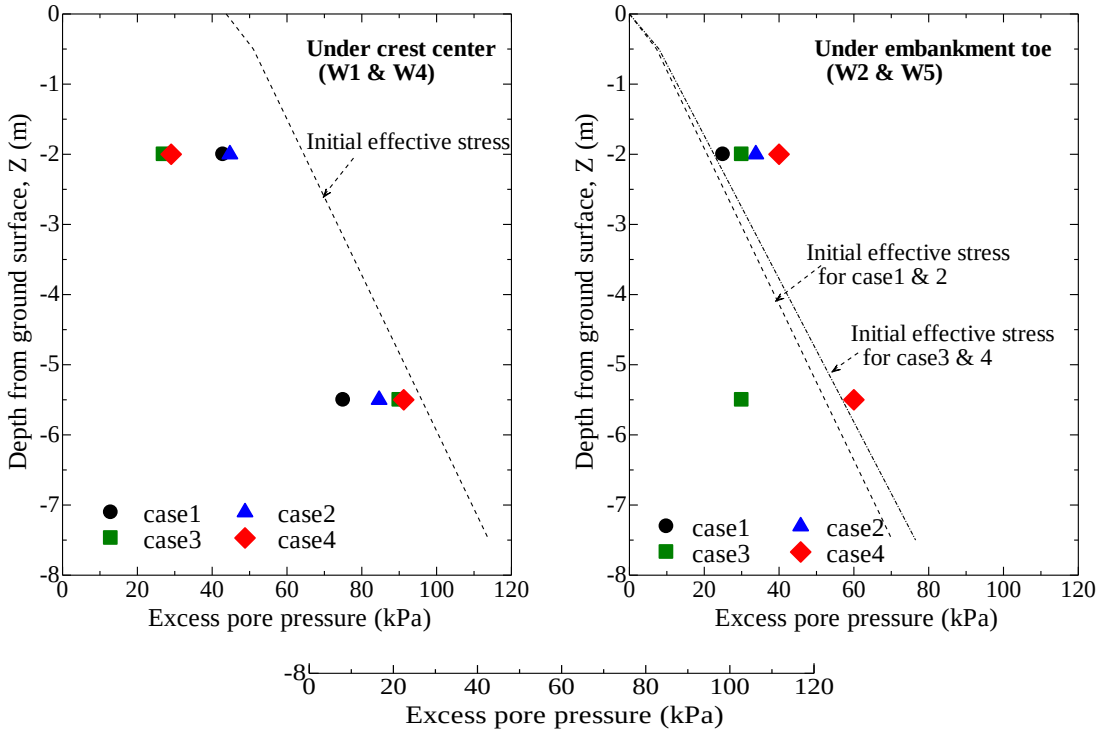

Figure 3.6.11 Maximum excess pore water pressure profiles during second shaking (A_{max}≈220gal)

As mentioned that the EPWP plays a vital role in the liquefaction phenomena and related effects, it is motivated to evaluate the effect of the angle of improvement zone on the generation of EPWP within the ground. In order to achieve that, Figure 3.6.12 depicts the relationship between the angle of the improvement zone and maximum EPWP at the representative locations within the ground subjected to the first and second shakings.

During the first shaking event (see Figure 3.6.12 (a)), the response in the free field seems almost the same irrespective to the angle of the improvement, since the values have no variation along the angle of the improvement zone. Beneath the embankment toe, the maximum EPWPs generated in the cases with 50 and 60 degrees improvement zone are smaller than the cases without improvement and with 90 degrees improvement zone. The same trend is also observed beneath the embankment center (see the black lines in Figure 3.6.12 (a)), especially at the deeper portion below the embankment center, where the EPWP values measured in Case3 and Case4 are approximately 20% of the values measured in Case1 and Case2. Overall, during the first shaking with relative smaller acceleration amplitude, the lower EPWP is observed in Case3 and Case4 when compare to Case1 and Case2, except in the free field.

The results of each case for the second shaking are shown in Figure 3.6.12 (b). In the free field, it seems that there is no relation the angle of the improvement. The similar trend is observed beneath the toe. In other words, there is no significant influence of the degree of improvement zone on the maximum EPWP in the free field and beneath the toe. However, under the embankment center, the maximum EPWP at a deeper portion (at a depth of 5.5 m) is larger in the improvement cases, especially in Case3 and Case4. This trend is the opposite of the situation in the first shaking. At the shallower portion beneath the embankment center, the maximum EPWP generated in Case3 and Case4 is smaller than Case1 and Case2, which is the same trend as that in the first shaking.

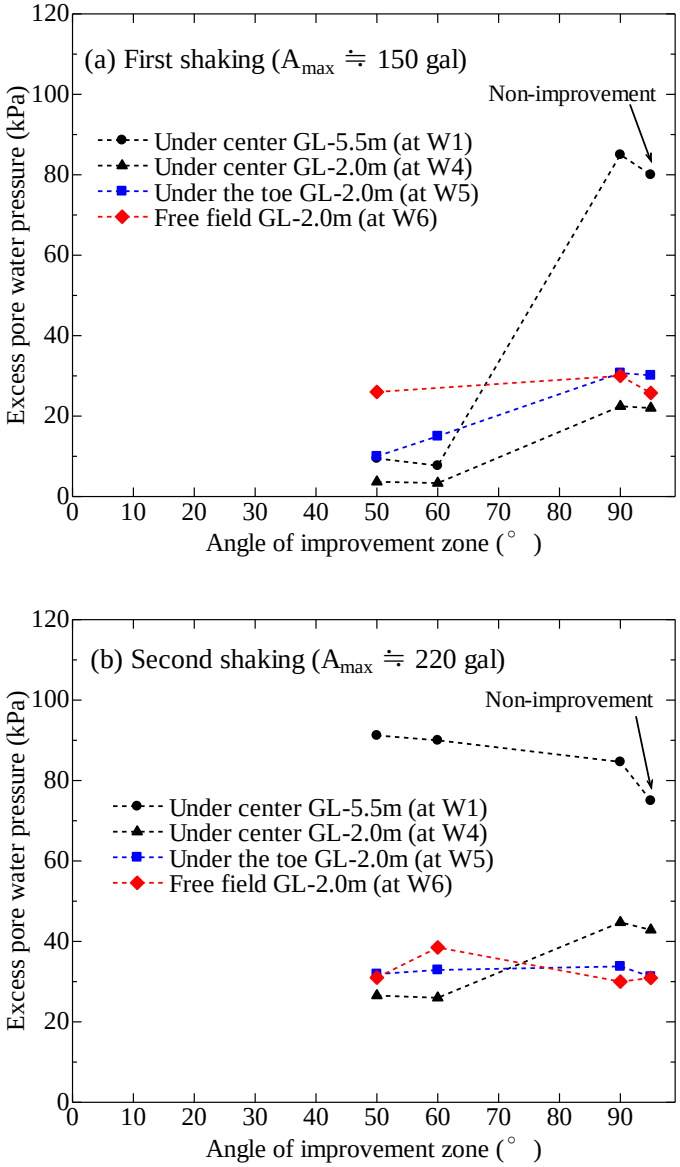

Figure 3.6.12 Relation between angle of improvement zone and maximum EPWP within the ground (at W1, W4, W5 and W6), (a) during first shaking, (b) during second shaking

3.6.4 Lateral displacement beneath embankment toe

As mentioned above, the major cause of the embankment settlement induced by liquefaction of the foundation ground is the lateral displacement of liquefied soil beneath the embankment away from the embankment center. Countermeasures in the remediation program for embankment, therefore, aiming at mitigating crest settlement by providing confinement to the liquefiable foundation soils by forming remediated stiff zones in the liquefiable soil layer under embankment toes. To evaluate the effectiveness of the improvement zone with a different angle, the lateral displacement beneath the embankment toe is discussed in this subsection.

Figure 3.6.13 depicts the lateral displacement distribution beneath the embankment toe after the first and second shakings, respectively. In the figure, the dashed lines present the results after the first shaking and the solid lines present those after the second shaking. It should be noted that the displacement distributions after the second shaking contain the displacement produced during the first shaking.

After the first shaking, the lateral displacement in Case1 is observed with a maximum value of about 0.2 m at a depth of 2.0 m, and decrease toward the ground surface and base. In Case2, the shape of lateral displacement distribution beneath the toe is similar to Case1, but the amount of displacement was mitigated compare to Case1 below a depth of 1.5 m. In Case3 and Case4, the lateral displacements are significantly smaller than the other two cases, which is attributed to the lower EPWP generation during the first shaking (see Figure 3.6.1 and Figure 3.6.10).

After the second shaking, a significant increment of lateral displacement is observed in Case1 at whole depth, especially at a depth from 1.0 to 3.5 m. It might be because the EPWP remains lower at the shallower portion beneath the center of the embankment (see Figure 3.6.10 and Figure 3.6.11), then the soil in that portion do not loss the strength and stiffness significantly. Whereas the EPWP at the deeper portion is high. Then large lateral displacement of sand can be expected below the portion that EPWP remains lower beneath the embankment. A similar deformation mechanism was also reported in other studies (Kawasaki *et al.*, 1998; Ghosh, 2003; Adamidis and Madabhushi, 2017). The lateral displacement in Case2 also increases during the second shaking, due to liquefaction occurred again beneath the toe and in the free field (see Figure 3.6.3), but the amount is smaller than Case1. In Case3 and Case4, the increment of lateral displacements is observed after the second shaking, caused by liquefaction occurred during the second shaking. It is noted that even though high EPWP is generated at the deeper portion below the embankment during the second shaking (see Figure 3.6.11), the lateral displacement at the deeper portion seems mitigated more effectively in Case3 and Case4, compared to the cases without improvement and with 90 degrees improvement zone.

From the above results, it is suggested that the main mechanism responsible for the settlement of the embankment is the form of soil softening due to decreased in effective stresses (generation of EPWP) in the foundation ground, permitting the vertical compression to accompany the lateral displacement. In this study, the ground improved by 50°angles improvement zones shows the most effective for mitigating the lateral displacement.

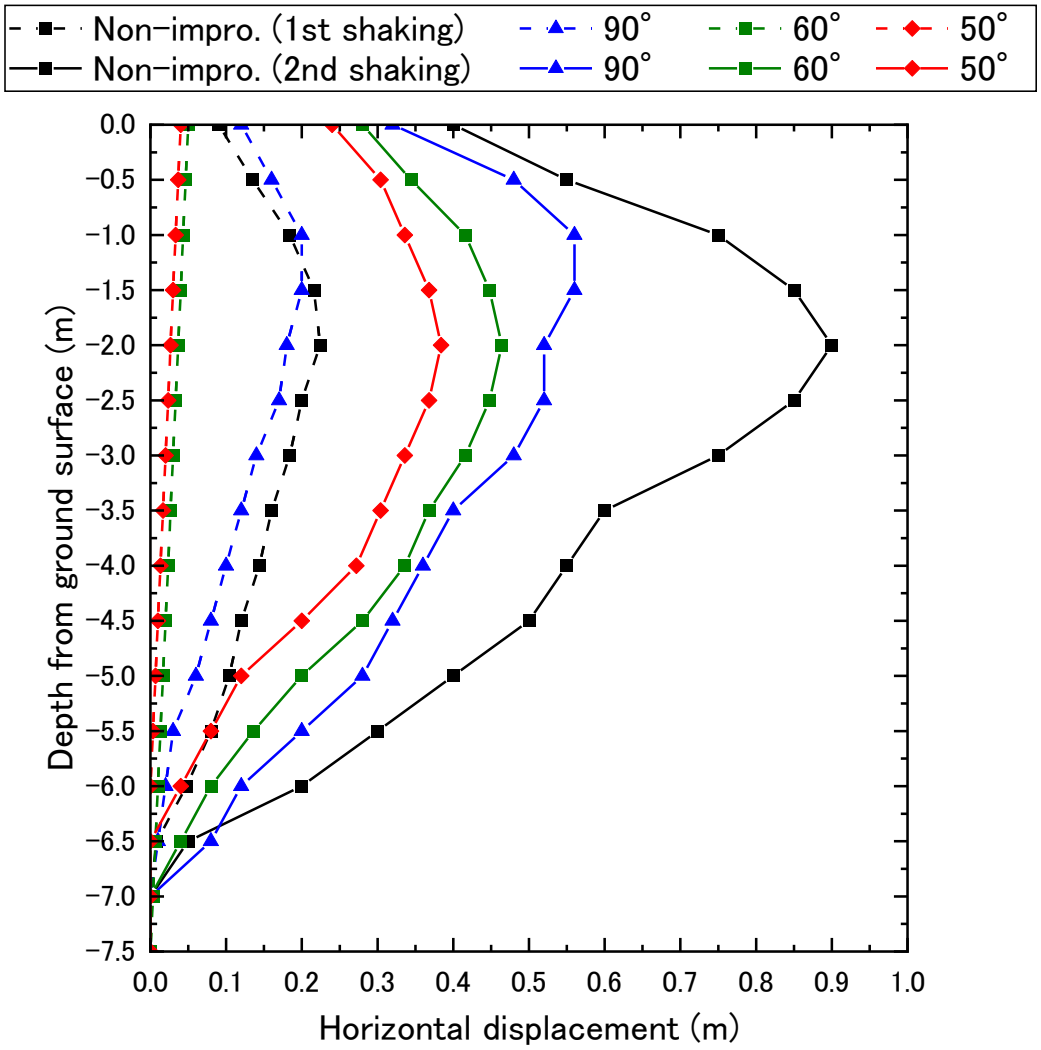

Figure 3.6.13 Lateral displacement beneath embankment toe (after first and second shaking)

To evaluate the effect of different improvement angle on mitigating lateral displacement quantitatively, the area of the lateral displacement distribution along the depth (i.e. the amount of the laterally deformed soil) is calculated from the distribution. Figure 3.6.14 presents the relationship between the angle of SCP improvement zone and area of lateral displacement. During the first shaking, the overall lateral displacement in Case3 and Case4 is significantly smaller than Case1 and Case2, due to much lower EPWP generated

in Case3 and Case4, compare to the other two cases (see Figure 3.6.12 (a)). During the second shaking, in all cases, the amount of total lateral displacement is more than that after the first shaking. It might due to the liquefaction state sustained a longer time than the first shaking (see Figure 3.6.1 and Figure 3.6.3). Overall, it can be seen from Figure 3.6.14 that the effectiveness of the inclined improvement zone on mitigating lateral displacement is confirmed. Among them, the improvement with 50° angle case shows the best performance.

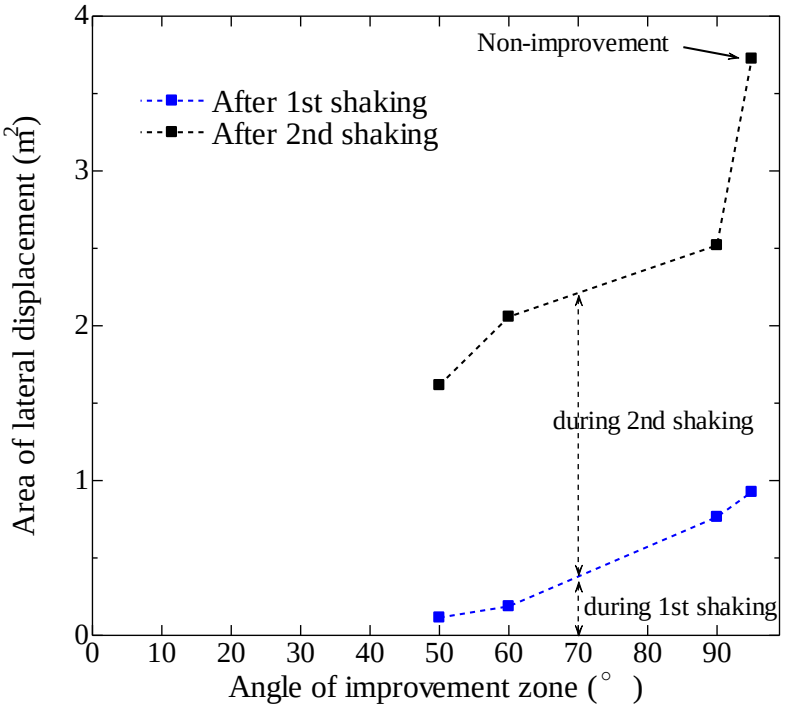

Figure 3.6.14 Relationship between angle of SCP remedial zone and area of lateral deformation

3.6.5 Settlement beneath embankment

Since the condition of the foundation ground during shaking is nearly undrained, the amount of lateral displacement is presumably equal to the amount of settlement after shaking if the densification of the ground is minimal. Several centrifuge tests (e.g. Adalier, Elgamal and Martin (1998)) as well as shaking table tests at 1g (e.g. Nasu, Fujisawa and Hikimoto (1987)) have been conducted to explore the effectiveness of remedial countermeasures beneath embankment toes for reducing crest settlement. The above-referenced studies showed that embankment crest settlement after shaking was greater than half of the settlement in the case without countermeasure, though the lateral displacements beneath the toes were significantly mitigated with a countermeasure. One

reason for this is that the embankment settlement contains the shaking-induced compression of the embankment itself. To eliminate this component from the embankment settlement, comparison of the settlement below the embankment is also useful.

Figure 3.6.15 depicts the settlement distribution at the embankment bottom after the first and second shakings, respectively. In the figure, the dashed lines present the results after the first shaking and the solid lines present that after the second shaking, respectively. In Case1, the bottom of the embankment is overall settles, where the largest settlement occurred under the crest and decrease toward the toe both for the first and second shakings. In Case2, the difference compared to Case1 is that the soil shows upward heave near the toe. It might be that the lateral displacement constraint is imposed by the vertical improvement zone, resulting in formations of a low strength exit path near the toes where liquefaction occurred (see Figure 3.6.10 and Figure 3.6.11). This deformation pattern would lead to an increase in the settlement under the crest. The same observation was also reported by the other centrifuge tests (e.g. Okamura and Matsuo (2002); Rasouli, Towhata and Akima (2016)). In Case3, the soil beneath the toe also heaves but smaller than Case2. In Case4, no significant heave deformation near the toe is observed. It might be due to that as the presence of stiff improvement zone below the toes, the volume of the deformable soil below the toes become less. Tis effect should be significant in Case4 as there is a larger improvement area below the toes.

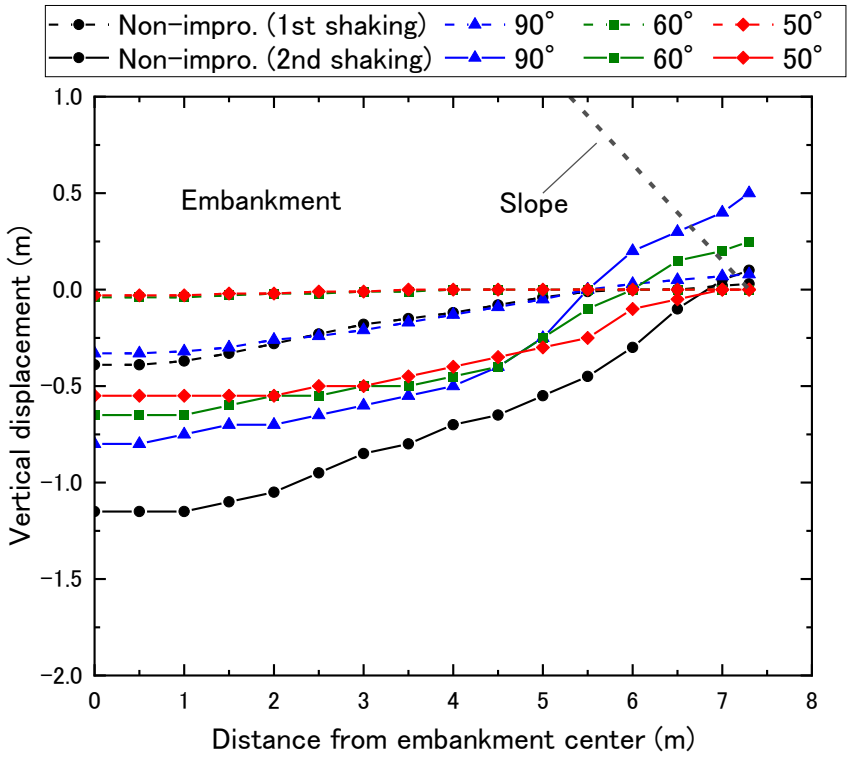

Figure 3.6.15 Vertical displacement of the ground under embankment

3.6.6 Settlement of embankment crest

Figure 3.6.16 plots the vertical displacement of embankment crest (P1 shown in Figure 3.5.2) against the angle of the improvement zone, for immediately after the first and second shakings, as well as the settlement due to the dissipation of EPWP after shaking. In every shaking event, the difference between settlement immediately after shaking and that after dissipation of EPWP is very small, which demonstrates that the main settlement occurs during shaking.

In Figure 3.6.16, the shape of the lines is very similar to that shown in Figure 3.6.14, which indicates the relationship between the angle of the improvement zone and area of lateral displacement has a one-to-one relationship. It is verified that there is a strong correlation between the lateral displacement beneath the toes and settlement of embankment. Also, it is suggested that the improvement conditions that can mitigate lateral displacement more effective, are also effective in mitigating the embankment settlement. It is clear from Figure 3.6.16 that all improvement cases show the effectiveness of mitigating embankment crest settlement. Among them, Case4 improved by 50° angle is the most effective in mitigating the settlement, which is considered as the lateral displacement beneath the toes is most mitigated in comparison with other cases.

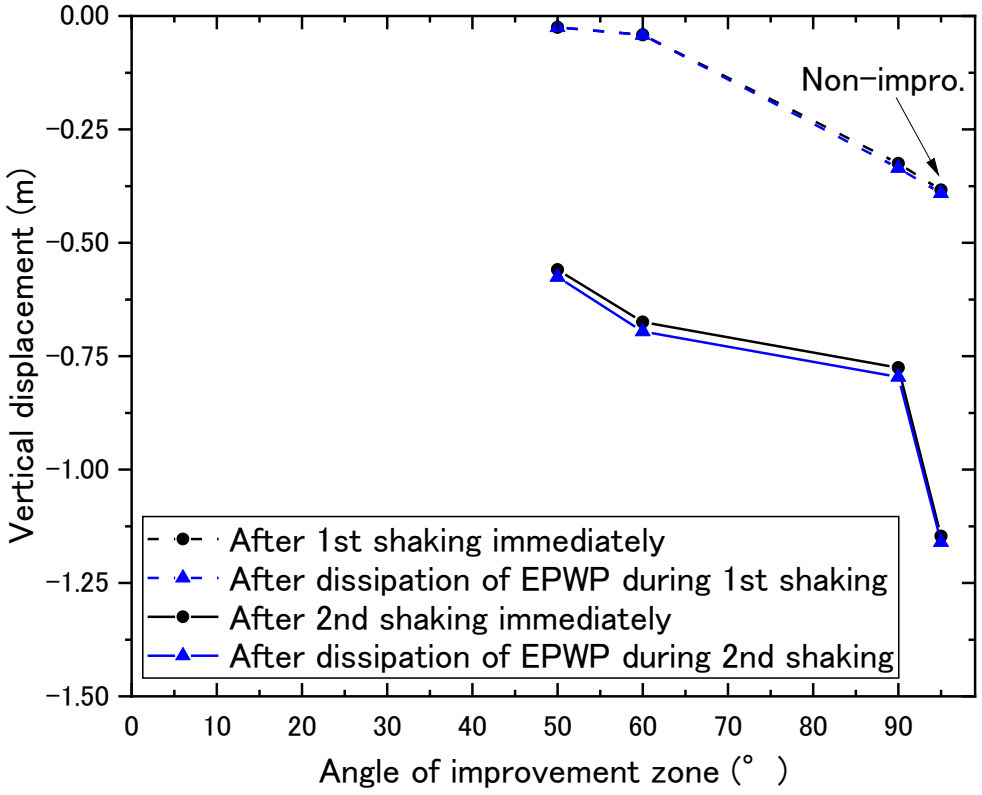

Figure 3.6.16 Relationship between angle of SCP remedial zone and vertical displacement

3.7 Summary

A series of dynamic centrifuge tests are carried out to investigate the effects of the angle of SCP improvement zone on mitigating liquefaction-induced settlement of embankment crest. The following major conclusions are drawn from the test results:

(1) The excess pore water pressure (EPWP) responses in the ground are influenced by the angle of the improvement zone. During the small shaking (150gal), the maximum EPWP under the embankment center and near the toe in case of 60° and 50° improvement zones is less in comparison with the unimprovement case and 90° improvement case. During the larger shaking (220gal), the maximum EPWP under the embankment center at deep layer tends to become higher values in cases of 60° and 50° improvement zones in comparison with the unimprovement case and 90° improvement case. At a shallower portion of the foundation ground under the embankment center, the trend of the maximum EPWP is similar to that during the small shaking, but there is a marginal difference between cases under the toe.

(2) It is confirmed that the lateral displacement beneath the embankment toes is mitigated by the presence of the improvement zone installed in the foundation ground. Especially, the case with 50° improvement zone is the most effective and contributes to the less settlement of the embankment.

(3) The deformation pattern of the soil below the embankment toe is also important for the mitigation of crest settlement. In the case with 90° improvement zone, relatively larger heave is observed beneath the embankment toe, whereas in the 60° and 50° improvement cases, such heave deformation near the toe is suppressed. Since this heave deformation beneath the toe makes the crest settlement larger, it is suggested that in addition to lateral displacement beneath the embankment toe, the deformability of the soil under the embankment toe is also important for mitigating the crest settlement of embankment.

Chapter 4

Numerical analyses on behavior of SCP improved ground with various geometries

The computational simulations are presented in this chapter for a series of centrifuge test described in chapter 3. Numerical method can not only consider almost all the factors influencing the response of embankment and foundation ground during an earthquake, but also be an efficient way to find effective mitigation to solve this problem. The numerical analysis is performed in this chapter for two main purposes: (i) to investigate the behavior of an embankment and foundation ground during an earthquake more detailed when the ground is improved by SCP with different geometric shapes; (ii) to validate the numerical model used in this study, prior to conducting a parametric study for other factors (i.e., wider angle and width of SCP improvement zone).

4.1 Finite element modeling assumption

Two dimensional finite element analyses were conducted under the plain strain condition(Takahashi, 2002). The constitutive model, extended sub-loading surface model proposed by Hashiguchi and Chen (1998), was adopted for the soil layers.

4.1.1 Numerical model mesh

The centrifuge model tests as described in Chapter 3 were numerically simulated. The finite element meshes used in these numerical analyses for Case1, Case2 and Case4 are designed with Model-1, Model-2 and Model-3, respectively, as shown in Figure 4.1.1. All input conditions (i.e., the dimension of model, the soil conditions and input motion) are set as much as possible in the same way as in the experiment, but only the width was set to 80 m to eliminate the influence of boundary conditions. The whole domain is divided into a number of uniform meshes, where all elements are set to a size of 0.5 m × 0.5 m, which is validated that the influence of element size is basically negligible.

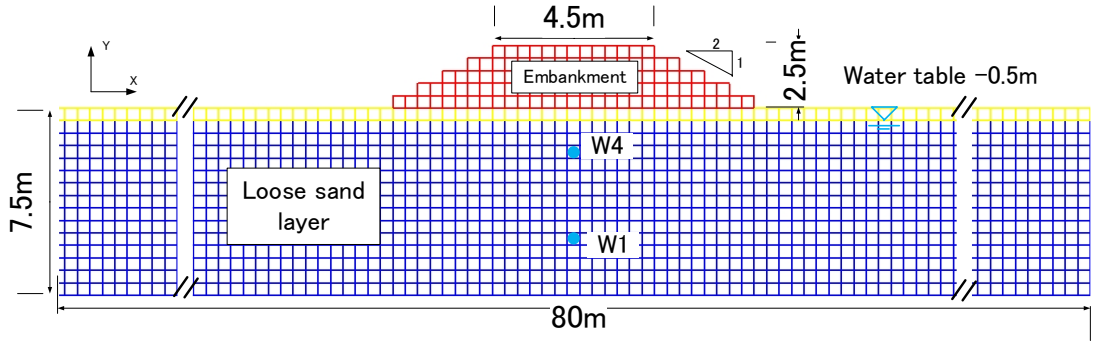

(a) Model-1: Non-improvement case

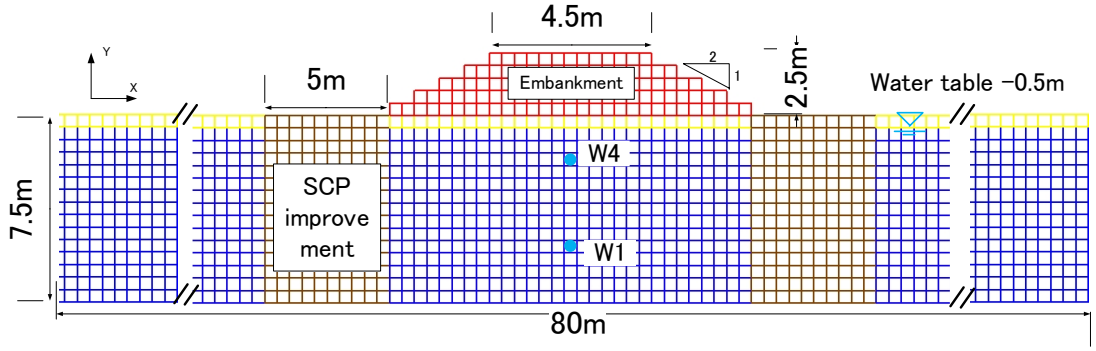

(b) Model-2: 90° improvement case

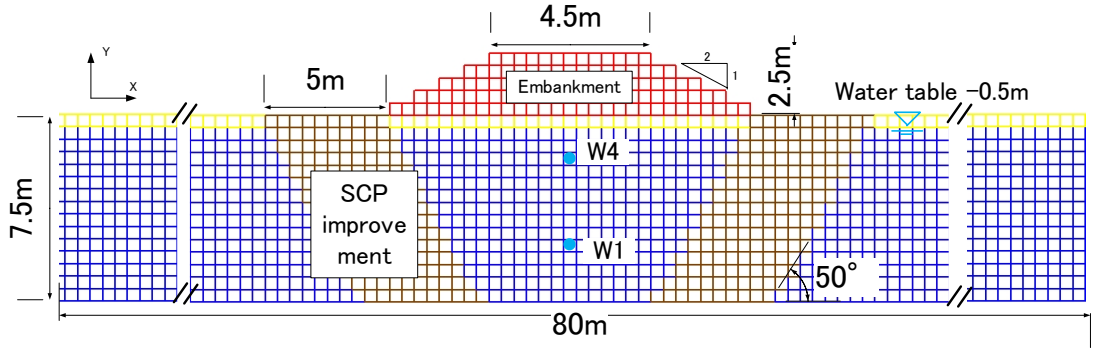

(c) Model-3: 50° improvement case

Figure 4.1.1 Numerical model mesh

4.1.2 Description of material parameters

The analysis model consists of embankment, loose sand layer and SCP improvement zones, and the values of the material parameters used in the analysis for each part are summarized in Table 4.1.1. For the loose sand layer, the relative density (Dr = 50%) is decided with reference to the conditions of the centrifugal model experiment that described in Chapter 3, and then the void ratio (e_0) and soil particle specific gravity (G_s) are determined. The values of the slope of the swelling curve κ and the slope of the normal compression curve λ are decided with reference to the experimental results (Fukushima and Tatsuoka, 1984). The coefficient of earth pressure K_0 was set as 0.5 for loose sand layer, and was set as 0.7 for SCP improvement zone to consider the K_0 effect due to the installation of SCP, irrespective of vertical and diagonal improvement cases. For other parameters, individual values were set so as to approach the results of the triaxial liquefaction test of Toyoura sand (Toki *et al.*, 1986). The liquefaction resistance curve is a relation between the ratio of the cyclic shear stress to the initial confining stress and the number of loading cycles required to cause shear strain of 5% in the double amplitude. As shown in Figure 4.1.2, the liquefaction strength curve obtained from the numerical simulation of the undrained cyclic triaxial compression test and the experimental result are almost the same for the liquefaction layer.

Table 4.1.1: Soil parameters for numerical analysis.

Param.	Loose sand layer (Dr=50%)	SCP improvement (Dr=90%)	Embankment	Description
κ	0.0013	0.00036	0.02	Isotropic normal consolidation and swelling curves.
λ	0.0072	0.0042	0.16	
e_0	0.791	0.642	0.8	Void ratio
ν	0.33	0.28	0.3	Shear modulus.
G_s	2.65	2.65	2.675	
φ	40°	50°	50°	Shape of sub-loading surface.
φ_d	25°	25°	25°	Undrained stress path and phase transformation line.
μ	0.9	0.24	1.8	
φ_b	30°	30°	40°	Rate and range of the evolution of anisotropic hardening
b_r	100	100	70	

u_1	4	9	9	Approaching rate to normal yield state.
m_1	1	1.8	1.8	
c	30	4.5	25	Width of hysteresis loop.
k(m/s)	0.0002	0.00015	0.0000002	Coefficient of permeability
OCR	1	5	1.6	Over consolidation ratio
S_{ij0}/σ_{ij0}	0.2	0.02	0.3	Shape of hysteresis loop.
K_0	0.5	0.7	0.7	Coefficient of earth pressure at rest

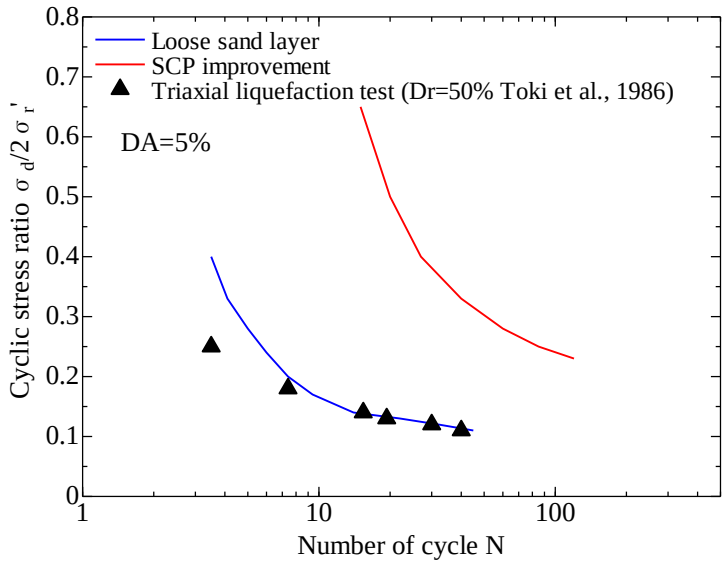

Figure 4.1.2 Comparison of experimental and numerical liquefaction resistance curve

4.1.3 Boundary condition and input motion

As the mechanical boundary conditions of the analysis model, the displacement in the horizontal direction is fixed and the displacement in the vertical direction is free on both sides of the ground. In addition, the bottom of the foundation ground is fixed so that it does not displace in both the horizontal and vertical directions. Next, the hydraulic boundary conditions are set to impermeable conditions on both sides and bottom of the ground. These boundary conditions are summarized in Table 4.1.2.

Before the dynamic response analysis, a static analysis is conducted to estimate the initial stress condition of the ground. In this study, a simple two-step loading of gravity is adopted in the static analysis to estimate the stress condition before the earthquake: in the first step, a stress analysis is conducted with the assumption that a deformation modulus of each soil is uniform irrespective of the confining pressure. Then, in the second step, the stress analysis is carried out with the stress-dependent deformation modulus using the stress condition obtained in the first step.

Acceleration time history recorded by an accelerometer that is attached to the base of the container during the centrifuge test is used in this analysis as an input ground motion. The input ground motion is shown in Figure 4.1.3.

Table 4.1.2 Boundary conditions

Mechanical boundary condition		Hydraulic boundary condition	
Both sides	Bottom	Both sides	Bottom
X: fixed Y: free	X, Y: fixed	impermeable	impermeable

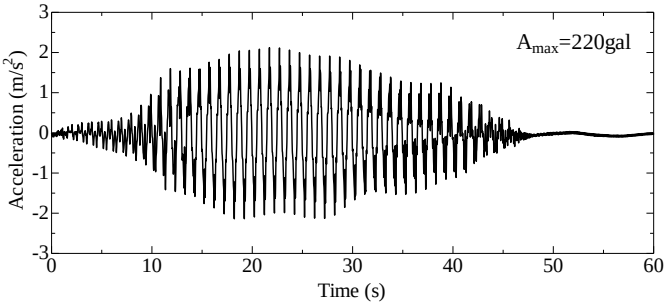

Figure 4.1.3 Input motion for numerical analysis

4.2 Numerical analysis results and discussions

4.2.1 Comparison of numerical and experimental results

In order to confirm the accuracy of the numerical tool used in this study, a validation is conducted through comparing the results of the numerical analyses and the centrifuge model experiments. Figure 4.2.1 - Figure 4.2.3 show the numerically computed and experimentally measured excess pore water pressure time histories at different depths within the liquefiable layer and the vertical displacement at embankment crest for each case. In these figures, black solid lines represent the responses in the centrifuge experiments, and red dashed lines represent the responses in the numerical analyses. However, what is compared here is the result of the second shaking with a maximum amplitude of 220 gal in the experiment.

For the unimprovement case (Model-1) as shown in Figure 4.2.1, the excess pore water pressure (E.P.W.P) responses measured in centrifuge test are captured well in terms of value and pattern, especially a complex behavior occurred at W4 beneath the embankment. At W4 beneath the embankment, as a complicated excess pore water pressure behavior, at first, the excess pore water pressure increased with shaking, but then changed to a downward behavior and then increased again. This response is captured well by the numerical analysis. In non-improvement case (Model-1), the excess pore water pressure under the embankment center at W4 initially increased (0-10s) and consequently decreased (10-15s), and then rise again. As shown in Figure 4.2.4, the decrease of excess pore water pressures during shaking may be attributed to a mechanism that the shear-induced dilation caused by the ground settlement. Ground shaking leads to the development of permanent vertical compressive and horizontal tensile strains, $\varepsilon_v \fallingdotseq 1\%$ and $\varepsilon_h \fallingdotseq -1\%$, respectively, or else to a permanent deviatoric strain of $\varepsilon_v - \varepsilon_h \fallingdotseq 2\%$. This deviatoric strain is sufficient to cause dilation of the sand and produce negative EPWP.

There is a discrepancy in the timing of the start of the rise in excess pore water pressure. The numerical results represented by red dashed lines in the Figures show a quick development of excess pore water pressure. Whereas, in experiment results, the generation of major excess pore water pressure starts after 10 s of shaking. Compared with the centrifuge experiment, the excess pore water pressures increased faster in the numerical analysis. This discrepancy is also seen in Model-2 and Model-3 as shown in Figure 4.2.2 and Figure 4.2.3. In actual soil behavior, it is considered that there is a shear strain threshold value for the occurrence of excess pore water pressure. The amplitude of acceleration in the first 10s of the input motion wave is small. Therefore, it is considered that no significant excess pore water pressure was generated in the experiment until 10 s, because the shear strain generated in the ground does not exceed the threshold. On the

other hand, in the analysis, excess pore water pressure is generated even for small shaking, which is considered to have caused the difference.

The numerical and experimental responses of the vertical displacement at embankment crest during shaking are also compared in Figure 4.2.1 - Figure 4.2.3. Numerical simulations underestimated vertical displacement at the crest during shakings. Dashti *et al.* (2010) identified volumetric strains due to sedimentation and drainage during cyclic loading as a primarily reason for settlement. Flow and loss of water that cause volumetric strains in soil may be significant during shaking because (1) the hydraulic conductivity of soil may increase drastically (Shahir *et al.*, 2012) when approaching a liquefied state ($r_u \approx 0.8 – 1.0$); and (2) hydraulic gradients are kept at their peak during the time of strong shaking while large excess pore water pressures are continuously being generated. The constitutive model incorporated in this numerical analysis is pressure-dependent, meaning that it can capture the loss of shear or volumetric stiffness as the effective stress decreases due to excess pore pressure generation. The vertical displacement in the numerical analyses are underestimated, partly because a constant value of hydraulic conductivity is used in the numerical simulations throughout the entire time history. The value of hydraulic conductivity assumed during shaking is expected to influence the total value of volumetric strain not just its rate, because during this time excess pore water pressures are continuously generated as they dissipate, and hydraulic gradients are kept at their peak. As a result, the model underestimated the flow velocity and the resulting volumetric strains during the time of shaking. However, if we focus on the magnitude relationship of the final settlement amount among the three cases, we can see that the characteristics are captured in the analysis.

Figure 4.2.5 - Figure 4.2.7 show the response acceleration of each case along with the experimental values. The analysis roughly captured the response acceleration in the ground, but did not capture the attenuation of acceleration well. As a result, the response acceleration at the embankment crest were greatly estimated in the numerical analyses.

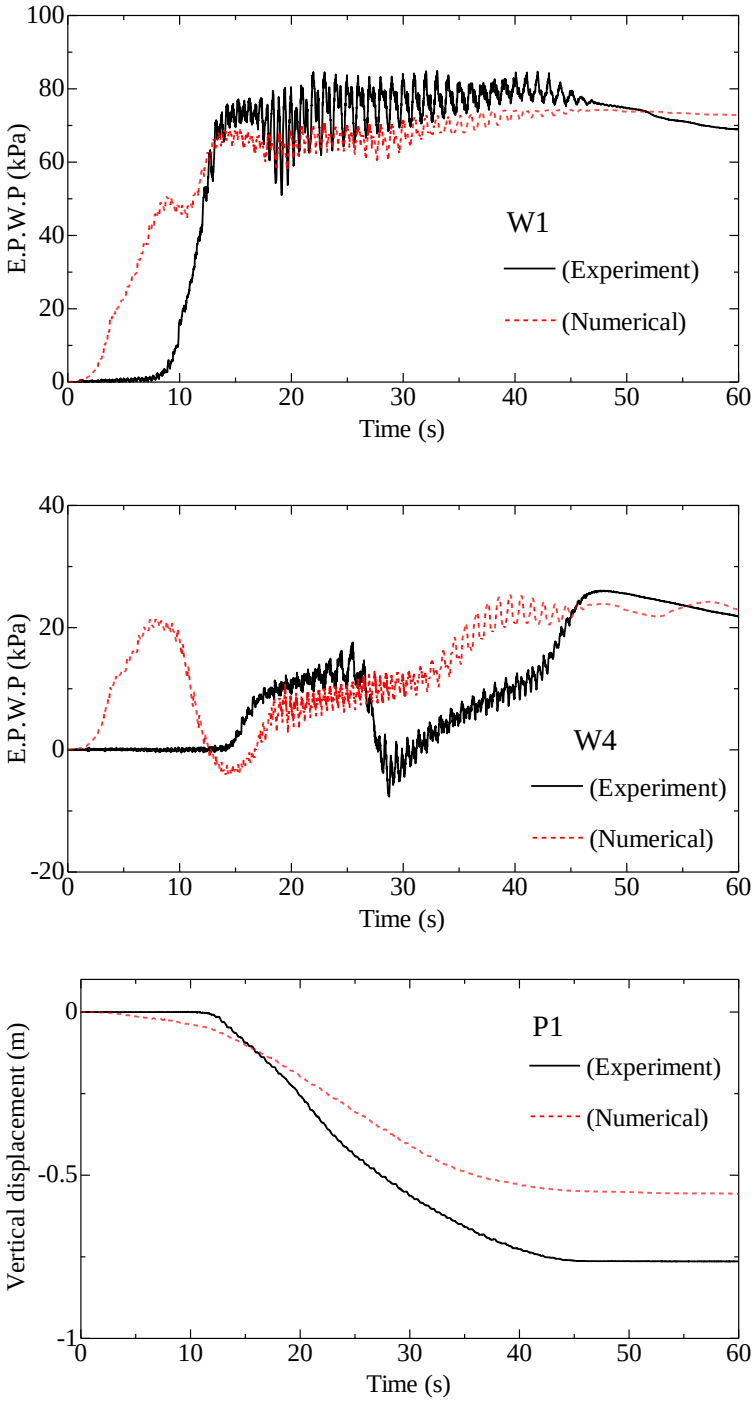

Figure 4.2.1 Excess pore water pressure time histories at W1 & W4 and vertical displacement at crest for Model-1 (Non-improvement)

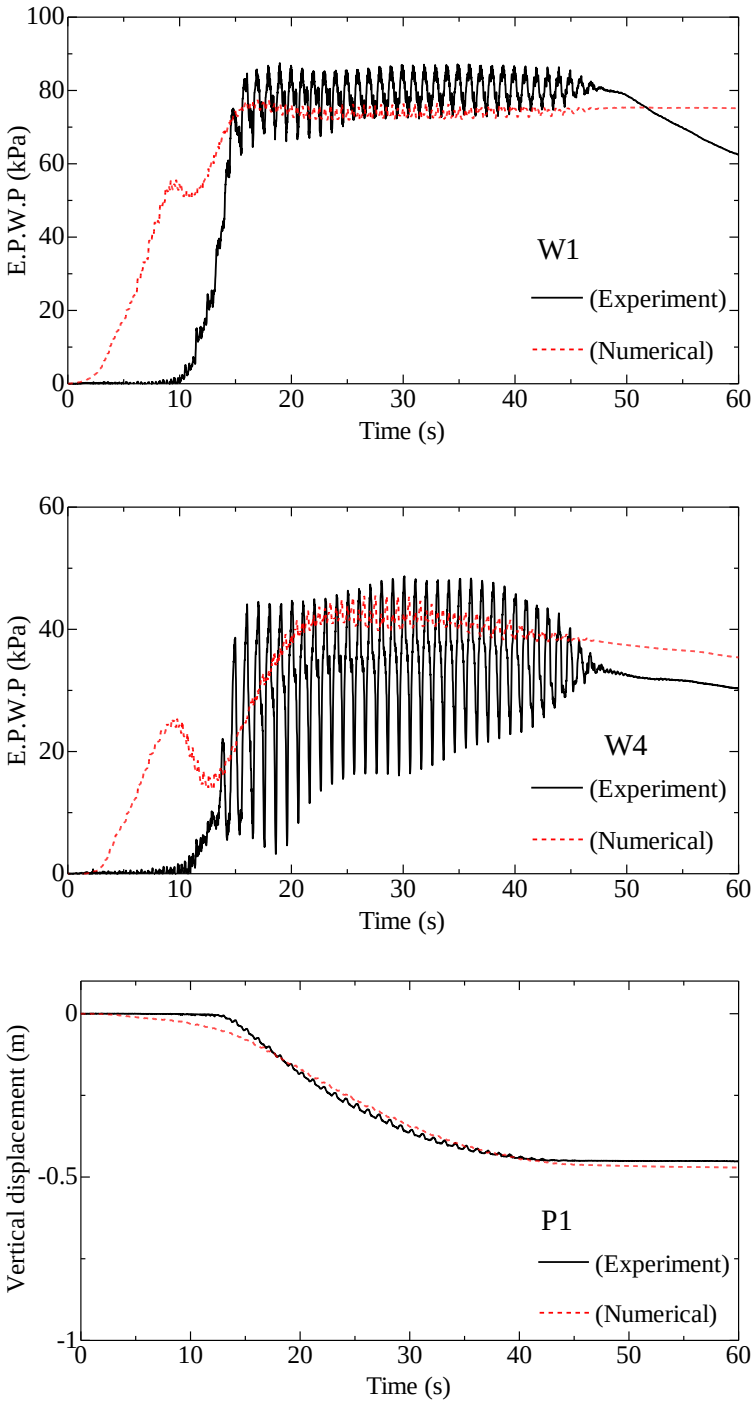

Figure 4.2.2 Excess pore water pressure time histories at W1 & W4 and vertical displacement at crest for Model-2 (90° improvement)

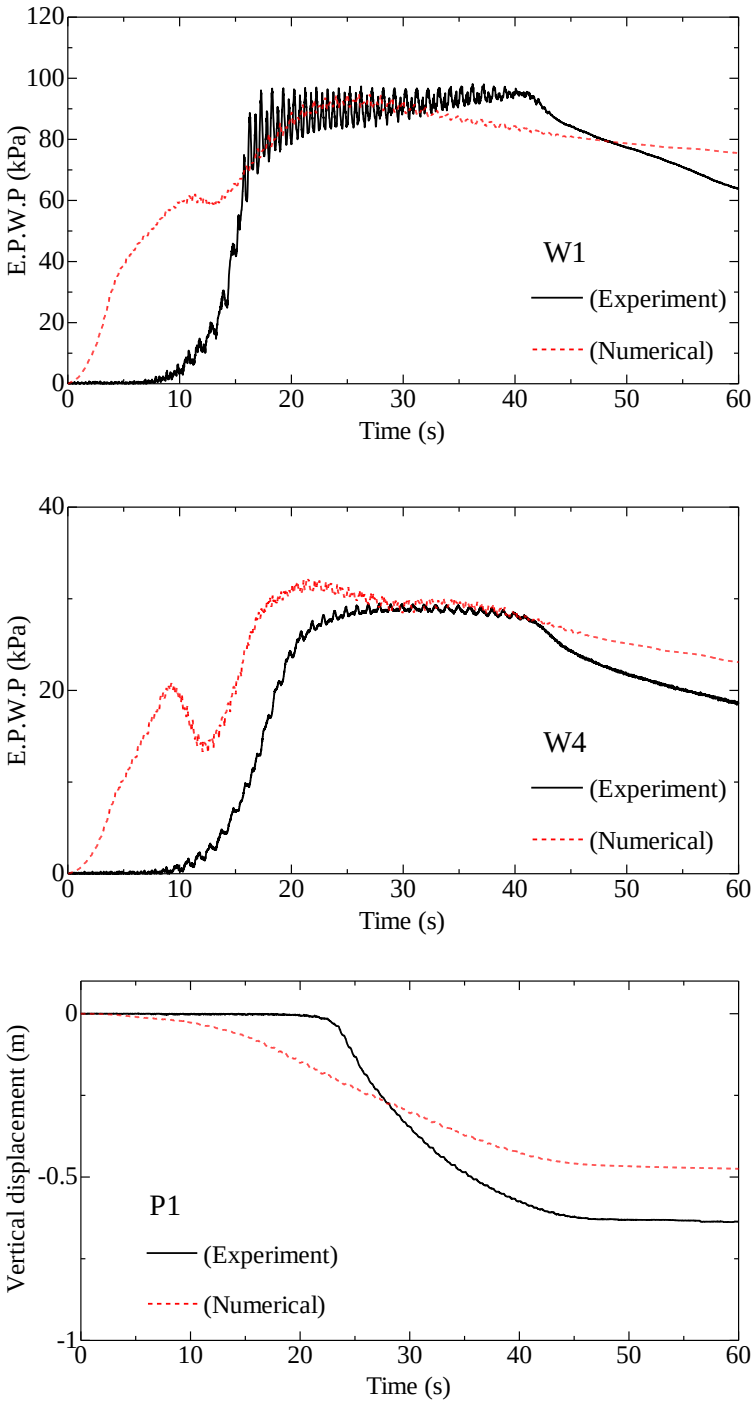

Figure 4.2.3 Excess pore water pressure time histories at W1 & W4 and vertical displacement at crest for Model-2 (50° improvement)

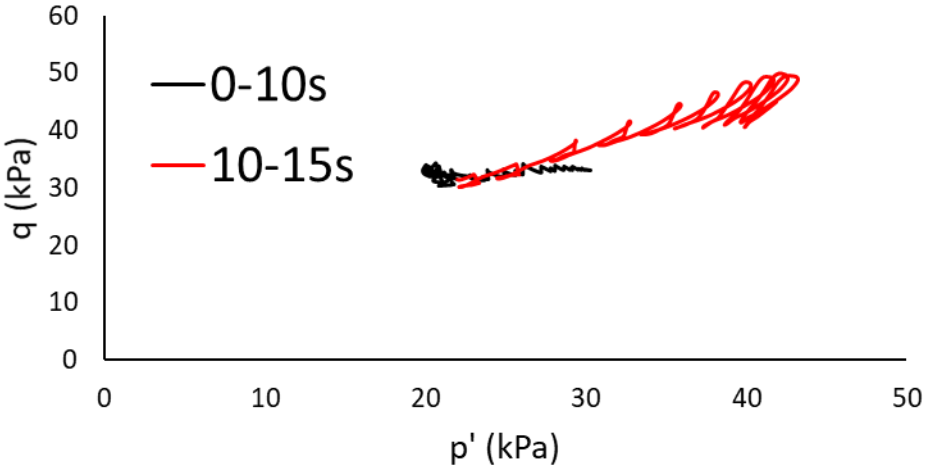

(a) Effective stress path

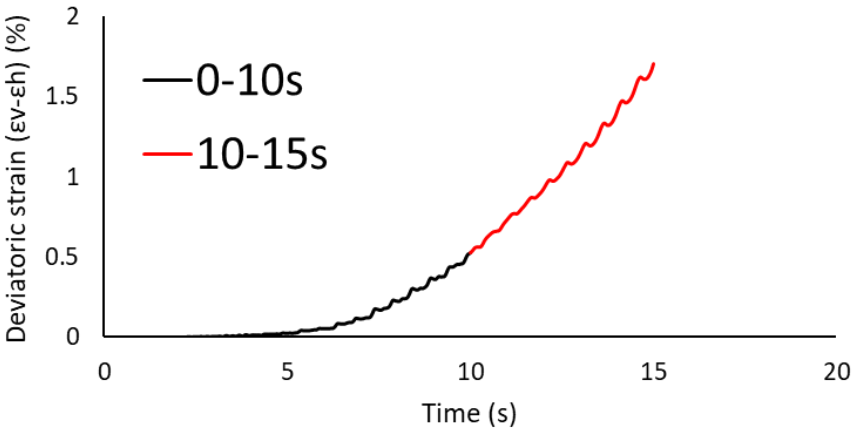

(b) Deviatoric strain

Figure 4.2.4 Effective stress path and deviatoric strain time history at W4 for Model-1 (Non-improvement)

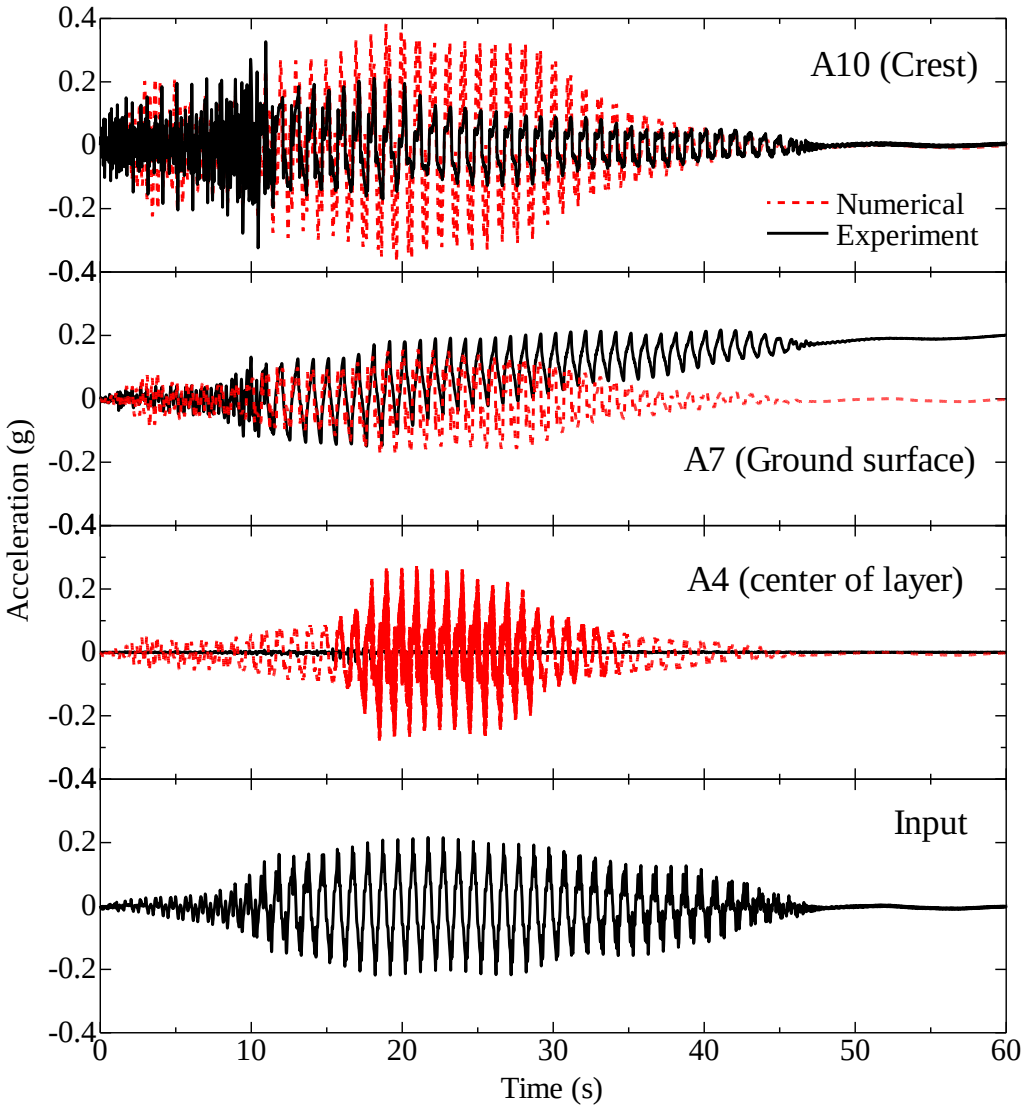

Figure 4.2.5 Acceleration responses in Non-improvement (Model-1)

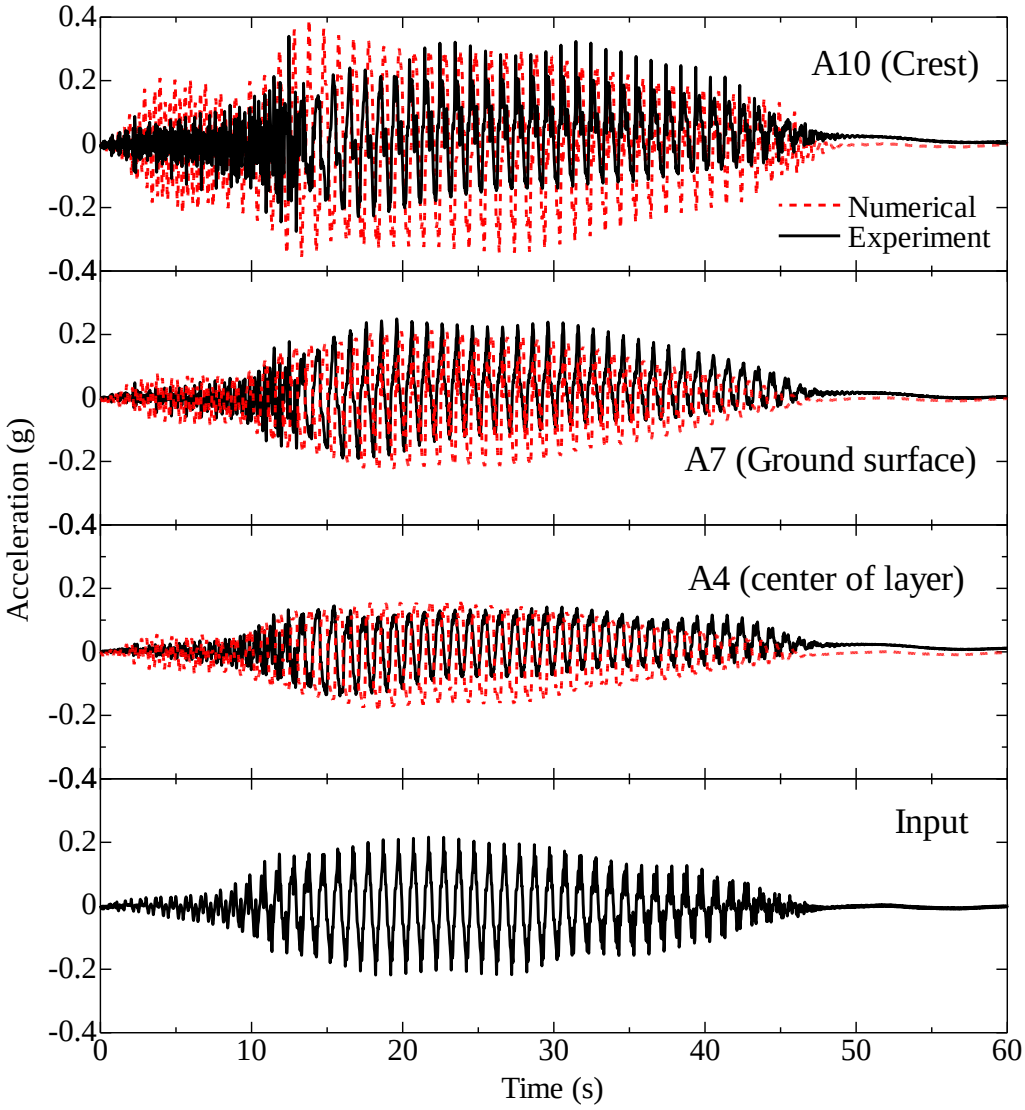

Figure 4.2.6 Acceleration responses in 90° improvement (Model-2)

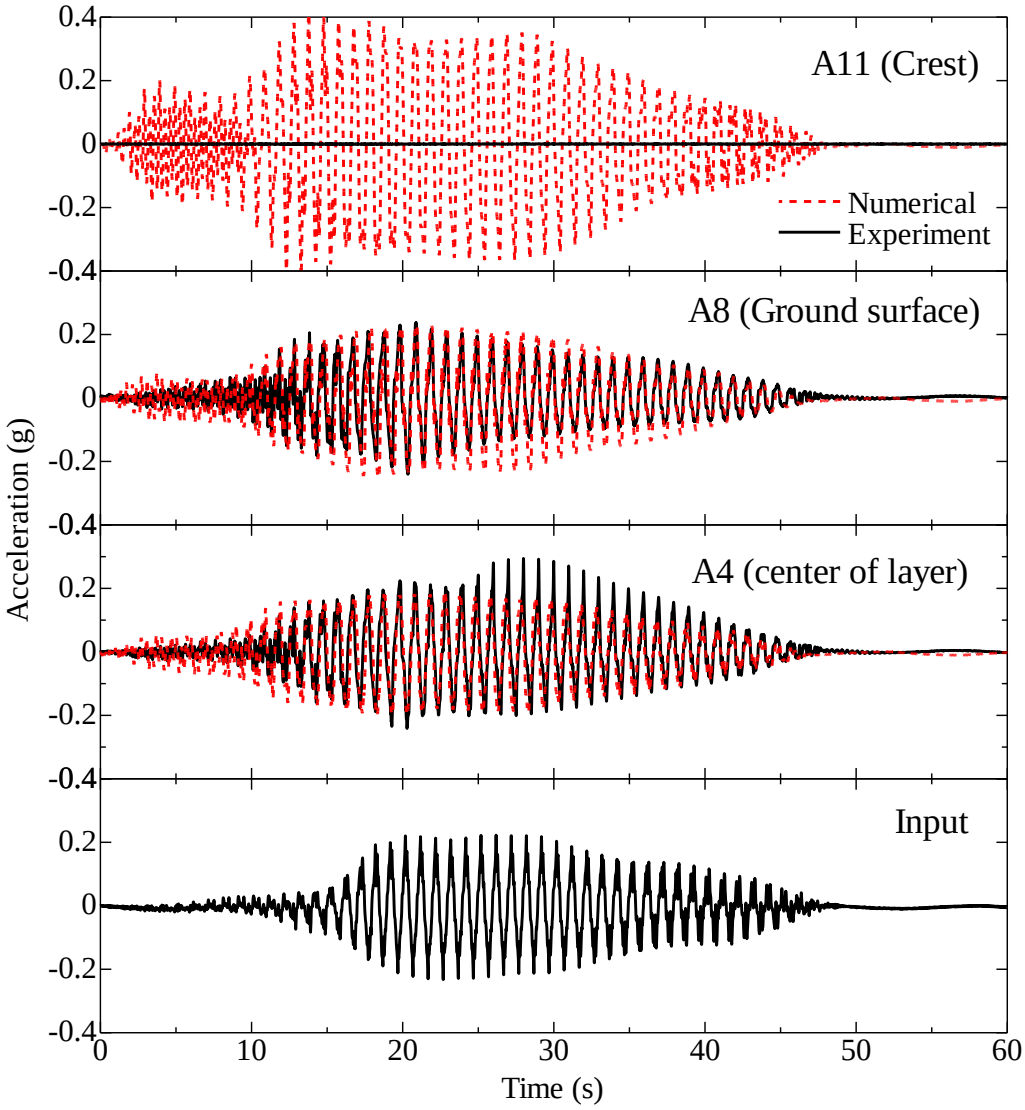

Figure 4.2.7 Acceleration responses in 50° improvement (Model-3)

4.2.2 Ground response during shaking

Figure 4.2.8 shows the distribution of the maximum response acceleration in the vertical cross section at the center of the embankment and slope. It should be noted that the maximum value of the response acceleration shown here is not the same time in each case, but is a plot of the maximum value of the response acceleration generated during shaking at each elevation. The vertical dashed line in the figure shows the maximum value of the input acceleration.

From the distribution of the maximum response acceleration at the center of the embankment shown in Figure 4.2.8 (a), in the case of unimproved ground, the maximum response acceleration tends to decrease from the bottom of the ground to the ground surface. In addition, the maximum value of the response acceleration at each depth tends to be smaller than the input acceleration. It can also be seen that the maximum value of the response acceleration increases from the ground surface to the top of the embankment, and the maximum response acceleration is shown at the top of the embankment. The same tendency applies to the slope shown in Figure 4.2.8 (b).

On the other hand, for the case of 90° improved ground (Model-2), the response acceleration and the input acceleration are almost the same at depths deeper than GL-6m, but the maximum value of the response acceleration from GL-6m to the ground surface is larger than the input acceleration, where there is a tendency for it to increase linearly toward the surface. Furthermore, it can be seen that the maximum value of the response acceleration increases rapidly from the ground surface to the top of the embankment.

For the case of the 50° improved ground, the response acceleration is almost the same as the input acceleration at a depth deeper than GL-4m, but the maximum value of the response acceleration increases linearly from GL-4m toward the ground surface. In the embankment, the two cases of improved ground have almost the same maximum response acceleration distribution. However, on the surface of the embankment slope, it was found that the two cases of the improved ground have a larger response acceleration than the case of the unimproved ground.

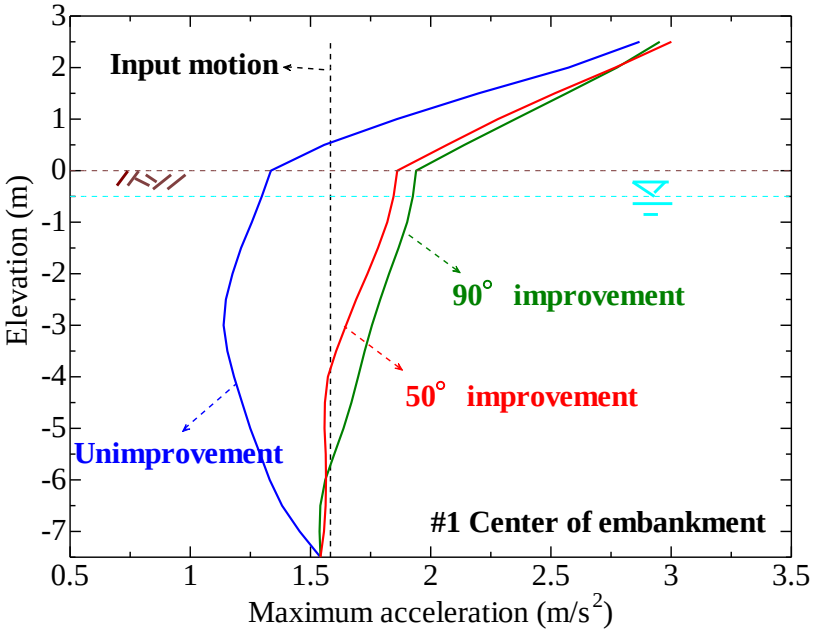

(a)

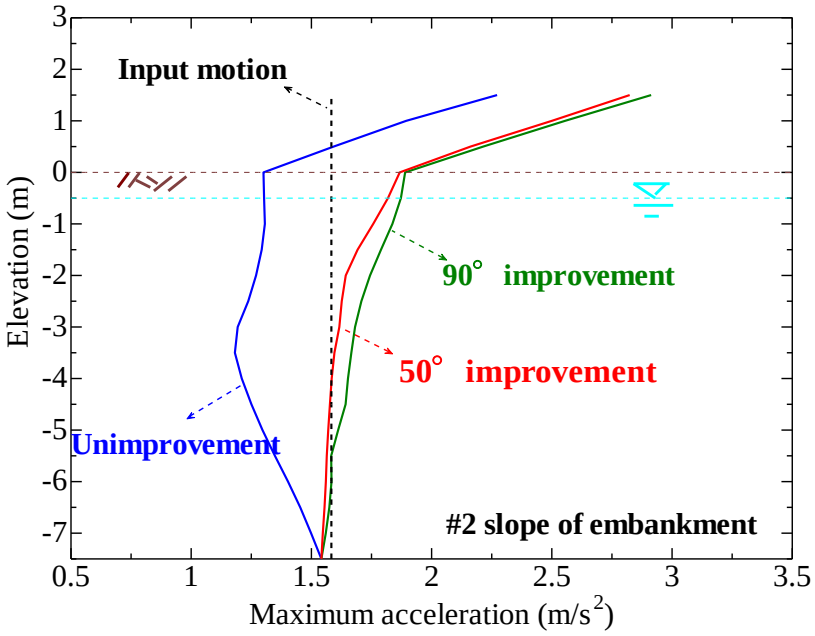

(b)

Figure 4.2.8 Distribution of maximum acceleration

4.2.3 Excess pore water pressure responses

Figure 4.2.9 displays the contours of the excess pore water pressure ratio immediately after shaking (t = 50 s). From Figure 4.2.9, it is considered that the excess pore water pressure ratio of the free field increased to unit at all depths regardless of the improvement, which represents liquefaction occurred in the free field. Regarding the foundation ground below the embankment, there is no region where the excess pore water pressure ratio became unit, and it is considered that the ground below the embankment is not liquefied in the unimprovement case (Model-1). On the other hand, in the 90° improvement case (Model-2), the excess pore water pressure ratio has not risen to unit in the ground below the center of the embankment, but the excess pore water pressure ratio has risen to unit in the vicinity of the vertically improved body, which is thought to be liquefied. For the case improved by 50°, the excess pore water pressure ratio has risen to unit in the vicinity of the improved body, which represents liquefaction occurred in the ground below the embankment.

From the above results, the two cases of improved ground are found to be more prone to liquefy. As shown in Figure 4.2.8, it is considered that one of the causes is that the response acceleration in the ground under the embankment is larger in the case of improvement ground.

4.2.4 Shear strain responses

Figure 4.2.10 shows the contours of maximum shear strain immediately after shaking. In the unimproved ground (Model-1), a maximum shear strain of 10% or more occurs in the entire area of the ground below the embankment. In particular, it can be seen that the maximum shear strain of 30% or more occurs in the deeper ground just below the embankment toe. This large deformation is thought to cause the significant settlement of the embankment. On the other hand, in the ground improved by 90° (Model-2), there are no region where the maximum shear strain exceeds 30% in the ground blow the embankment, but the ground under the slope has a larger shear strain than the central region, which is considered that the ground under the slope has lager deformation. For 50° improvement case (Model-3), the shear strain is smaller overall than other two cases. This means that in the ground improved by 50°, the shear deformation in the ground below the embankment was smaller than in the other two cases.

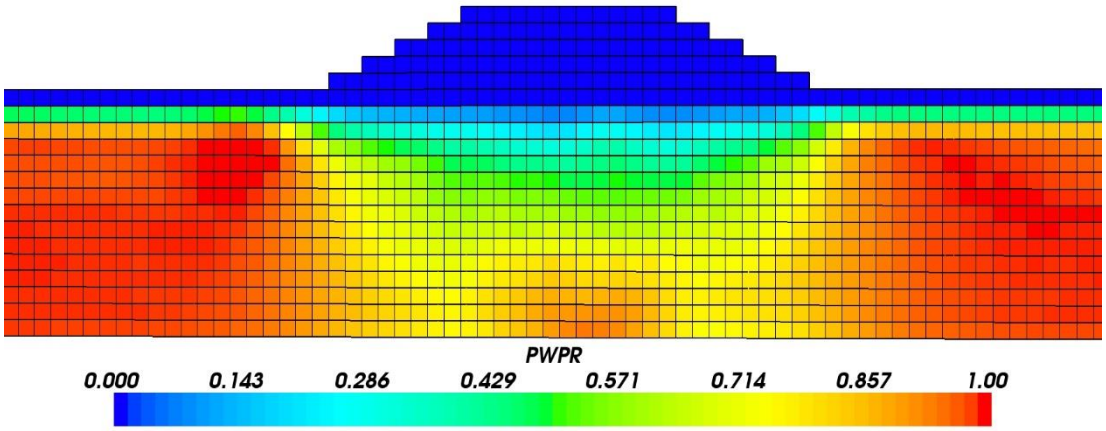

(a) Unimprovement (Model-1)

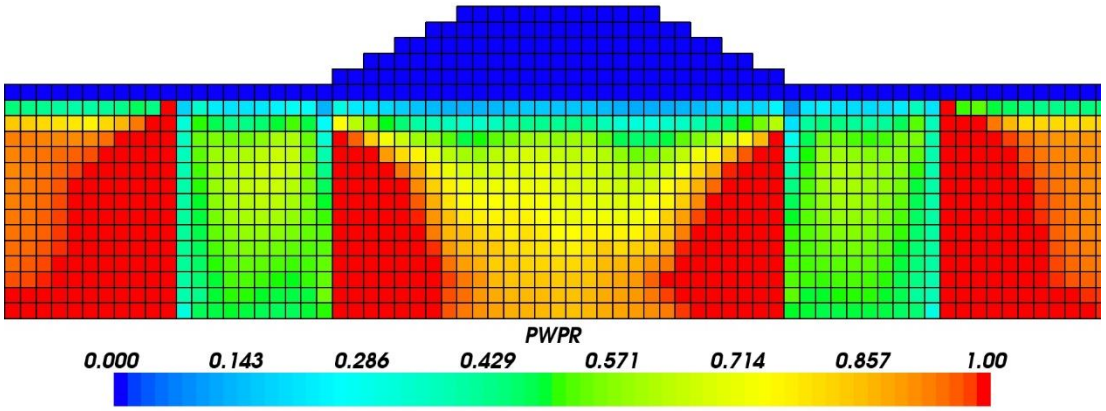

(b) 90° improvement (Model-2)

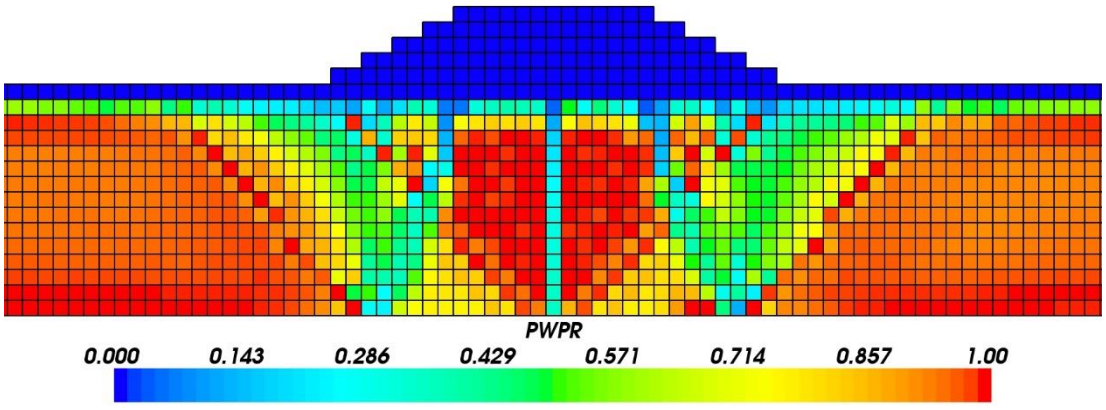

(c) 50° improvement (Model-3)

Figure 4.2.9 Contours of excess pore water pressure ratio distribution immediately after shaking (t = 50 s)

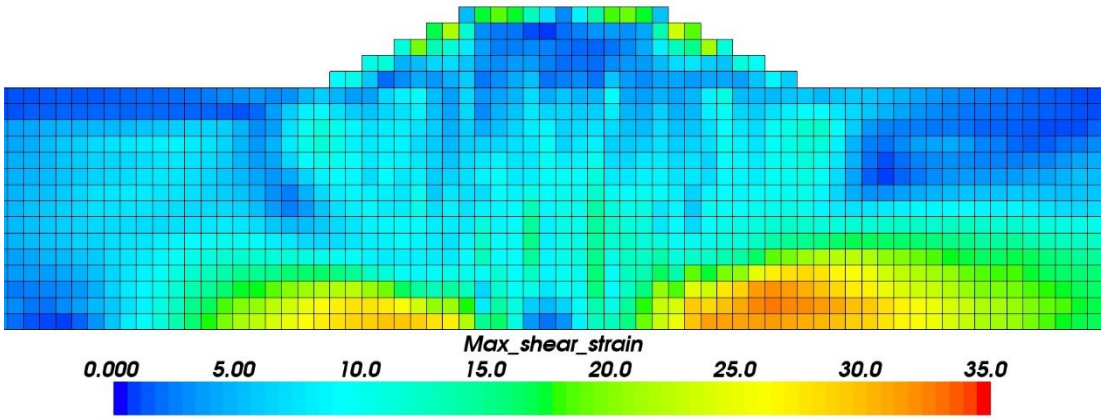

(a) Unimprovement (Model-1)

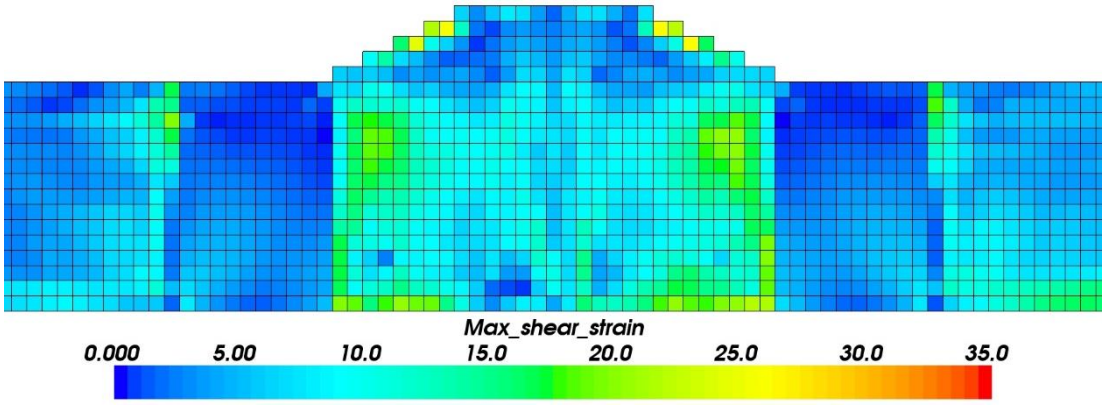

(b) 90° improvement (Model-2)

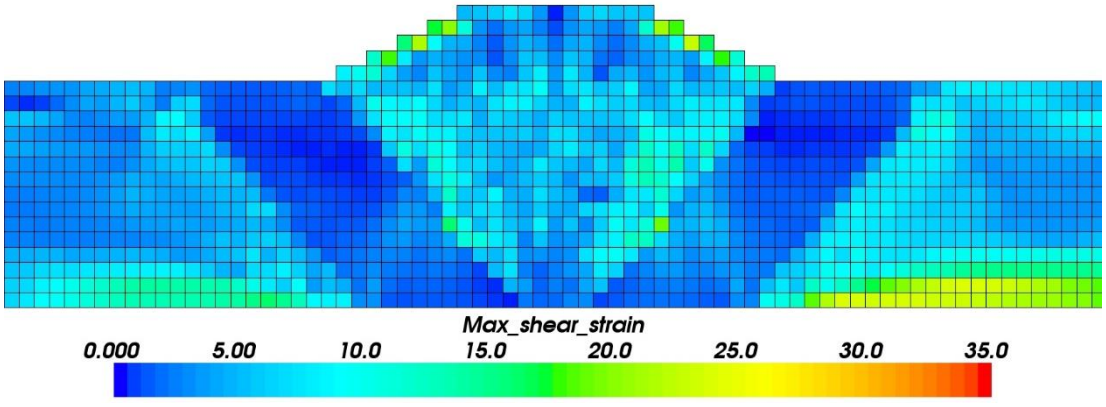

(c) 50° improvement (Model-3)

Figure 4.2.10 Maximum shear strain contours immediately after shaking (t = 50 s)

4.2.5 Horizontal and vertical displacement distribution

The horizontal displacement distribution under the embankment toe at three selected time is shown in Figure 4.2.11. In the unimproved case (Model-1) that represented by blue line, there is no significant horizontal displacement under the embankment toe before liquefaction occurred in the free field (t = 12 s). At 22 s after the start of shaking, it was found that remarkable horizontal displacement occurred as liquefaction occurred in the free field and the deeper region of the ground just below the center of the embankment. After that, the horizontal displacement further expanded as the shaking continued (t=50s).

In the 90° improvement case (Model-2) that represented by green line, it is clear from Figure 4.2.11 that the horizontal displacement is greatly suppressed compared to the unimprovement ground, except that at the ground surface (GL 0 m). From this result, it is considered that the settlement of the embankment caused by the horizontal displacement of the ground can be reduced, but there is not much effect in reducing the settlement amount due to the horizontal deformation of the embankment itself.

On the other hand, in the 50° improvement case (Model-3) that represent by red line, the suppression of horizontal displacement seems to be more effective than in the 90° improved ground, and the displacement on the ground surface is also smaller than other two cases, which is suggested that the horizontal deformation of the embankment itself is also smaller.

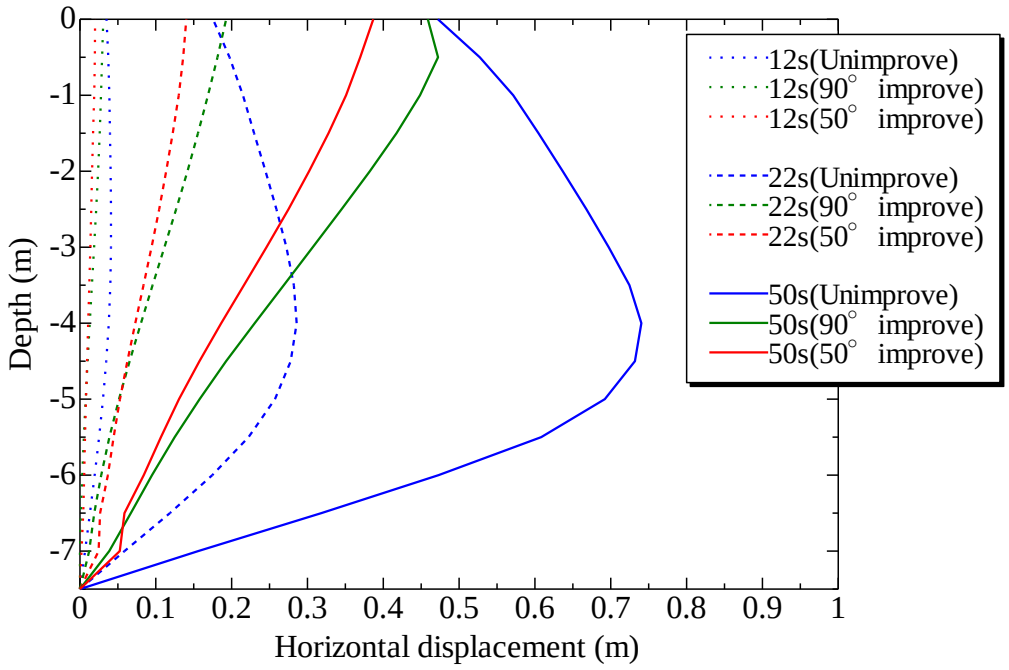

Figure 4.2.11 Horizontal displacement under the embankment toe

Figure 4.2.12 indicates the vertical displacement distribution at the bottom of the embankment at three time same with Figure 4.2.12 (t = 12, 22, 50 s). In the case of unimproved ground (Model-1), no significant vertical displacement occurred until the free field is liquefied (t = 12s). At 22 s after the start of shaking, it is observed that about 0.2 m vertical displacement occurred blow the embankment crest. After that, with the shaking continued until 50s, the amount of the vertical displacement has increased overall, especially under the embankment crest.

In the 90° improvement case (Model-2), despite the fact that the horizontal displacement under the embankment toe is significantly suppressed (see Figure 4.2.11), the amount of vertical displacement blow the embankment crest have not been suppressed much compared to the unimproved ground. It is considered that the significant uplift displacement at the embankment toe is attributed to the larger vertical displacement blow the crest.

For the 50° improvement case (Model-3), the vertical displacement under the crest is about 50% of the 90° improvement case (Model-2), although there is not much difference in the situation of suppressing horizontal displacement.

From the results above, it is considered that the pattern of vertical displacement distribution under the embankment is influenced by the improved angle, even though there is not significant difference in the horizontal displacement under the embankment toe.

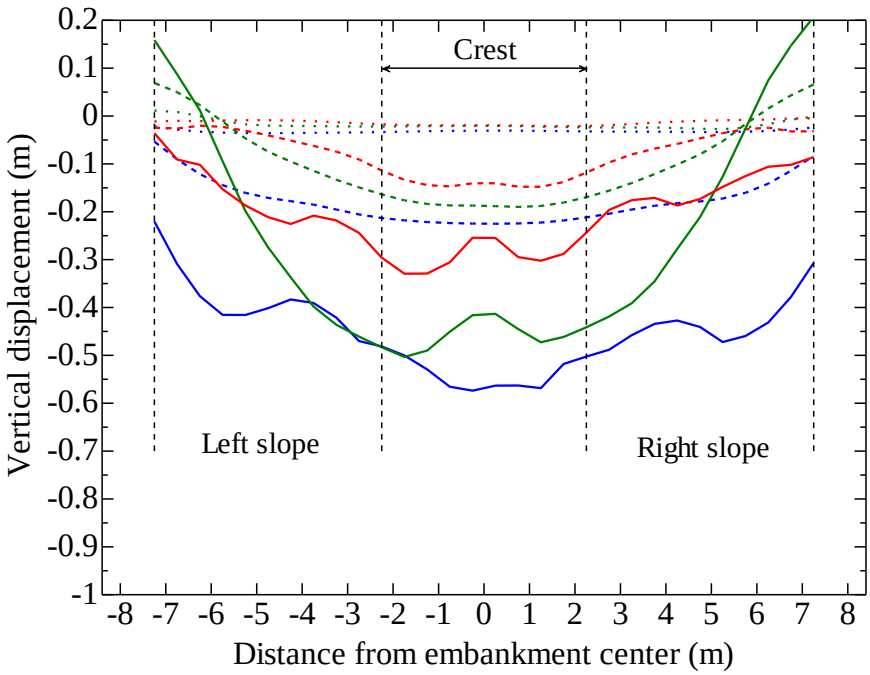

Figure 4.2.12 Vertical displacement at the embankment bottom

4.2.6 Average vertical displacement for each factor

Regarding to the settlement of embankment, there are the following three major factors contributes the crest settlement; i) shear deformation of embankment due to horizontal deformation of underlying liquefied soil, ii) lateral deformation of loose sand layer and iii) contractive volume change of loose sand under embankment (Okamura and Matsuo, 2002; Okamura and Tamura, 2004). The factors ii) and iii) are associated with settlement of the embankment base, while factor i) is associated with a change in the embankment height. Herein, the effect of the SCP improvement angle on the factors ii) and iii) are discussed.

Figure 4.2.13 shows the total average vertical displacement of the ground surface under the embankment (solid line) and the vertical displacement due to lateral deformation of the foundation ground under the embankment (dashed line) in each case. It should be noted that the average vertical displacement mentioned here assume uniform vertical displacement along the base of embankment, though uneven vertical displacement is observed in the numerical analysis results (see Figure 4.2.12). Therefore, vertical displacement represented in Figure 4.2.13 do not agree qualitatively with displacement obtained from the numerical results shown in Figure 4.2.1 - Figure 4.2.3 but provide the relative contribution of each factor to the vertical displacement. In addition, the average vertical displacement due to shear deformation was defined as the average vertical displacement due to volume change is subtracted from the total average vertical displacement.

From the results show in Figure 4.2.13, the total average vertical displacements in the 90° improvement case (Model-2) and the 50° improvement case (Model-3) are about 65% and 50%, respectively, compared to the unimprovement case (Model-1). It also can be seen that the vertical displacement due to shear deformation of foundation ground is dominant in all cases. In addition, the amount of vertical displacement due to shear deformation (dashed line) is about 50% or less in the case of improved ground compared to the case of unimproved ground. Furthermore, the case of 50° improved ground has a smaller amount of vertical displacement due to shear deformation than the case of 90° improved ground.

On the other hand, it is found that the amount of vertical displacement due to volume compression is 1.8 times and 1.4 times larger in the case of the 90° improved ground and the 50° improved ground than in the unimproved ground, respectively. It may be due to the larger excess pore water pressure occurred in the improved ground as shown in Figure 4.2.9.

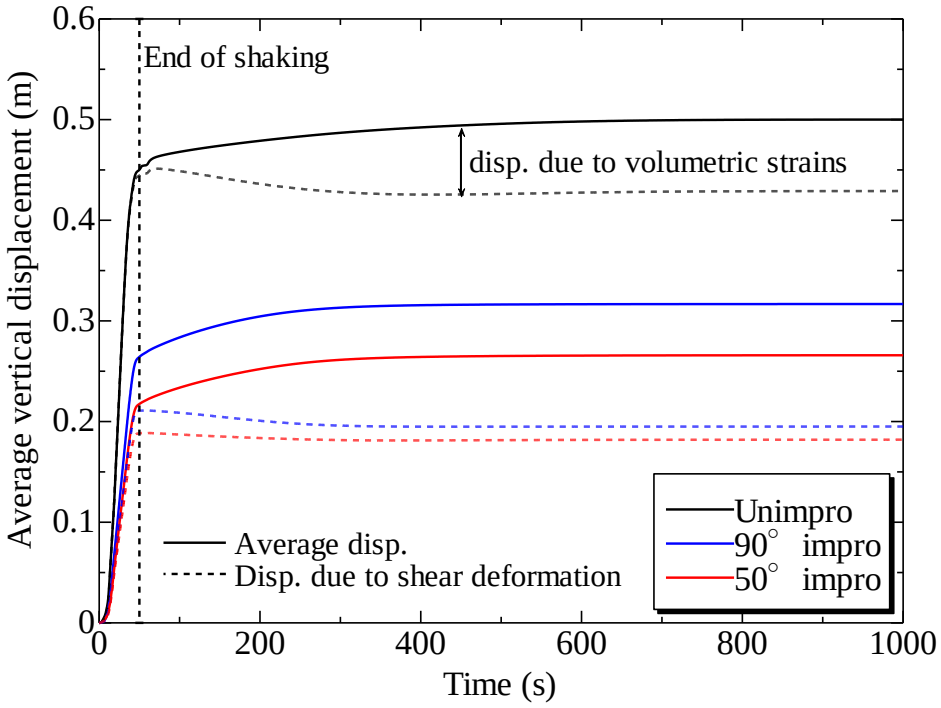

Figure 4.2.13 Average vertical displacement for each factor

4.3 Summary

After the validation of the numerical tool, the numerical model was applied to simulate the centrifuge experiments to study the effects of the SCP improvement angle on the seismic performance. By comparing the experimental and analytical results, it can be said that the numerical tool has confidence in ability of simulation for the realistic behavior on embankments and saturated soils during dynamic loading events.

It is found from the results that the shear deformation of the foundation ground under the embankment is a major factor in settlement. In the improved cases, the lateral deformation of the foundation ground under the embankment can be significantly reduced, while the settlement due to contractive volume change is observed larger in improved cases because the larger excess pore water pressure occurred. The total average vertical displacements in the 90° improvement case (Model-2) and the 50° improvement case (Model-3) are about 65% and 50%, respectively, compared to the unimprovement case (Model-1).

Chapter 5

Effect of angle of SCP improvement on the mitigation of embankment settlement

5.1 Introduction

The lateral spreading of the liquefied foundation triggers the seismic settlement or deformation of the embankment resting on the loose sandy foundation ground (Bhatnagar, Kumari and Sawant, 2016). Countermeasures in the remediation program are designed and constructed so as to provide containment for deformation of liquefied foundation soils away from embankment centerline toward free field by forming remedied stiff zones under embankment toes (Adalier, Elgamal and Martin, 1998; Okamura and Matsuo, 2002). In practical design procedure for liquefaction countermeasures of embankment, the specification and scope of improvement are determined according to the seismic performance requirements of the structure (PWRI, 2016). In recent times, engineering concern has been extended to the seismic resistance of lifelines and long embankments. Since these facilities are often too long and too wide to allow economically for an overall soil improvement, an alternative idea has been developed in which liquefaction is allowed to occur but the facilities are designed to resist a certain magnitude of ground deformation. Although mitigation to prevent the occurrence of liquefaction are desirable, it is important from an economical viewpoint that there is a level of allowable displacement and deformation below which the induced ground movement does not cause serious problems to concerned structures.

In the previous chapters, it was found that the angle of the SCP improvement zone affects the dynamic behavior of the ground and the embankment during a shaking. Despite the valuable insight that can be gained from field observations and physical modeling tests, the relative importance and influence of various parameters on the structure's response cannot be determined in a systematic manner from field observations and physical modeling tests only. A comprehensive numerical parametric study was performed with a wider range of angle and width of SCP improvement zones, to evaluate their influence and relative importance on the performance of embankment. Yet, there are still no reliable

engineering procedures for predicting liquefaction-induced ground displacement near structures, which is a necessary step for reliable mitigation of this hazard. This understanding and the dataset produced are necessary steps before the benefits of performance-based engineering can be realized in the evaluation of liquefaction consequences on embankment structures.

In this chapter, as shown in Figure 5.1.1, the angle of the SCP improvement zone is changed from 30° to 90°, and the effect on the deformation of embankment is investigated. The conditions other than the angle of the improvement zone are kept in the same way as the conditions of the centrifuge model experiments, and are the same in all cases. Acceleration time history recorded by an accelerometer that is attached to the base of the container during the centrifuge test is used in this analysis as an input ground motion. The input ground motion is shown in Figure 5.1.2.

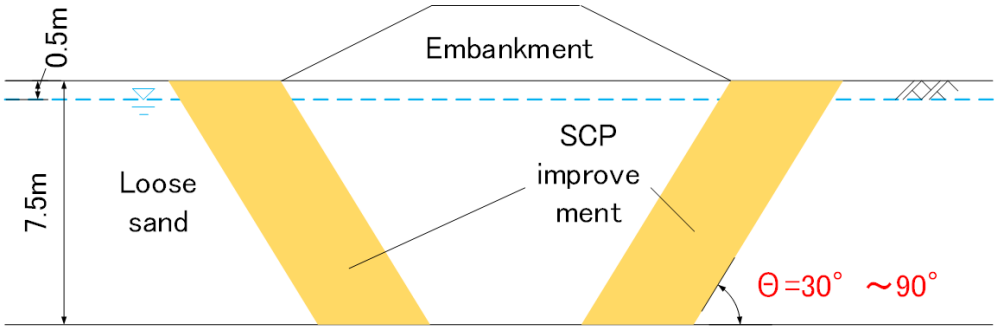

Figure 5.1.1 Schematic of FE analysis model

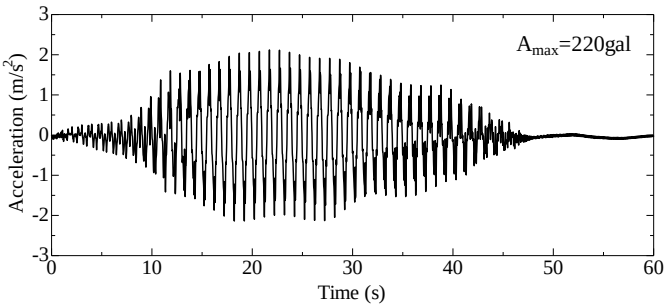

Figure 5.1.2 Input motion for numerical analysis

5.2 Description of model mesh

Two-dimensional finite element simulation of the centrifuge experiment is conducted under plain-strain condition considering a domain with a unit width in the transverse direction. The discretized mesh of the numerical models are shown in Figure 5.2.1. A uniform mesh having the dimensions of 0.5 m × 0.5 m in X and Y direction, respectively, is used throughout the whole model. Boundary conditions in the numerical model are imposed in such a way that all the movements of the nodes are restricted at the bottom boundary, and the nodes along the vertical boundary are kept free to move vertically and are restricted to move horizontally during the analysis.

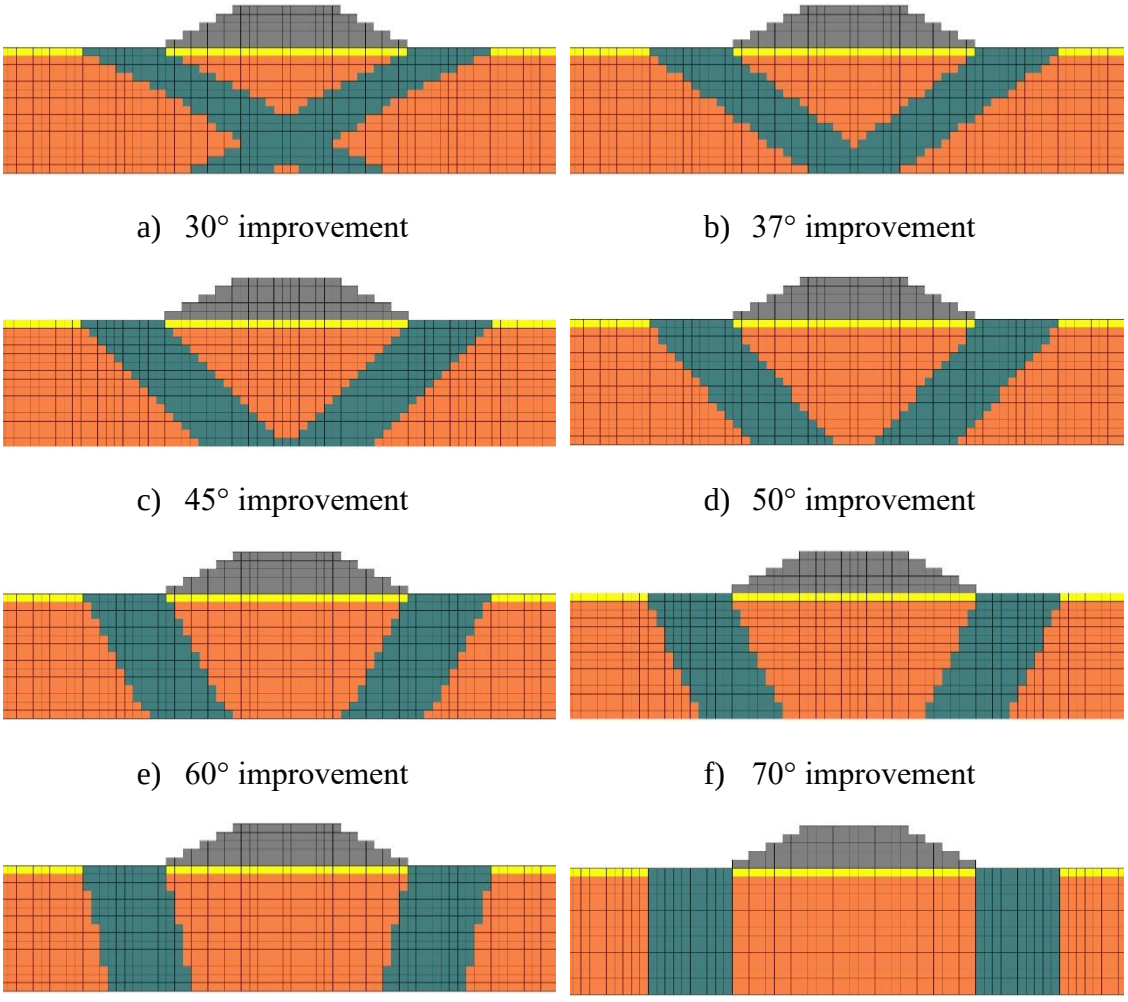

a) 30° improvement b) 37° improvement

c) 45° improvement d) 50° improvement

e) 60° improvement f) 70° improvement

g) 80° improvement h) 90° improvement

Figure 5.2.1 Discretized mesh for the 2D FE analysis models

5.3 Results and discussions

As mentioned in the preamble, the settlement and deformation of the embankment on the liquefied ground is considered to be mainly caused by the deformation of the underlying ground. Therefore, it is expected that the current measures against liquefaction of embankment will reduce the settlement of embankment by suppressing the lateral deformation of the foundation ground. In the current design of liquefaction countermeasures for embankment structures, the extent and shape of SCP improvement zone must be determined according to the required seismic performance of the structure. In this chapter, the angle of SCP improvement zone that can be constructed in practice is changed from 30° to 90°, and examine the effects of the angle of SCP improvement zone on the deformation of the embankment.

5.3.1 Excess pore water pressure responses

Previous studies have shown that the generation of excess pore water pressure in the ground due to an earthquake plays an important role in the deformation of the foundation ground and embankment(Koga and Matsuo, 1990; Dobry and Liu, 1994). Therefore, in herein, the generation of excess pore water pressure at some representative locations in the ground is investigated first. And then, the behavior of excess pore water pressure and displacement in the cases with different angle of the SCP improvement zone is compared.

Figure 5.3.1 shows the time history of excess pore water pressure at three locations with different initial stress states in the foundation ground. When compare the excess pore water pressure under the center of the embankment shown in Figure 5.3.1(a), the excess pore water pressure in the ground improved by 37° to 90° is larger than the ground without improvement, except for the ground with an improved angle of 30°. On the other hand, in the ground of 30° improvement, the excess pore water pressure at P1 rise until 12s and then decrease until 22s. It is considered to be the typic undrained shear behavior of the sand (Ishihara, Tatsuoka and Yasuda, 1975; Alarcon-Guzman, Leonards and Chameau, 1988). Attention should be paid to another behavior in addition to the magnitude of excess pore water pressure. In the unimproved ground, the excess pore water pressure at P1 reached the maximum value at about 15s and then continued during the shaking, whereas in the improved ground, the excess pore water pressure decreased even during the shaking. This behavior is particularly remarkable as the distance from the improved zone is closer (i.e., the excess pore water pressure decreased the fastest in the improved ground with 37 °). It may be due to that the difference occurred in excess pore water pressure between the unimproved area and the improved area created a large hydraulic gradient, which caused the drainage even during the shaking.

Figure 5.3.1(b) shows the time history of the excess pore water pressure at P2. The excess pore water pressure generated higher in the 90 ° improved ground than that in the

unimproved ground. It is considered that the excess pore water pressure is prone to generate larger in the vicinity of the dense improvement zone due to the larger response acceleration. On the other hand, in the improved ground with 30°, 37°, 45° and 60°, the P2 location is within a dense improved zone, so the excess pore water pressure increased from the start of shaking to 10 s, but then decreased. However, it rises again after that and reached the same value as the unimproved ground.

Figure 5.3.1(c) shows the time history of excess pore water pressure in free field away from the embankment. In the free field, the excess pore water pressure is almost the same in all cases regardless of the angle of the improvement zone.

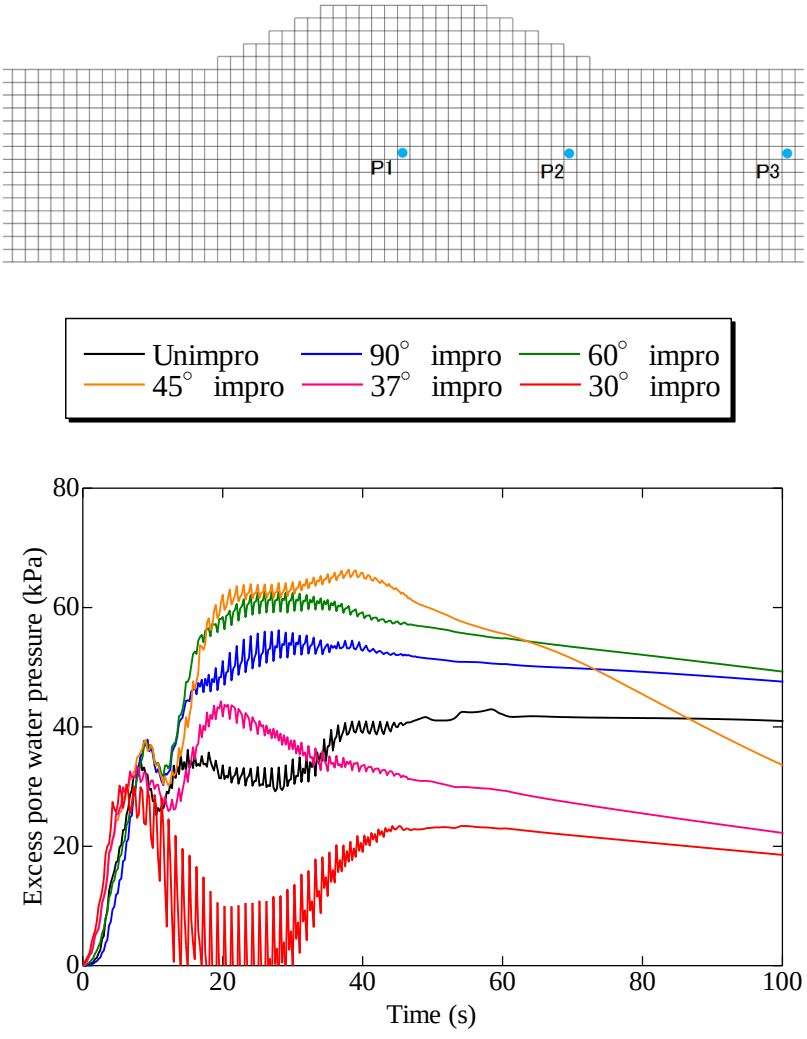

a) Under embankment center (P1)

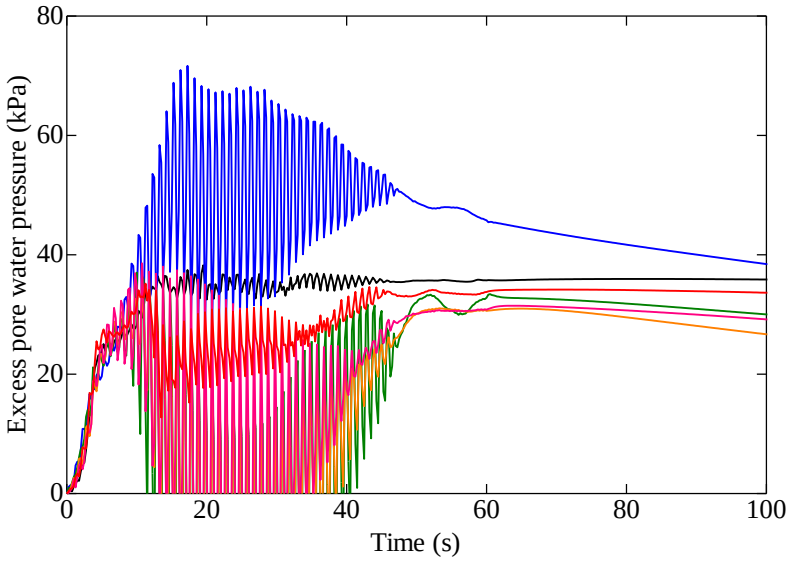

b) Under embankment toe (P2)

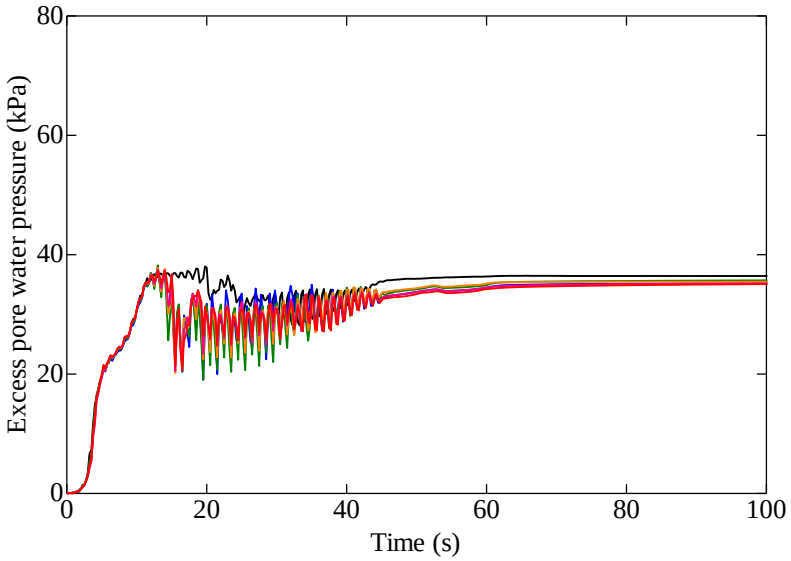

c) Free field (P3)

Figure 5.3.1 Time histories of excess pore water pressure at P1, P2 and P3

5.3.2 Displacement responses

In this section, the time histories of displacement of embankment and ground at several representative locations are compared. The representative locations is shown at the top of Figure 5.3.2. Figure 5.3.2(a) shows the time history of vertical displacement at D1 that is the center of embankment base, Figure 5.3.2(b) shows the horizontal displacement at the embankment toe (D2) and vertical displacement at the embankment toe (D3) is shown in Figure 5.3.2(c). The vertical displacement at D1 increases rapidly occurred from 10 s in the unimproved ground, and finally a vertical displacement of about 0.6 m occurred. On the other hand, it is clear that the vertical displacement in the improved ground is smaller than that in the unimproved ground. Among them, as the angle of the improvement zone is changed from 90 ° to 30 °, the vertical displacement D1 becomes smaller in terms of the increasing rate (i.e., the gradient of the line), leading to the final settlement becomes smaller.

Next, looking at the horizontal displacement at embankment toe (D2) shown in Figure 5.3.2(b), the behavior of the horizontal displacement is almost the same in all cases except for the ground with 30 ° and 37 ° improvement zone. On the other hand, it can be seen that the horizontal displacement is smaller in the ground improved by 30 ° and 37 ° than that in other cases, and the horizontal displacement is the smallest in the ground improved by 30°. The horizontal displacement at the embankment toe is considered to be directly related to the shear deformation of the embankment. Therefore, it is expected that the smaller the horizontal displacement at the embankment toe, the smaller the shear deformation of the embankment. As a result, it is expected that the amount of settlement of the embankment due to the shear deformation of the embankment could be reduced.

Figure 5.3.2 (c) shows the time history of vertical displacement at the embankment toe. In herein, "+" represents an upward displacement, and "-" represents a settlement. First, looking at the unimproved ground indicated by the black line, the part of the embankment toe settled from the start of shaking, and finally a vertical displacement of about 0.3 m was generated. On the other hand, it can be seen that in the improved ground of 30 ° to 45 °, the settlement occurred at the embankment toe, but the amount is smaller than that of the unimproved ground. On the other hand, it can be seen from the graph that when the angle of the improvement zone changed from 60 ° to 90 °, the vertical displacement at the embankment toe does not settle but shows a upward movement. This may be due to the deformation pattern of the ground below the embankment. The deformation pattern of the ground below the embankment will be discussed in a later section.

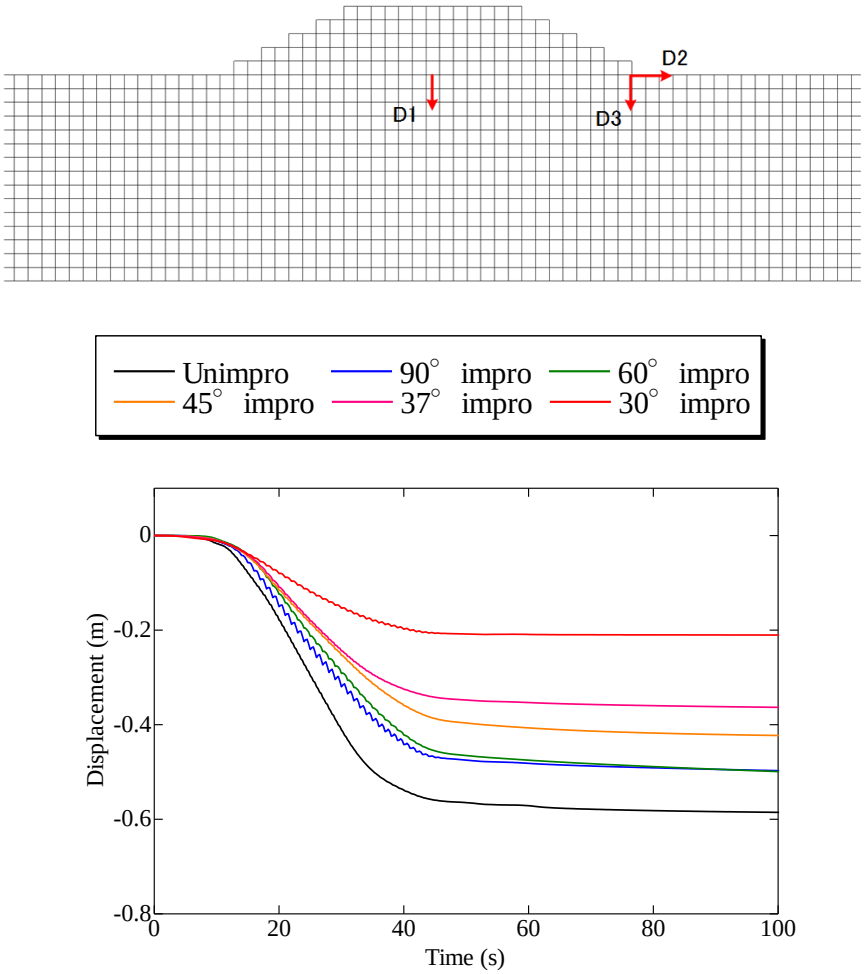

a) Vertical displacement at center of embankment bottom (D1)

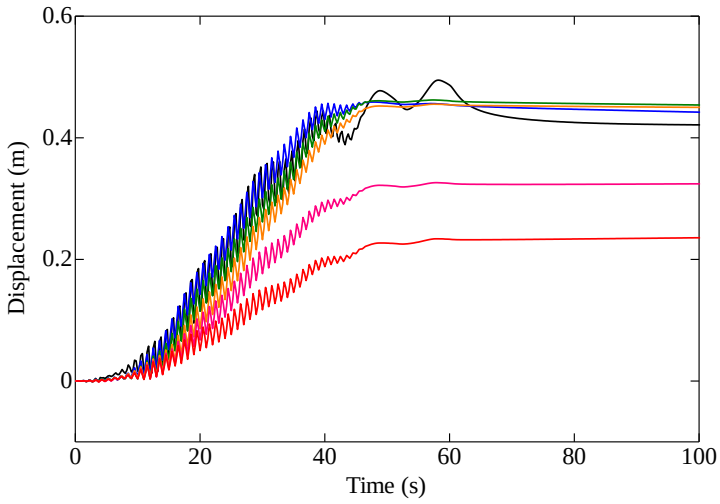

b) Horizontal displacement at embankment toe (D2)

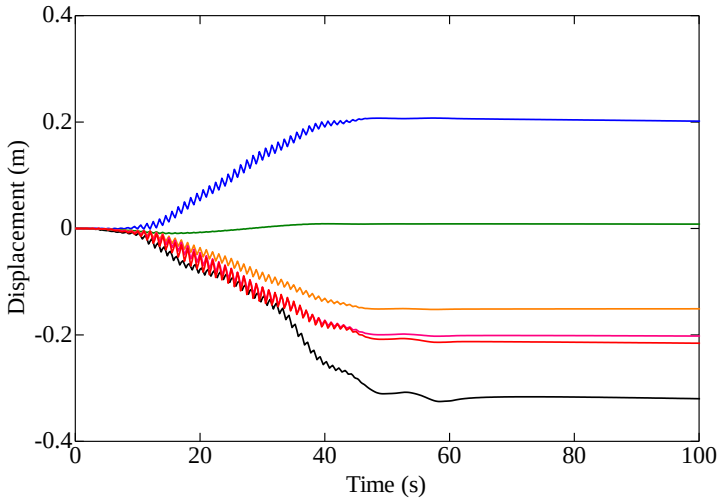

c) Vertical displacement at embankment toe (D3)

Figure 5.3.2 Time histories of displacement at D1, D2 and D3

5.3.3 Maximum acceleration at embankment crest

Figure 5.3.3 shows the maximum response acceleration at the crest of the embankment together with the experimental values in each case. There is little difference in the maximum response acceleration when the improvement angle is between 90 ° and 50 °, but when it is smaller than 50 °, the maximum response acceleration becomes significantly larger. It is considered that this is because the improvement ratio in the ground below the crest of the embankment increases, which makes it easier for the shaking waves to propagate upward. The observed performance illustrates the importance of considering potential changes in the character and intensity of the ground motion transmitted to the embankment when the improvement ratio is large under the embankment center.

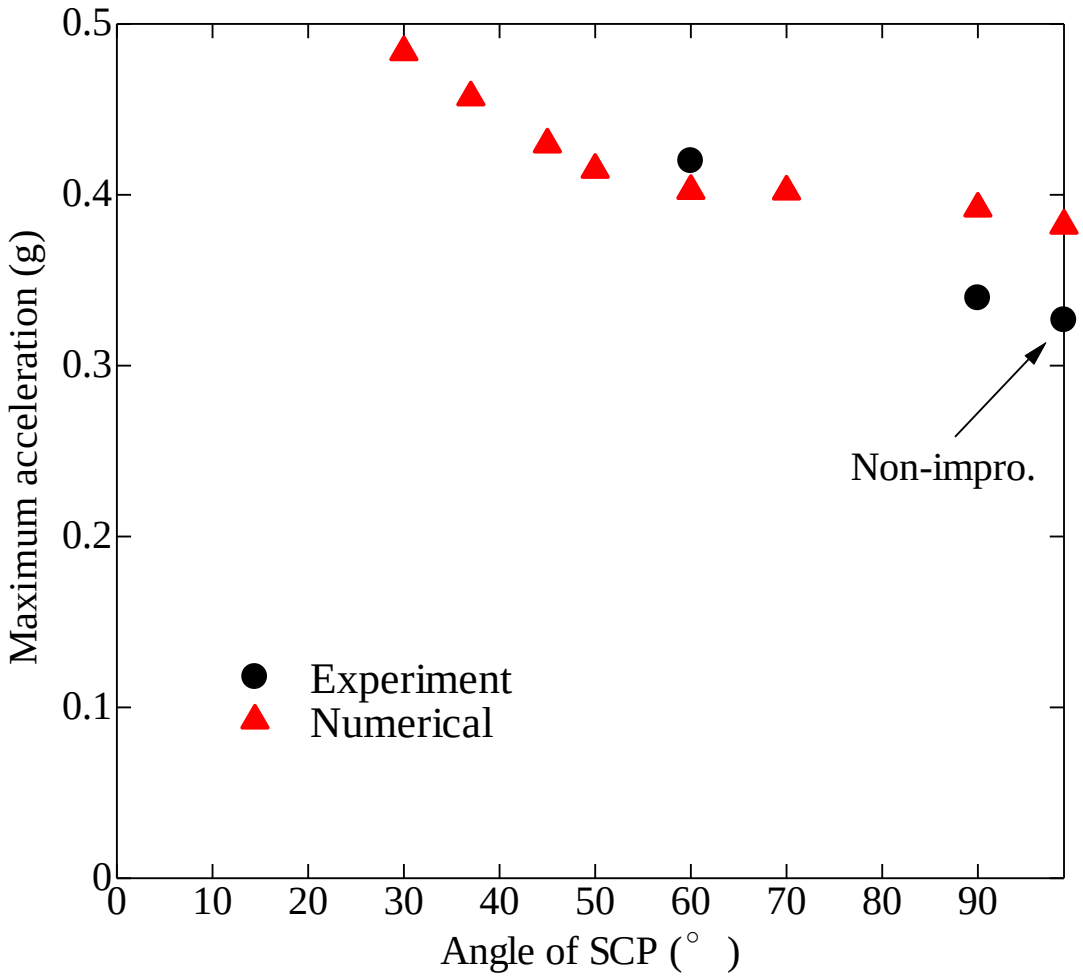

Figure 5.3.3 Maximum accelerations at embankment crest

5.3.4 Degree of liquefaction in foundation ground

In the above section, the behavior of excess pore water pressure and displacement at some representative location is discussed. As already mentioned, the deformation of the foundation ground and embankment is considered to be greatly related to the circumstances of excess pore water pressure in the ground. In this section, the effect of the difference in the angle of the improvement zone on the overall circumstances of excess pore water pressure in the foundation ground is investigated and discussed. In order to achieve this objective, as shown in the schematic diagram at the top of Figure 5.3.4, the ground blow the embankment is divided into three areas, where the region beneath the center of the embankment is defined as Area 1, the region below the top of slope is defined as Area 2, and the region blow the embankment toe is defined as Area 3. The excess pore

water pressure ratio in the mesh at the same depth at each region was calculated and the average value was taken along the depth direction. The distribution of excess pore water ratio along the depth at each region is shown in Figure 5.3.4.

In the unimproved ground, the average excess pore water pressure ratio does not reach 1.0 in all areas under the embankment, but the average excess pore water pressure ratio is 0.6 or more in most areas. In the 90° improved ground, it can be seen that the excess pore water pressure ratio under the center of the embankment tends to be smaller than that in the unimproved ground, but the excess pore water pressure ratio becomes larger than the unimproved ground under the slope and embankment toe. In the ground improved by 70 ° and 60 °, the average excess pore water pressure ratio reaches 1.0 below the depth of -2.0 m under the center of the embankment, indicating that this region is completely liquefied. The average excess pore water pressure ratio beneath the slope has also reached 1.0, which indicates liquefaction occurred at this region. Whereas, the excess pore water pressure ratio under the embankment toe is smaller than that in the unimproved ground and the ground improved with 90°. It is considered that this is because the generation of excess pore water pressure was suppressed by the presence of the dense improvement zone. On the other hand, it can be seen that the excess pore water pressure ratios in the three regions are smaller in the improved ground with 30° and 37°.

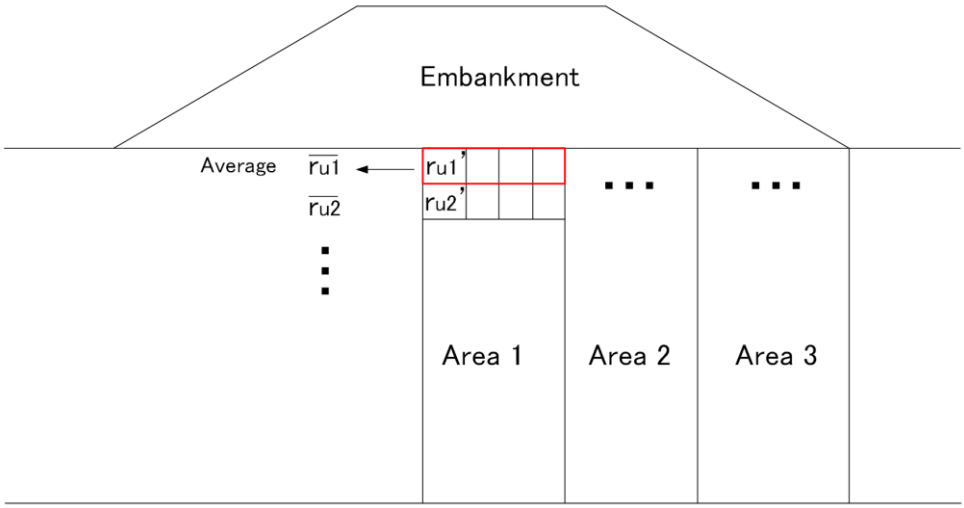

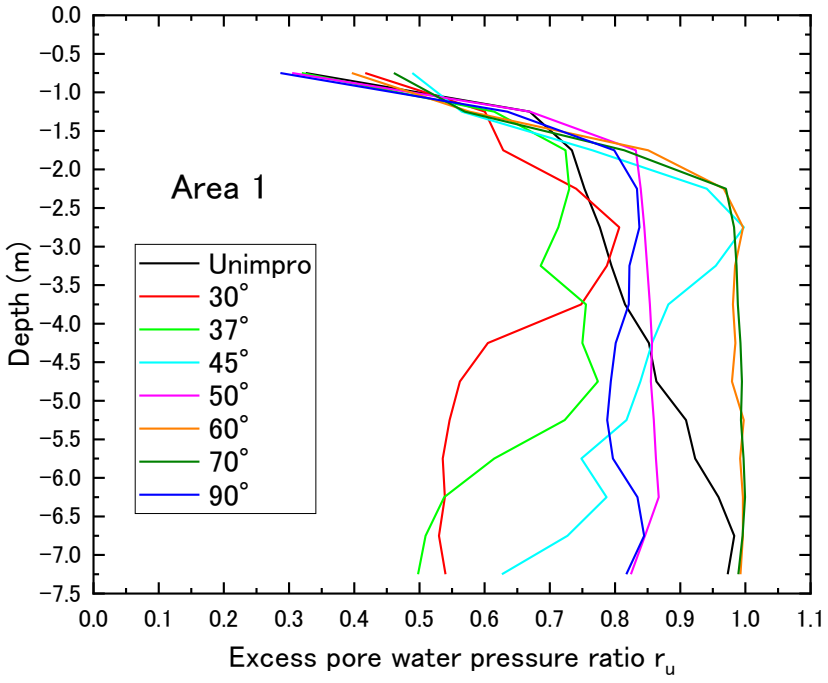

a) Excess pore water pressure ratio under embankment the center (Area 1)

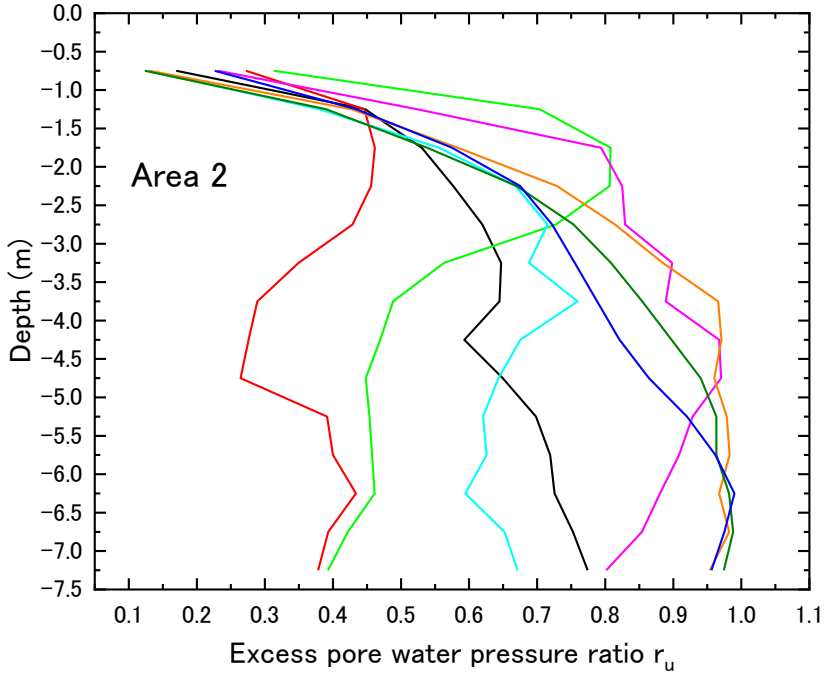

b) Excess pore water pressure ratio under the slope (Area 2)

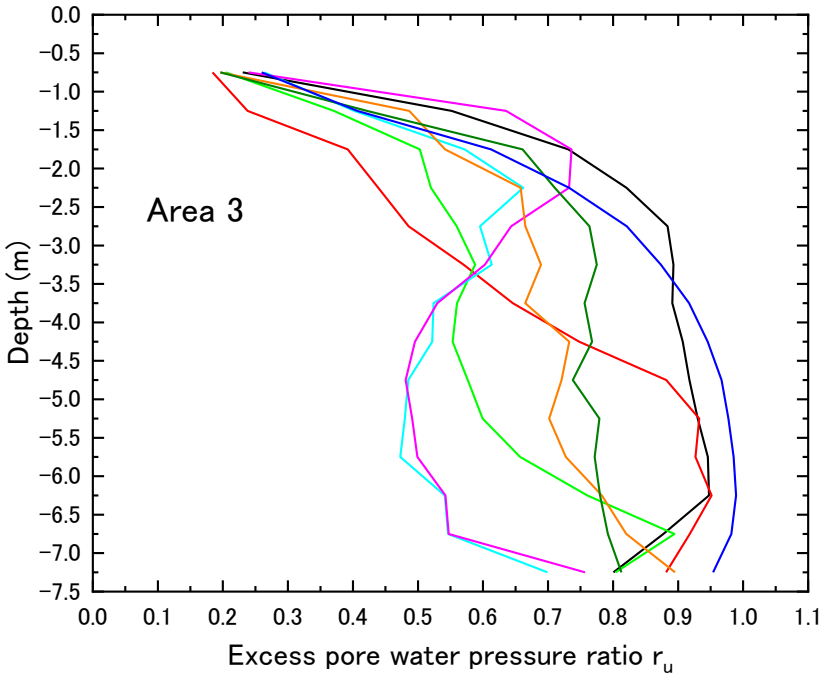

c) Excess pore water pressure ratio under the toe (Area 3)

Figure 5.3.4 Distribution of excess pore water pressure ratio under the embankment (at t = 50s)

Furthermore, in order to quantitatively investigate the effect of the angle of SCP improvement zone on the liquefaction of the foundation ground, the degree of liquefaction, $U_{liquefaction}$, is defined using the results shown in Figure 5.3.4. the degree of liquefaction is calculated as following,

$$U_{liquefaction} = \frac{S1}{7.5*1.0} \qquad (1)$$

Where S1 is the area surrounded by the distribution of the excess pore water pressure ratio and the y-axis as shown in Figure 5.3.5. it indicates that the larger the degree of liquefaction $U_{liquefaction}$, the more element in the area reached liquefaction, and if the degree of liquefaction $U_{liquefaction}$ becomes 1.0, it means that the entire element in the area is completely liquefied. Using the above equation, the degree of liquefaction of the foundation ground was calculated in each case at the end of shaking. Furthermore, in order to examine the degree of liquefaction in different regions in more detail, the three regions shown in Figure 5.3.3 were divided into upper and lower parts, and the degree of liquefaction in a total of six regions was calculated. The results are shown in Figure 5.3.5.

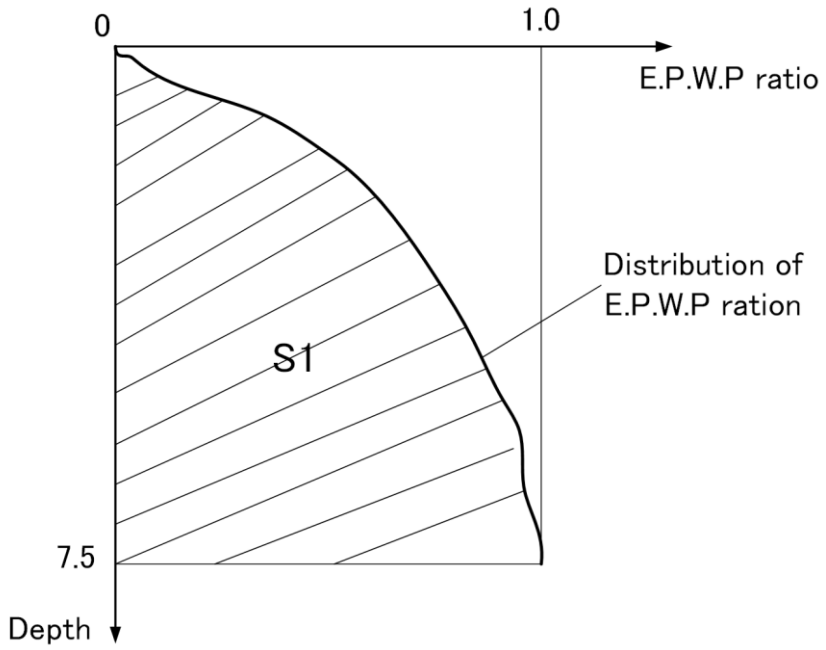

Figure 5.3.5 Schematic diagram of degree of liquefaction

It can be seen that in the ground below the center of the embankment as shown in Figure 5.3.6(a), the degree of liquefaction increases as the angle of the improved body decreases from 90 ° to 60 °, compared to the unimproved ground. As the angle of the improved body becomes smaller than 50 °, the degree of liquefaction tends to decrease.

The degree of liquefaction in the Area 2 shown in Figure 5.3.6(b), when the angle of the improvement zone is in the range of 90 ° to 60 °, the degree of liquefaction in both the upper and lower layers of the ground becomes larger than unimprovement case. It can be seen that the degree of liquefaction of the ground decreases when the angle of the improved body becomes smaller than 50 °.

As shown in Figure 5.3.6(c), As the angle of the improvement zone becomes smaller, the degree of liquefaction becomes monotonously smaller in the upper layer of the ground. On the other hand, in the range of 90 ° to 45 °, the degree of liquefaction decreases in the lower layer of the ground as the improvement angle decreases, but the degree of liquefaction increases when the angle is smaller than 45 °.

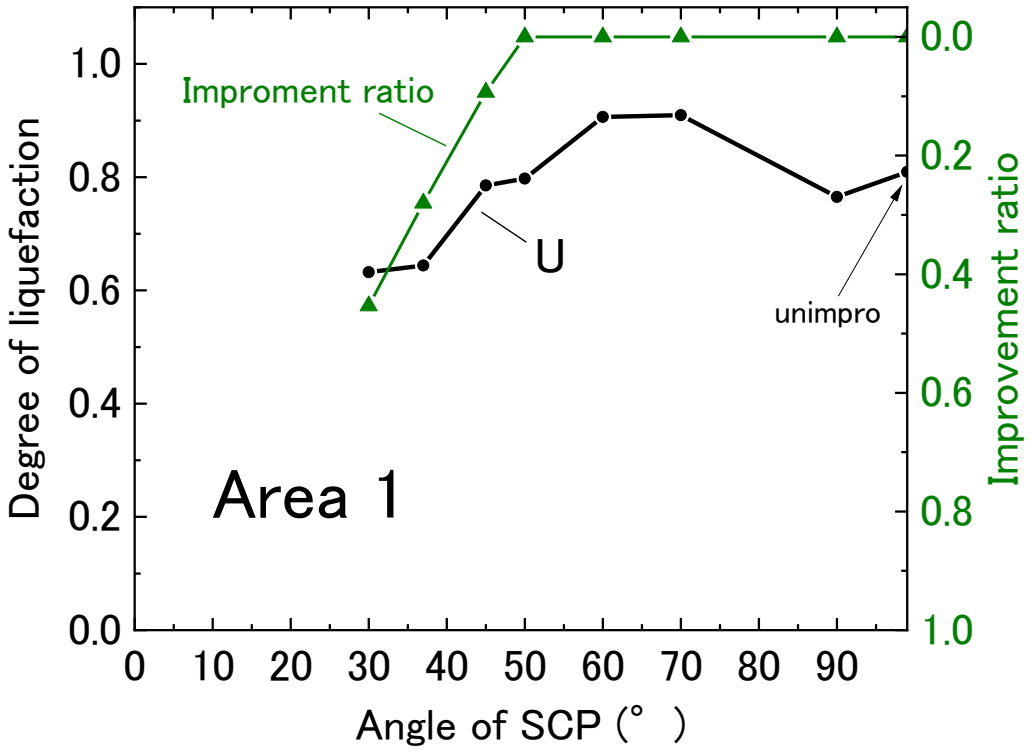

a) Under the center of embankment (Area 1)

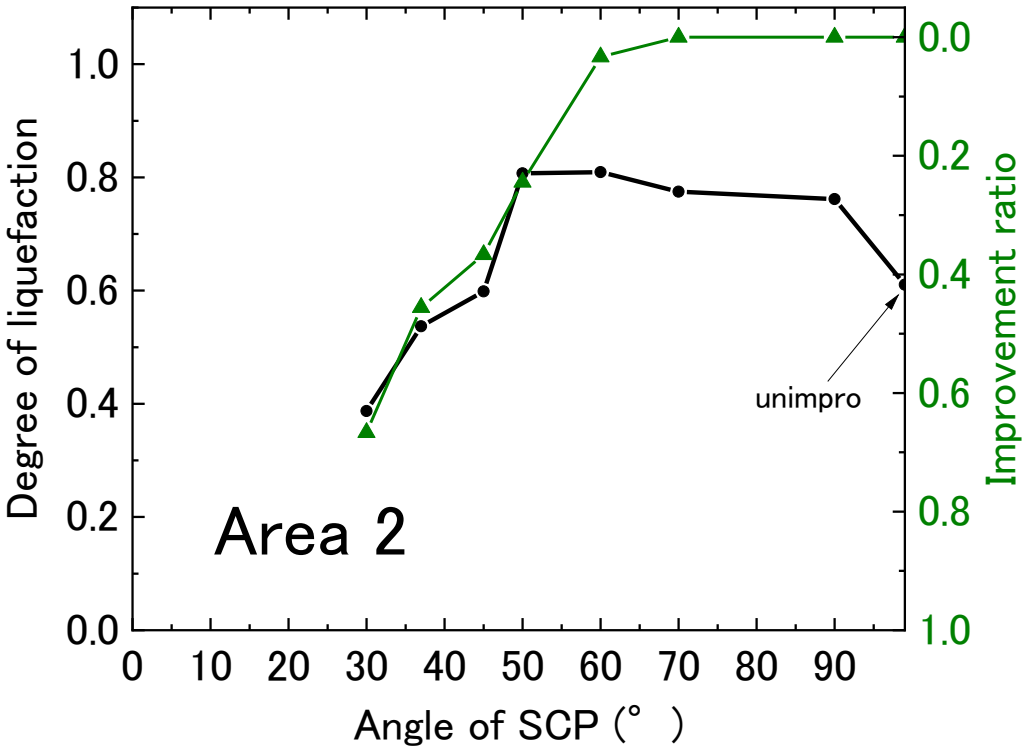

b) Under the top of slope (Area 2)

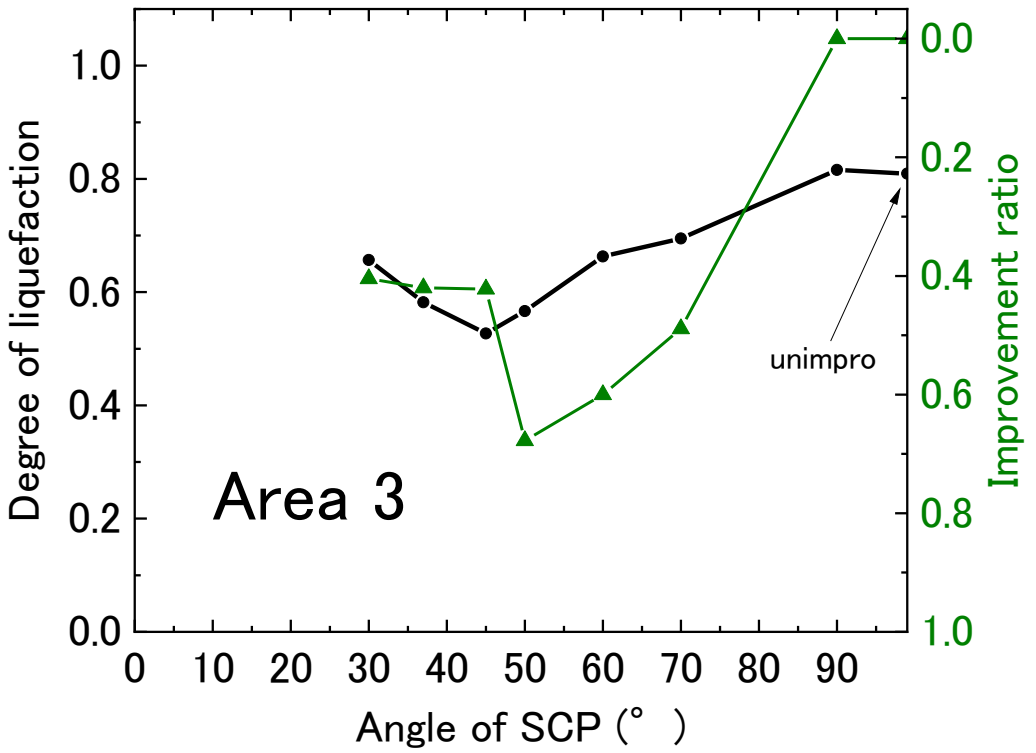

c) Under the embankment toe (Area 3)

Figure 5.3.6 Degree of liquefaction in foundation ground under embankment

5.3.5 Lateral deformation of foundation ground

The SCP improvement zone constructed below embankment toe is aimed to reduce the settlement of embankment by mitigating the lateral deformation of ground below the embankment. Hence, in this section, the effects of improved ground with different angles on the lateral displacement of the ground is investigated.

Figure 5.3.7 shows the distribution of the horizontal displacement under the embankment toe at the end of shaking (at t=50s). In the unimproved ground, a large horizontal displacement under the embankment toe can be confirmed, where the largest horizontal displacement occurred near the central depth of the ground. In the ground improved by 90° that is the conventional SCP improvement case, the horizontal displacement of the ground could be greatly reduced except for the part of the ground surface. In the improved ground with 90° to 45 °, there is no significant difference in the distribution of horizontal displacement. On the other hand, it can be seen that the horizontal displacement at the depth above -4.5 m can be further reduced in the ground

improved by 37 ° and 30 °. However, it can be seen that the horizontal displacement is slightly larger than the ground improved by 90° to 45° below the depth of -4.5m.

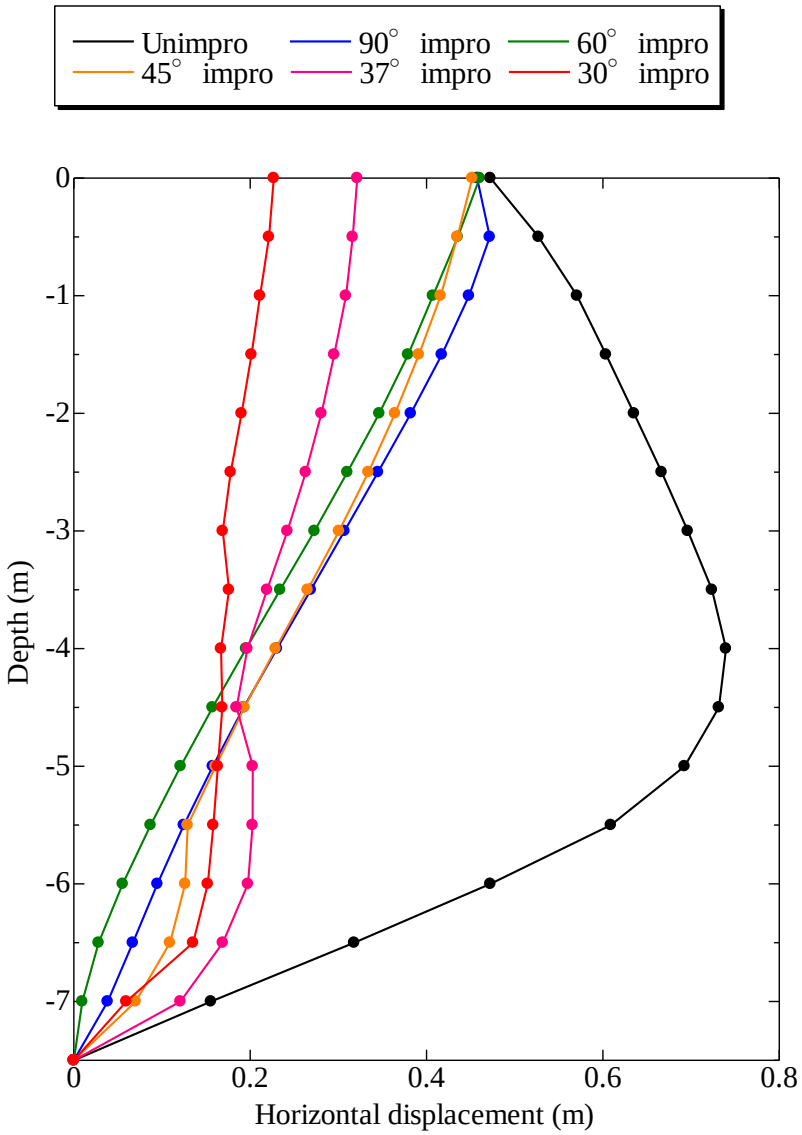

Figure 5.3.7 Distribution of horizontal displacement under embankment toe (t = 50 s)

It is considered that the amount of lateral deformation of the soil under the embankment is greatly related to the settlement at the embankment base (Okamura and Tamura, 2004). In order to quantitatively evaluate the effect of the angle of the improvement zone on the lateral deformation of the ground, the area of the horizontal displacement in each case is calculated from the result of Figure 5.3.7, and the relationship with the improved angle is

shown in Figure 5.3.8. It can be seen that the area of horizontal displacement in all the improved ground can be reduced to less than half compared to the unimproved ground. In the improved ground, there is no significant difference between each case when the improved angle is in the range of 90 ° to 45 °. Whereas, when the improved angle become smaller than 45°, the area of horizontal displacement decrease. If the area of lateral displacement of the ground decreases, the amount of settlement of the ground below the embankment may also decrease, but the distribution of the vertical displacement at the embankment base will be changed depending on the condition of the ground below the embankment.

When the SCP improvement zone cross (< 45°in this study), the improvement ratio in the ground below the embankment crest (Area 1) begins to increase. Until the SCP improvement zone cross, even though the improvement ratio in the ground below the embankment slope increases, but it just can suppress the uplift deformation of the ground below the slope. In order to suppress the lateral deformation of the ground, the improvement ratio in the ground below the embankment crest is important.

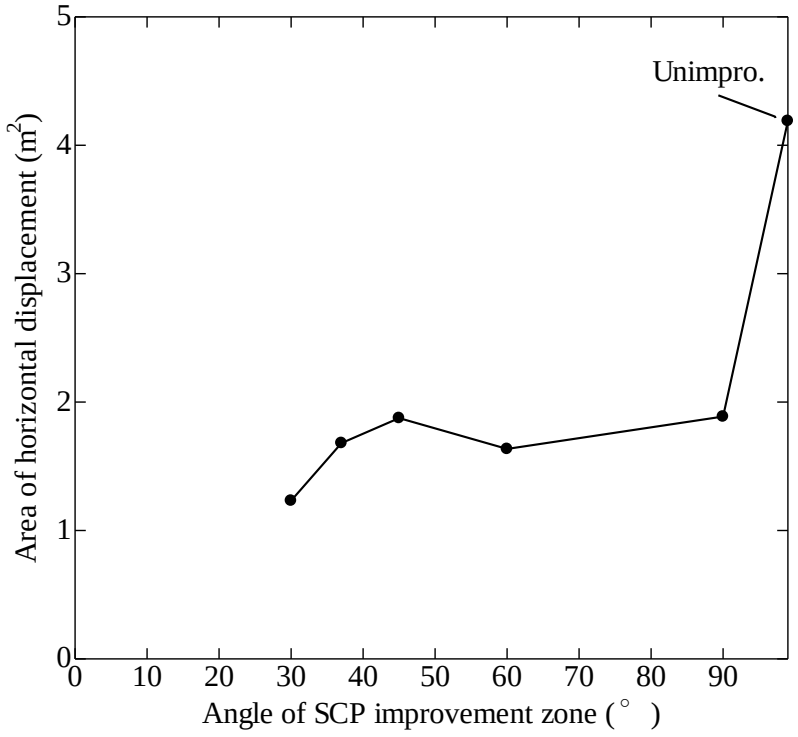

Figure 5.3.8 Relation of angle of SCP improvement zone and area of horizontal displacement under embankment toe

5.3.6 Liquefied soil pressures under embankment

The cause of the lateral displacement of the ground below the embankment is that the excess pore water pressure generated due to shaking in the ground below the embankment, which acts toward the ground next to soil under the embankment toe (in herein, defined as Area 4 shown in Figure 5.3.9) (Okamura, Ishihara and Tamura, 2006).

In this section, the effect of the angle of the improvement zone on the liquefied soil pressure acting on the soil next to the region under the embankment toe is investigated. As shown in Figure 5.3.8, the horizontal soil pressure, Pe, from the lower embankment ground, the horizontal soil pressure, Pf, from the free field, the inertial force, I, due to the earthquake and the shearing force T acting on the base must be in balanced.

$$Pe + Pf + I + T = 0 \qquad (2)$$

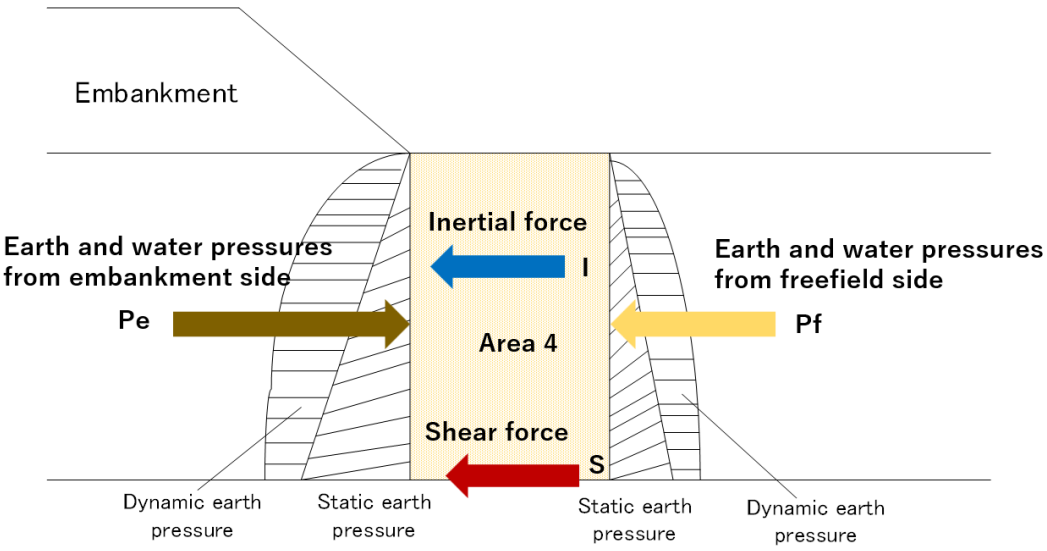

Figure 5.3.9 Schematic diagram for equilibrium of forces

Figure 5.3.10 (a) shows the soil water pressure from the embankment side, and Figure 5.3.10 (b) shows the soil water pressure from the free ground side. The soil water pressure distribution shown here is the situation at 22s. The reason for choosing 22s is that at this time, the excess pore water pressure in the foundation ground below the embankment reaches its maximum value.

Regarding the distribution of soil water pressure on the embankment side, the soil pressure of 90 ° improved ground is higher than that of unimproved ground at all depths. It is considered that this is because the excess pore water pressure rises significantly in the ground below the buttock in the ground improved by 90 °. On the other hand, in the ground where the improved body angle is smaller than 60 °, the soil water pressure from the embankment side becomes smaller. It is considered that this is because the excess pore water pressure in the ground below the buttock was suppressed by reducing the angle of the improved body and the ground below the buttock became a dense improved body, or the ground was deformed.

Figure 5.3.9(b) shows the soil pressure distribution from the free ground side. From the figure, the distribution of soil water pressure is almost the same in cases other than the ground improved by 90°. It is probable that the soil water pressure generated in the ground improved by 90° is larger than in other cases because the excess pore water pressure was generated in the vicinity of the vertically improvement zone.

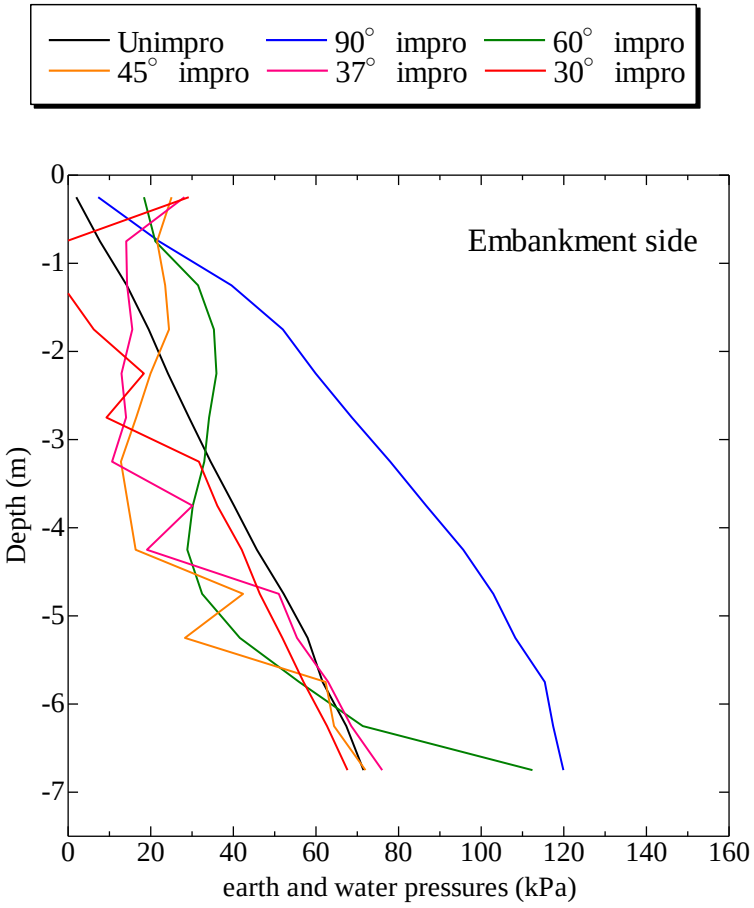

a) Earth and water pressures from embankment side

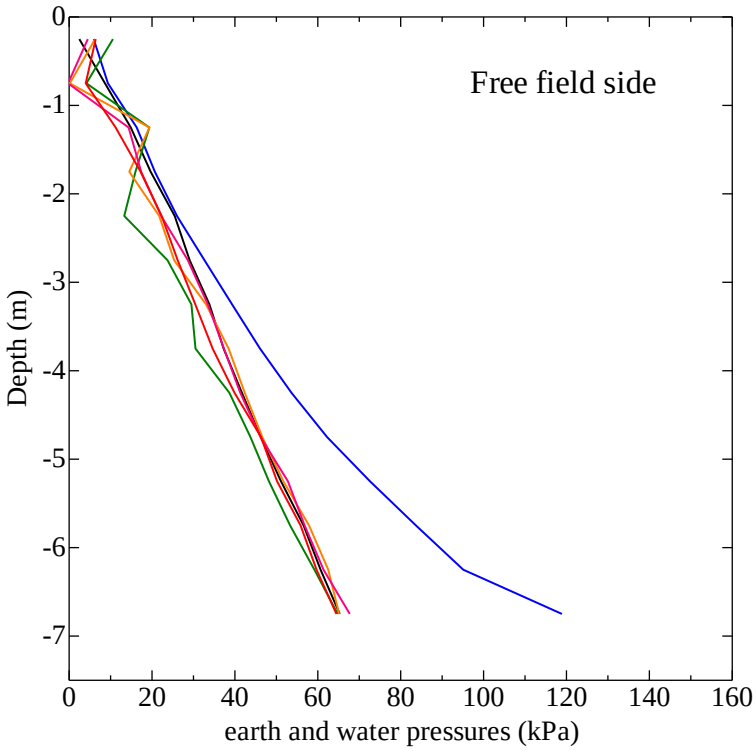

(b) Earth and water pressures from free field side

Figure 5.3.10 Earth and water pressures from embankment side and free field side

Figure 5.3.10 shows the relationship between the resultant force of soil water pressure from the embankment side and the area of horizontal displacement under the embankment toe. This figure shows the relationship from before the shaking (t = 0 s) to when the excess pore water pressure completely dissipated(t = 1000s). The resultant force of the soil water pressure from the embankment side is integrated with respect to the total depth from the distribution of the soil water pressure shown in Figure 5.3.9 (a). In the unimproved ground, the soil water pressure from the embankment side increased after the shaking began, and when it increased to about 280 kPa, the horizontal displacement increased rapidly. This indicates that when the soil pressure from the embankment side increases to 280 kPa, many soil elements next to the region under the embankment toe (i.e., in Area 4 shown in Figure 5.3.8) have reached a state of failure, resulting in causing a large deformation. On the other hand, in the improved ground of 90 °, it can be seen that the soil water pressure from the embankment side does not cause a large horizontal displacement up to 550 kPa. The horizontal displacement increased sharply from the time when it exceeded 550 kPa, but the final amount of horizontal displacement was only about half of the unimproved ground. As the angle of the improvement zone decreases from 90 ° to 60 °, the magnitude of the maximum soil water pressure from the embankment side decreases. Furthermore,

when the angle of the improved body is smaller than 50 °, it can be seen that the magnitude of the maximum soil water pressure from the embankment side is almost the same as that of the unimproved ground. However, the amount of horizontal displacement is also mitigated significantly than that in unimproved ground.

From the above results, as the angle of the improved body is reduced from 90 ° to 60 °, the area of the improvement zone decreases in Area 4, so that the overall stiffness of the ground in Area 4 become smaller. As a result, it is conceivable that the magnitude of the maximum soil water pressure from the embankment side, where the horizontal displacement increases rapidly, also decreases. When the angle of improvement zone is reduced to 50 ° or less, it is seemed that the overall stiffness of Area 4 will be almost the same as the unimproved ground. Nevertheless, in the case where the improved body angle is smaller than 50 °, the final horizontal displacement is more than half smaller than that without improvement.

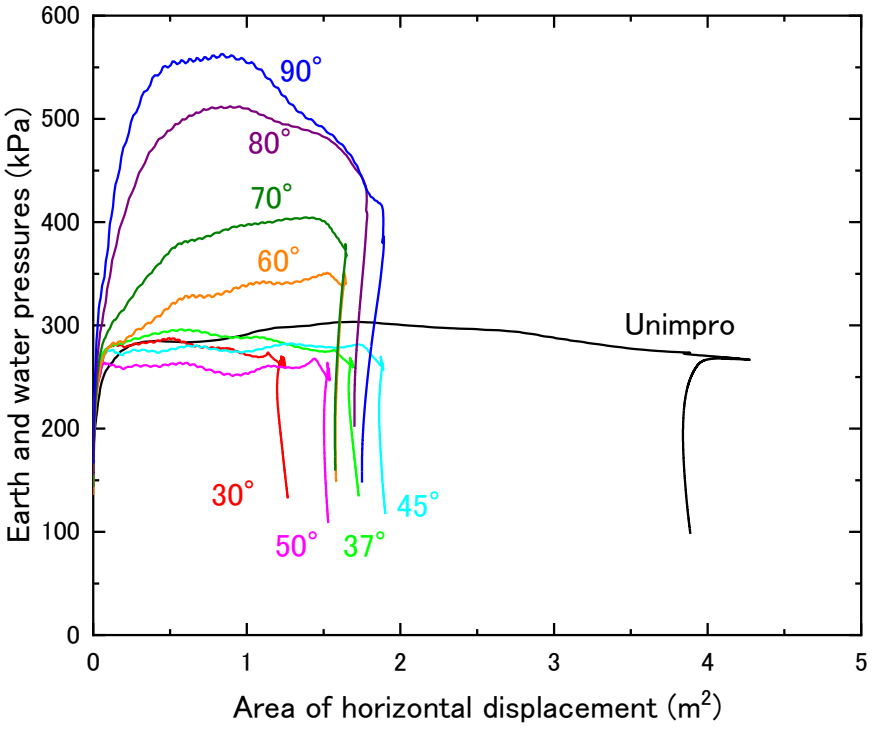

Figure 5.3.11 Relation of Area of horizontal displacement and earth water pressures

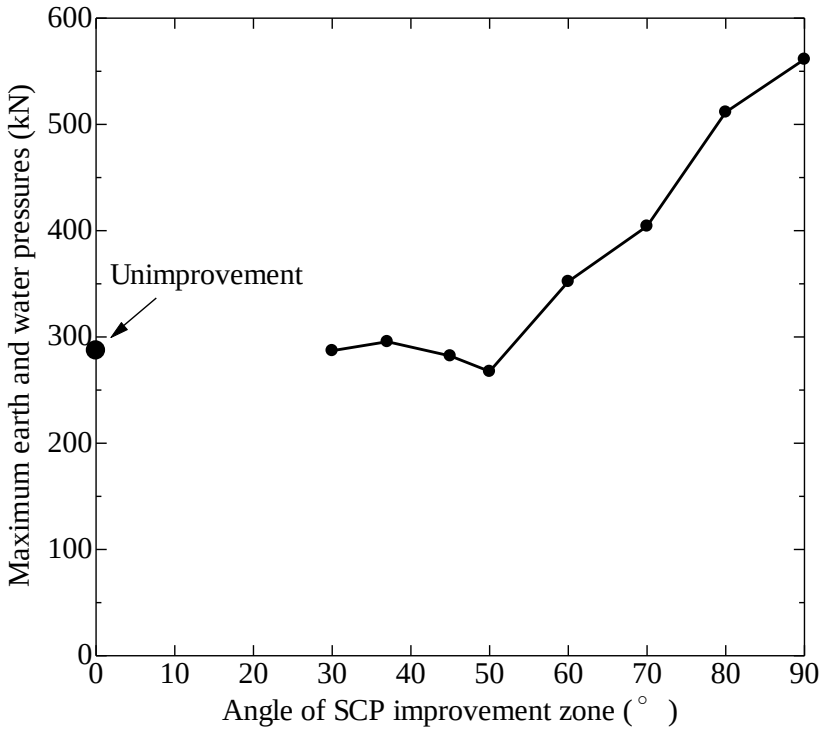

Figure 5.3.12 Relation of maximum earth water pressures and angle of SCP improvement zone

5.3.7 Vertical displacement during and after shaking

In the previous section, the horizontal displacement of the ground is discussed. However, the amount of horizontal displacement of the ground does not directly relate to the amount of settlement of the embankment. That is, just because the same amount of horizontal displacement occurs does not mean that the situation of subsidence of the embankment is the same. The situation of subsidence of the embankment differs depending on the ground conditions at the bottom of the embankment. Figure 5.3.12 shows the distribution of ground subsidence on the bottom of the embankment immediately after the shaking. From Figure 5.3.12, in the unimproved ground, the ground under the embankment settled significantly. On the other hand, it is clear from the figure that the ground with 90 ° improvement has a smaller amount of settlement on the bottom of the embankment than the ground without improvement. In the ground improved by 60 ° and 45 °, the settlement of the ground under the embankment is smaller than that of the ground improved by 90 °, but the amount of subsidence in the central part is almost the same as that of the ground improved by 90 °. In the ground improved by 30 ° and 37 °, the amount of settlement near the embankment toe is larger than in the other improved cases, but the settlement near the embankment center is smaller.

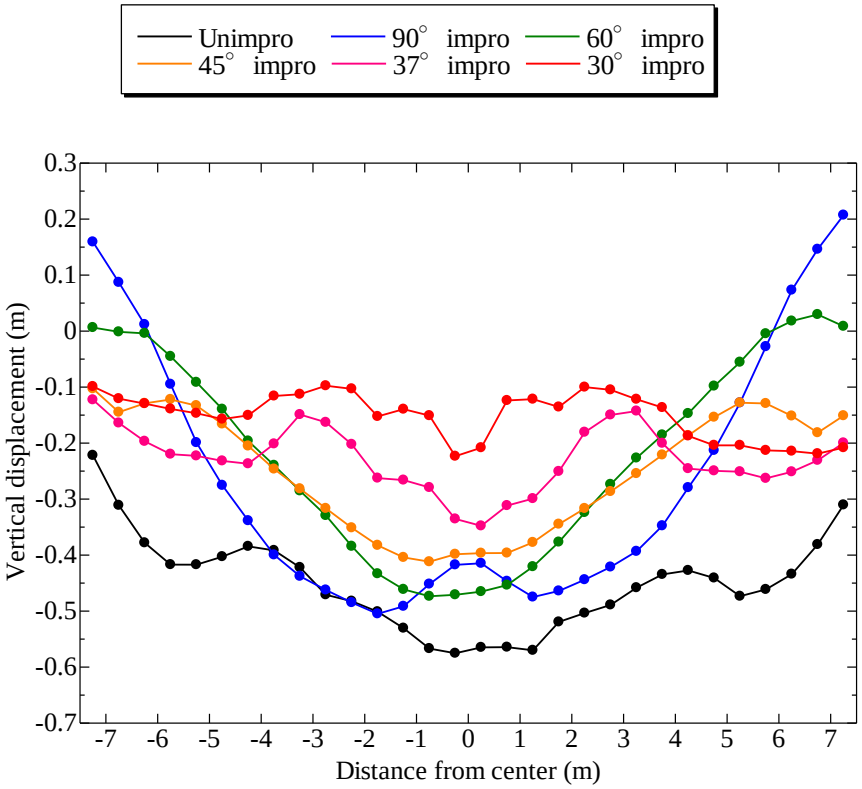

Figure 5.3.13 Distribution of vertical displacement at embankment bottom immediately after shaking (at t = 50s)

It can be seen from the above figure that the distribution of settlement at the bottom of the embankment is affected by the difference in the improvement angle. The distribution of settlement on the bottom of the embankment is influenced by various factors and is the result of very complex behavior. Among these factors, the occurrence of excess pore water pressure in the ground below the embankment is thought to have a significant effect on its deformation. Therefore, the relationship between the degree of liquefaction in the three areas of the ground below the embankment and the average settlement of the bottom of the embankment in that area is shown in Figure 5.3.14. As shown in the figure below, it can be seen that almost all points are distributed according to the fitting curve. That indicates that the settlement of the bottom of the embankment has a strong relationship with the degree of liquefaction of the ground below it.

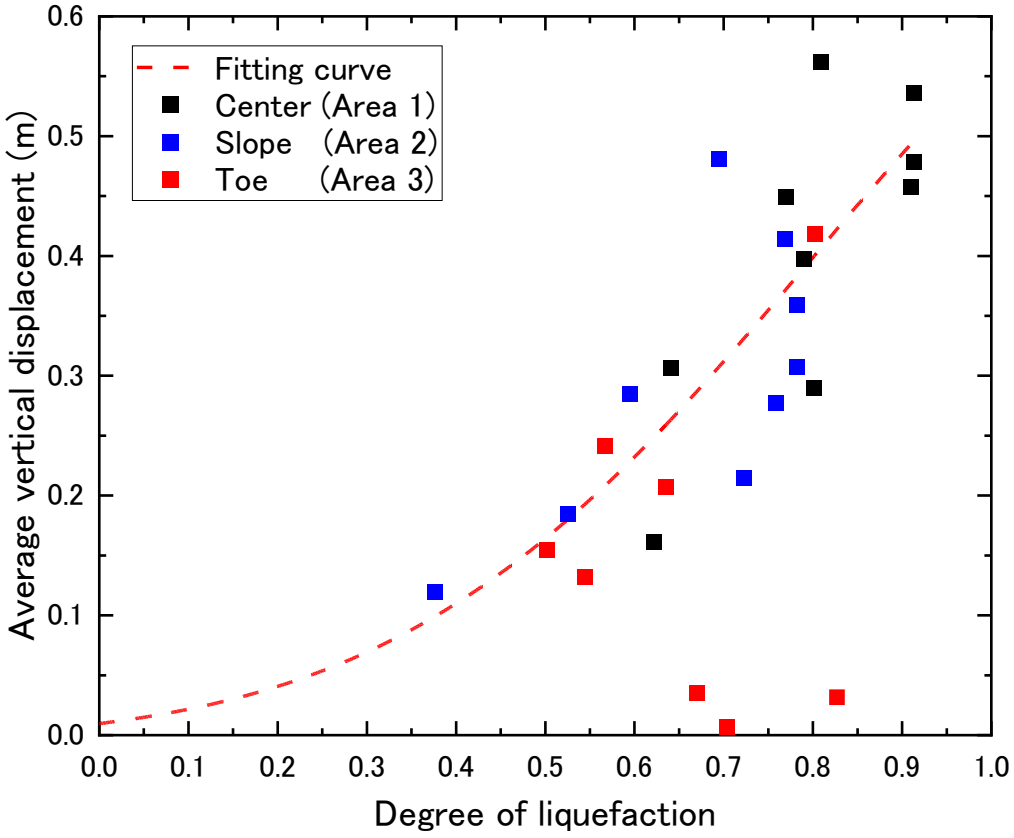

Figure 5.3.14 Relation of Average vertical displacement and degree of liquefaction under embankment (at t = 50s)

Figure 5.3.14 shows the settlement distribution on the bottom of the embankment from the end of shaking until the excess pore water pressure in the ground completely dissipated. In the unimproved ground, the amount of settlement near the embankment toe is larger than that in the center. It is considered that this is because the excess pore water pressure was larger under the embankment toe. In the 90 ° improved ground, the area below the slope of the embankment has more settlement than the central area. It is considered that this is also because the excess pore water pressure increased significantly in the ground below the slope, especially in the vicinity of the improvement zone. On the other hand, in the ground improved by 45 ° to 30 °, the settlement due to dissipation of excess pore water pressure is smaller than other cases, which may be due to the smaller excess pore water pressure generated under the embankment.

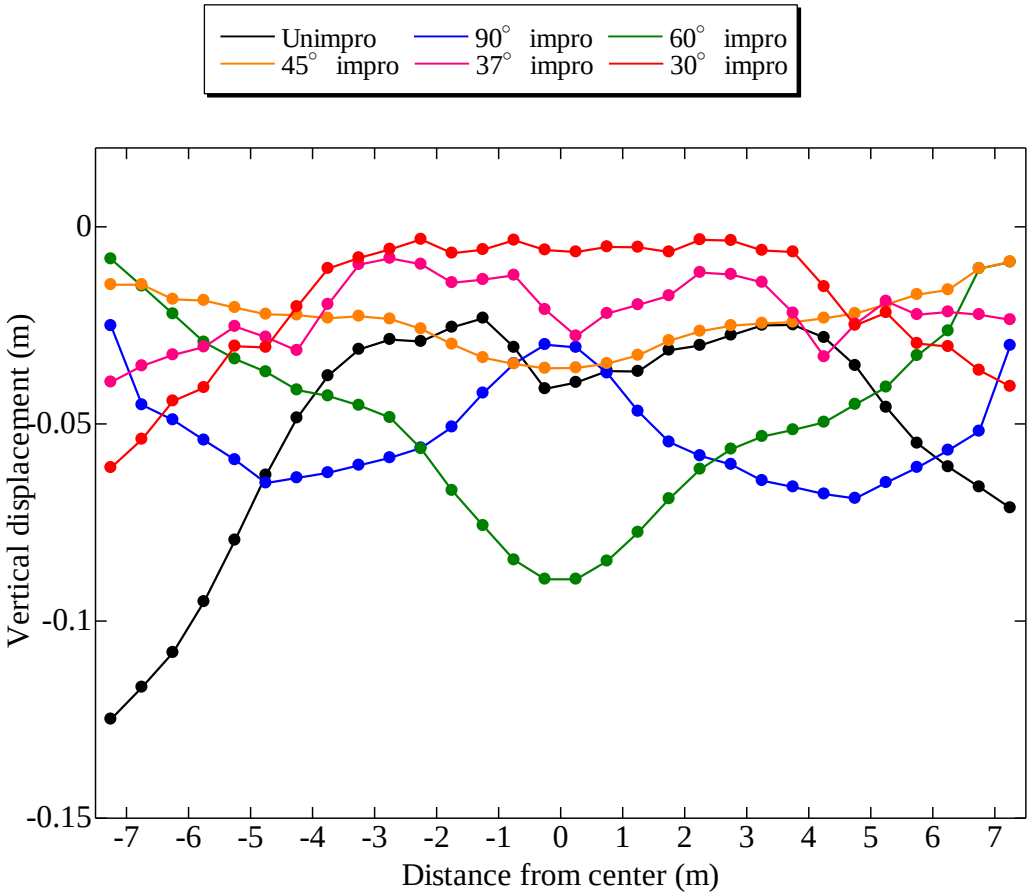

Figure 5.3.15 Distribution of vertical displacement at embankment bottom during dissipation of E.P.W.P (during t = 50～1000s)

Figure 5.3.15 shows the relationship between the improvement angle and the amount of ground settlement at the end of shaking and after the dissipation of excess pore water pressure. The black line shows the amount of ground settlement immediately after the shaking, and the red line shows the amount of land subsidence after the excess pore water pressure in the ground has completely dissipated. From the figure, it can be seen that the amount of ground settlement decreases as the angle of the improved body decreases from 90 ° to 30 °. In particular, when the temperature is smaller than 45 °, the amount of ground settlement can be further reduced.

5.3.8 Main factors on embankment settlement

researchers have previously used experimental and numerical methods to study the seismic behavior of earth embankments on liquefiable soil deposits. Some of these studies have focused on the performance of unmitigated embankments (Matsuo et al. 2000; Pagano et al. 2009; Aydingun and Adalier 2003; Maharjan and Takahashi 2014), whereas others have analyzed the influence of liquefaction mitigation strategies such as compaction, preloading, and sheet pile enclosures on the overall response of the embankment (Adalier and Aydingun 2003; Elgamal et al. 2002; Bhatnagar et al. 2015; Lopez-Caballero et al. 2016). These studies have generally identified the embankment crest settlement, arising from a combination of volumetric and shear-type deformations in the embankment and the liquefiable soil below, as the main predictor of performance. An attempt is made to quantify the settlement of the embankment induced by each fact. From the previous studies that mentioned above, it appeared that the following three major factors contributed the embankment settlement; (i) shear deformation of the embankment caused by horizontal deformation of the underlying liquefied ground, which is dominated by the horizontal displacement at the ground surface, (ii) lateral deformation of the liquefied loose sand layer below the embankment and (iii) contractive volume change of the liquefied loose sand below the embankment. These factors are schematically illustrated in Figure 5.3.16. the factors (ii) and (iii) are associated with settlement of the embankment base, while factor (i) is associated with a decrease in the embankment height. Generally, a change in volume of embankment during an earthquake is expected to be very small.

Assuming uniform settlement along the embankment base as well as uniform shear deformation of the embankment, the embankment settlement, S, due to shear deformation of embankment, S1, due to lateral deformation of soil below embankment, S2, and the contractive volume change of soil below embankment, S3, can be written as,

$$S = S1 + S2 + S3$$

$$S1 = \frac{2dH_e}{B}$$

$$S2 = \frac{2A}{B}$$

$$S3 = \varepsilon_v H_t$$

Where A=area of the later displacement under embankment toe, ε_v=volumetric stain of the liquefied soil beneath the embankment, Ht=thickness of the soil layer, dt=horizontal displacement at embankment toe, B=width of the embankment base and He=embankment height.

It should be noted that factors (ii) and (iii) assume uniform settlement along the base of embankment, while factor (i) assumes uniform shear strain and constant volume in the embankment, though uneven settlement and strain were occurred in the cases. Therefore, settlements calculated from these factors do not agree qualitatively with settlement of the embankment crest but provide the relative contribution to the crest settlement.

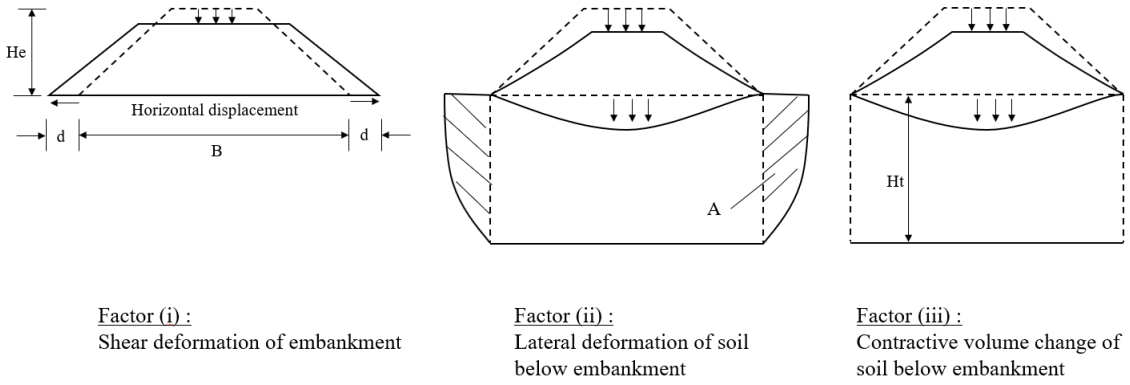

Figure 5.3.16 Three major factors contributing embankment settlement

From Figure 5.3.17, the settlement due to lateral deformation of ground can be reduced 50% to 75% in improved cases. The settlement due to shear deformation of embankment can only be reduced when the angle is smaller than 45°. The settlement due to the volumetric compression will become 2 times larger compare to unimproved case in the range from 90° to 50°, and will be reduced when the angle is smaller than 45°. In Figure 5.3.20, when compared 60° and 45° improvement, it is the case for "(a) the settlement is reduced, but the lateral spreading remains large". It is because the settlement due to the degree of liquefaction decreased, resulting in smaller contractive volume change of the ground under the embankment.

When compared 90° and 60° improvement, it is the case for "(b) the lateral spreading is reduced, but the settlement remains large". It is due to that the degree of liquefaction in 60° improvement was larger than 90° (Figure 5.3.6 (a), (b)). Therefore, it results in a large amount of settlement due to volume compression.

For "(c) both the settlement and lateral spreading are reduced.", it is the case of 30° improvement where the smallest degree of liquefaction is shown in this case. All of the settlement due to the three factors become small.

Figure 5.3.19 shows the relationship between the crest settlement and the settlement calculated from the three factors. In Figure 5.3.19, there is a good correlation of the settlements. The settlement of crest is proportional to that from three factors, irrespective of angle of SCP. The slope of the least-square-fit straight line provided in the figure depend on unevenness of the settlement profile along the embankment base and heterogeneity of strain in the embankments.

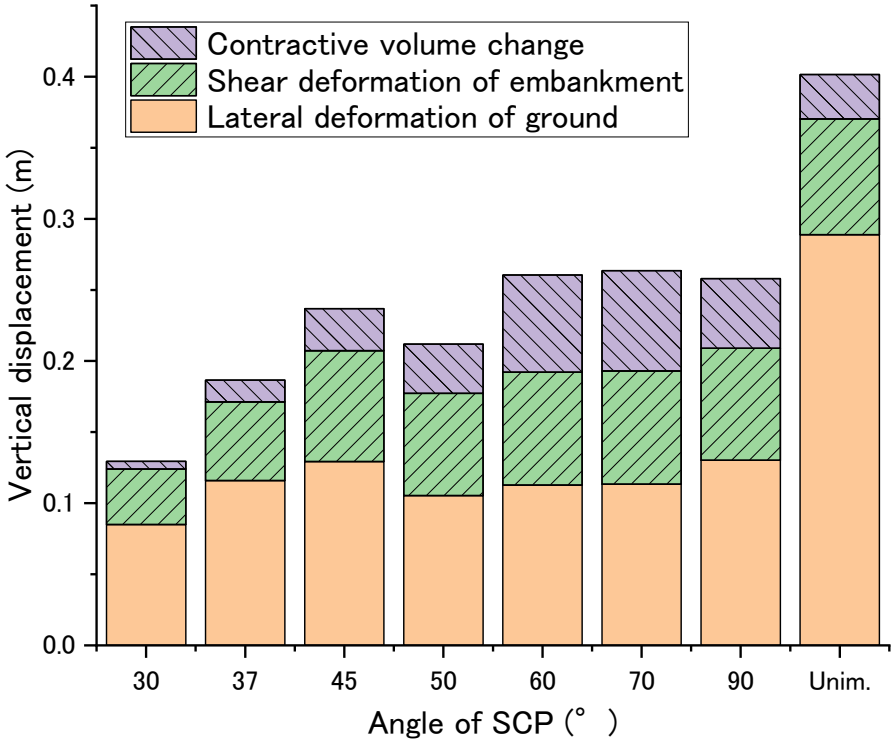

Figure 5.3.17 Main factors of embankment settlement

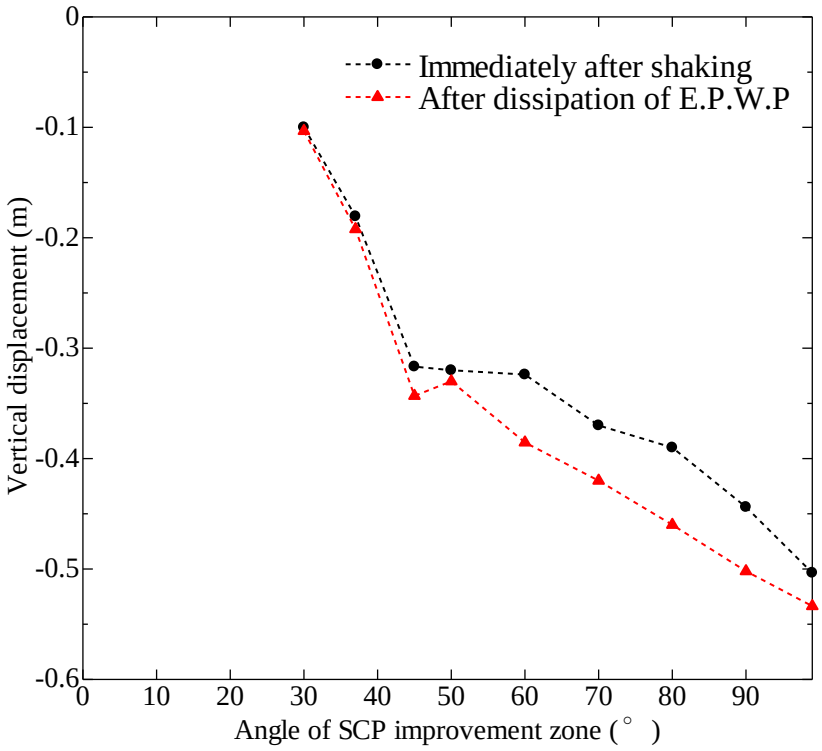

Figure 5.3.18 Relation of angle of SCP improvement zone and vertical displacement

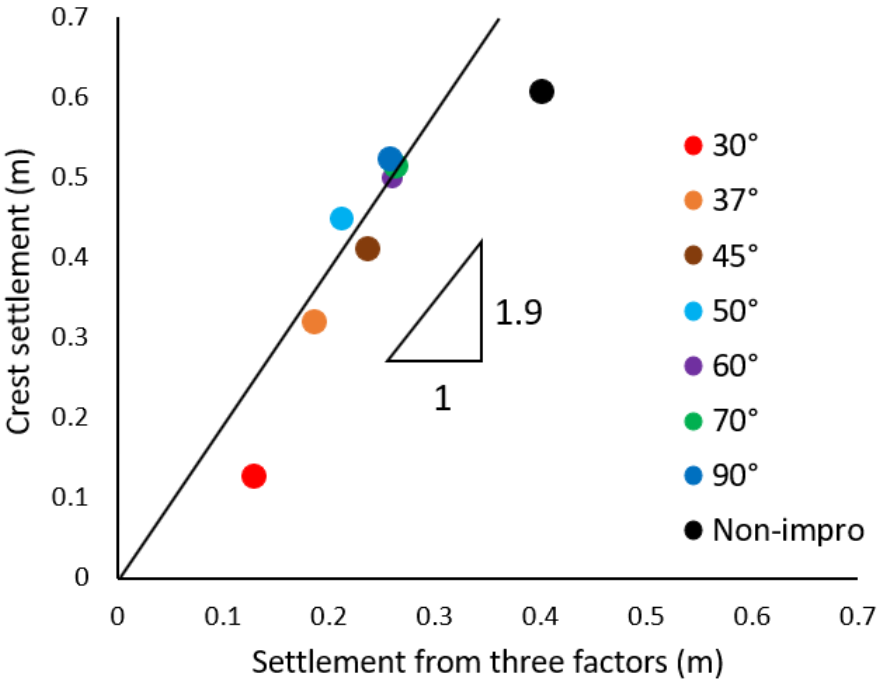

Figure 5.3.19 Relationship between crest settlement and calculated settlement

5.4 Summary

In this chapter, two-dimensional finite element analysis was used to widely change the angle of the improved body in the range of 90 ° to 30 °, and the effect of the improved angle on the deformation and settlement of the embankment on the liquefied ground was examined.

From the results of the analysis, it was found that the angle of the improved body affects the magnitude of excess pore water pressure in the ground and its distribution in the ground during the earthquake. In the ground improved by 90 ° to 60 °, the excess pore water pressure in the ground below the embankment tends to rise more easily than in the ground without improvement. The degree of liquefaction in each region in the foundation ground can be reduced by making the improvement angle smaller than 60 °. As a result, it is considered that the soil water pressure from the embankment side becomes small and the horizontal displacement under the embankment toe becomes small. Since the deformation of the ground during shaking is almost under undrained condition, it is expected that the amount of settlement of the embankment will be smaller if the horizontal displacement is suppressed. However, even if the horizontal displacement is suppressed, the shape of the settlement distribution at the bottom of the embankment differs due to the difference in the improvement angle. It was confirmed that by making the improvement angle smaller than 60 °, the excess pore water pressure in the foundation ground is suppressed, and the amount of settlement due to drainage after the end of vibration is also reduced.

Chapter 6

Effect of extent of SCP improvement on the performance of embankment

6.1 Introduction

In current, the design procedure in Japan for the extent of SCP improved ground for an existing embankment structure is limited to the area that: (1) assure the stability of the embankment structure, even if liquefaction occurs over a wide area; (2) the seismic performance of the embankment structure is satisfied with the level 2 earthquake (PWRI, 2016). But the area that controls the stability of the structure is complex because the lateral distance that is necessary to confine the liquefiable zone beneath the embankment structure from significant post-earthquake strength loss and settlement is quite uncertain. The extent of SCP improved ground for liquefaction mitigation should be designed according to the following considerations: (a) propagation of excess pore water pressure into improved area; (b) earth and water pressures applied by the liquefied sand layer beneath embankment; (c) shear strength reduction of liquefied area. Several physical model tests and numerical analyses were conducted to investigate the effect of extent of SCP improved ground on the seismic performance. Shaking table tests and seepage analyses performed by PHRI (1997) indicate that an area of softening or instability exists above a failure plane at 30 degrees with the vertical plane between the improved and unimproved zone. The strength of this area should not be expected to contribute to bearing capacity, and the improvement area should be designed wide enough to obtain sufficient bearing capacity from shear resistance. Hiro-oka *et al.* (1995) performed 25 centrifuge tests to investigate the behavior of densified sand surrounded by liquefied loose sand. The density and the extent of the improved area were varied. In all cases with an improved zone, the densification extended to the bottom of the model container. However, no structure was used in these tests. As the improved zone increased in density and extent, the weak zone becomes narrower and shallower. Hatanaka *et al.* (1987) performed 1g shaking table tests to investigate the effect of the extent of compaction area, extent of the structure, and height-to-width ratio of the structure on settlement of the structure due to liquefaction. The authors tested 13 different combinations of remediation zone geometry

and building dimensions. They found that the settlement decreases with increasing ratio of improvement width to building plan.

In the practical design of SCP improvement for an embankment resting on liquefiable ground, the extent of SCP improvement is one of the essential specifications in the design procedure. Hence, it becomes essential to investigate the effects of extent of SCP improvement on the performance of embankment. This chapter presents parametric studies of SCP improved ground by changing the extent of SCP. The analysis and computation results of the different cases are compared to investigate the efficiency and the critical extent of SCP.

6.2 Model mesh

Two-dimensional finite element simulation of the centrifuge experiment is conducted under plain-strain condition considering a domain with a unit width in the transverse direction. The discretized mesh of the numerical models are shown in Figure 6.2.1. A uniform mesh having the dimensions of 0.5 m × 0.5 m in X and Y direction, respectively, is used throughout the whole model. Boundary conditions in the numerical model are imposed in such a way that all the movements of the nodes are restricted at the bottom boundary, and the nodes along the vertical boundary are kept free to move vertically and are restricted to move horizontally during the analysis.

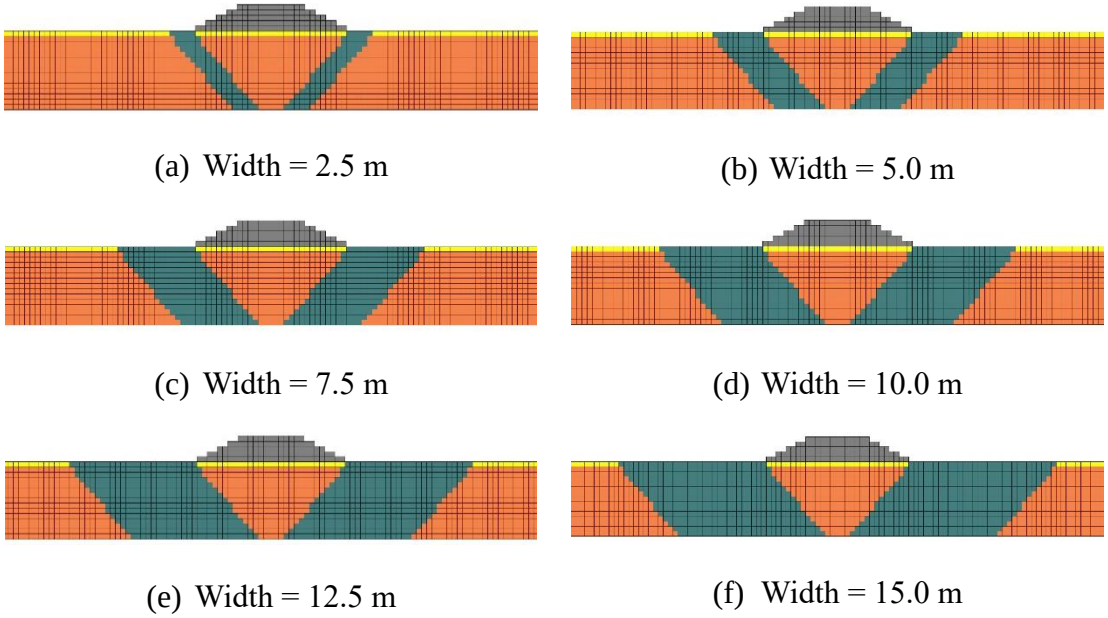

(a) Width = 2.5 m (b) Width = 5.0 m

(c) Width = 7.5 m (d) Width = 10.0 m

(e) Width = 12.5 m (f) Width = 15.0 m

Figure 6.2.1 Discretized mesh for the 2D FE analysis models

6.3 Result and discussions

6.3.1 Degree of liquefaction in foundation ground

The excess pore water pressure generated in the ground due to the earthquake reduces the effective stress of the soil, thereby reducing the stiffness and strength of the soil. Therefore, the occurrence of excess pore water pressure in the ground plays an important role in embankment and ground deformation and settlement. Therefore, in this chapter, the effect of the extent of improvement zone on the generation of excess pore water pressure in the ground is investigated first.

To graphically illustrate the magnitude of excess pore pressures at various locations within the soil profile, as an example, Figure 6.3.1 presents a comparison of different extent of improvement zone for the excess pore water pressure ratio along with the depth in the three areas below embankment in 50° improvement case at the end of shaking. The reason why chooses the point at the end of shaking to compare is mainly due to the three considerations as follow. First, at this point the fluctuation of the pore water pressure was negligible. Second, excess pore water pressure was high enough at this time to show the possibility of liquefaction. Third, the excess pore water pressure at the end of shaking accumulates the effects of the reduction in the E.P.W.P generation and dissipation.

Under the embankment center shown in Figure 6.3.1 (a), when the extent of the improvement zone is 2.5 m, the excess pore water pressure ratio increases from the ground surface toward the depth of -2 m. The excess pore water pressure ratio is almost the same in the part from the depth of -2m to the base of the ground, which is about 0.8. When the extent of the improvement zone is increased to 5 m, the distribution of excess pore water pressure ratio in the lower part of the center of the embankment is almost the same as in the case of 2.5 m in terms of shape and magnitude along with the depth. When the improvement extent is larger than 7.5 m, the excess pore water pressure ratio does not change much from the ground surface to the depth of -2 m, but the excess pore water pressure ratio become larger and has risen to around 1.0 below the depth of -2 m.

In Area 2 below the top of sloe shown in Figure 6.3.1 (b), there is no difference from the tendency seen in Area 1. That is, as the extent of the SCP improvement increases from 2.5 m to 12.5 m, the excess pore water pressure ratio also increases in the ground below the embankment. Under the embankment toe shown in Figure 6.3.1 (c), when the extent of the improvement zone is increased from 2.5 m to 5 m, the excess pore water pressure ratio becomes smaller in the ground. When the extent of the SCP improvement is larger than 5 m, the excess pore water pressure ratio increases significantly. The cause of the high excess pore water pressure in the unimproved ground below the embankment due to

the presence of the improved body is that the response acceleration propagating to the ground below the embankment increases due to the presence of the improved body, and the ground It is conceivable that the cyclic shear stress inside will increase. Similar phenomena have been confirmed in other centrifugation experiments and numerical analysis (Okamura and Matsuo, 2002; Adalier and Aydingun, 2003; Bhatnagar, Kumari and Sawant, 2016; Olarte *et al.*, 2017).

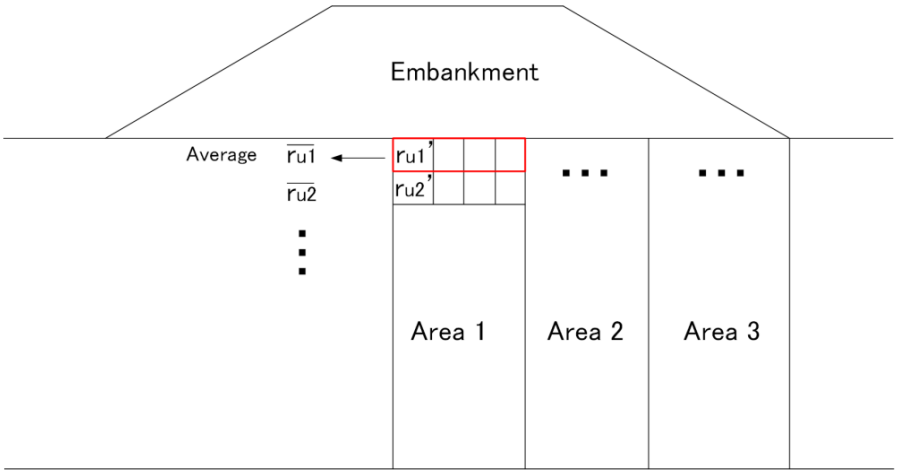

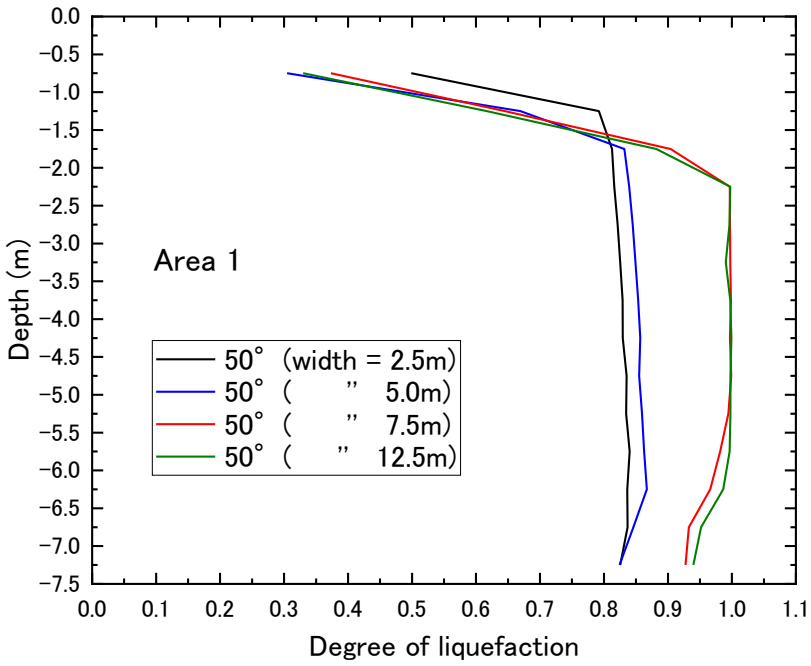

(a) Under embankment center (Area 1)

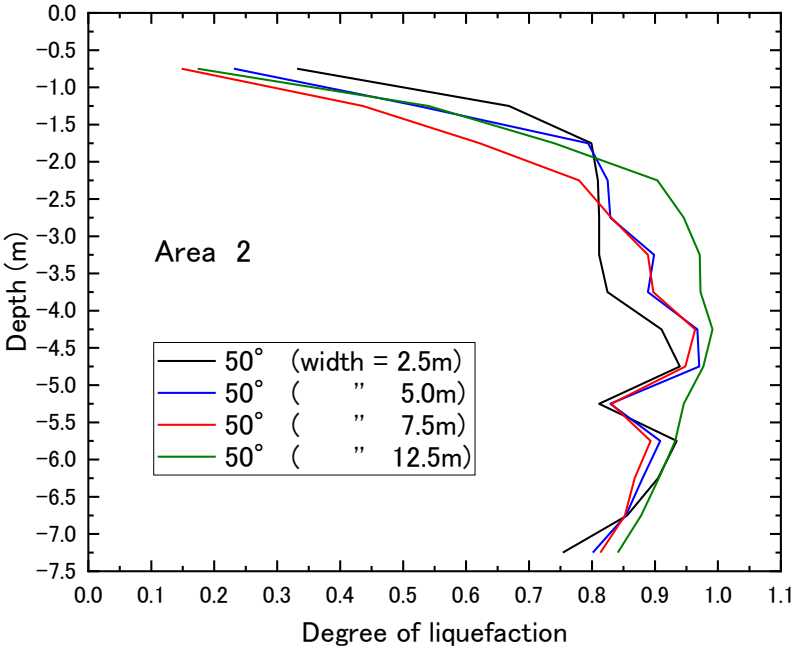

(b) Under top of slope (Area 2)

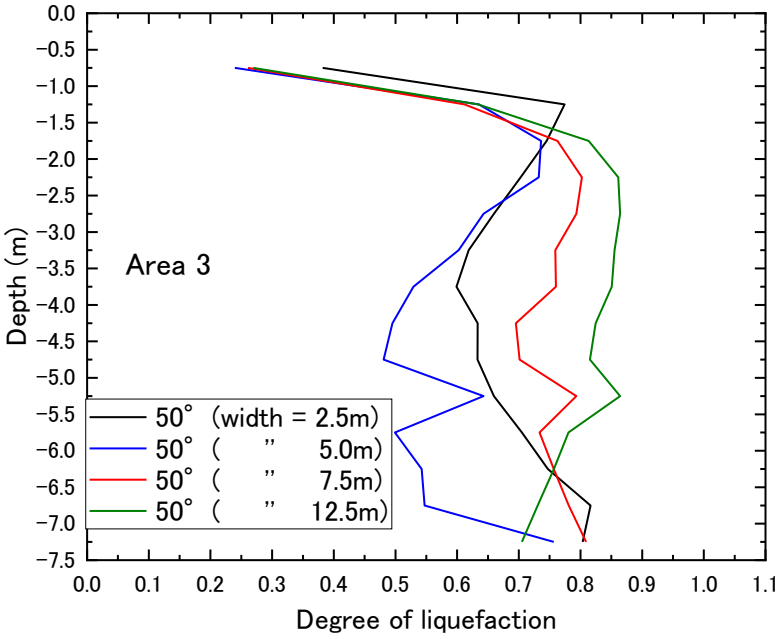

(c) Under embankment toe (Area 3)

Figure 6.3.1 Distribution of excess pore water pressure ratio under embankment at the end of shaking

In order to quantitatively examine the effect of the extent of the improvement zone on the occurrence of excess pore water pressure in the ground, the degree of liquefaction of each of the three regions under the embankment is compared. The calculation method of degree of liquefaction is described in chapter 5. Figure 6.3.2 shows the relationship between the extent of the improvement zone and the degree of liquefaction in the three areas of the ground below the embankment. In addition, in order to see the effect of the difference in the angle of the improved body together, the improved ground with improved angles of 30 °, 37 °, 50 ° and 90 ° is taken up and compared. From the definition of the degree of liquefaction, when the value becomes 1.0, it means that the excess pore water pressure ratio of all the elements is 1.0 in the region, and it is considered that the region is completely liquefied. In the region below the center of the embankment shown in Figure 6.3.2 (a), it can be seen that the value of the degree of liquefaction increases as the SCP improvement increases by 5 m or more regardless of the improvement angle. This tendency can also be confirmed in Area 2 shown in Figure 6.3.2 (b). In the areas under the center of the embankment (Area 1) and under the top of slope (Area 2), the degree of liquefaction increases as the extent of the improvement zone increases in all cases, but the magnitude is affected by the angle of the improvement zone. When the angle of the improvement zone is from 90 ° to 50 °, the degree of liquefaction is not significantly affected, but when it becomes smaller from 50 ° to 30°, it can be seen that the degree of liquefaction shifts downward. This is consistent with the trends seen in chapter 5.

In the region under the embankment toe shown in Figure 6.3.2 (c), the situation of the degree of liquefaction differs considerably not only by the extent of the improvement zone but also by the difference in the angle. In the 90 ° improved ground, the situation is the same as under the embankment center and the top of slope, that is, the degree of liquefaction increases as the extent of the improvement zone increases. In the 37 ° improved ground, the degree of liquefaction decreases from 2.5m to 7.5m, and the degree of liquefaction increases again when it reaches 7.5m or more. In the 30 ° improved ground, the degree of liquefaction decreases from 5 m to 10 m, and the degree of liquefaction does not change even if the SCP improvement increases to 10 m or more.

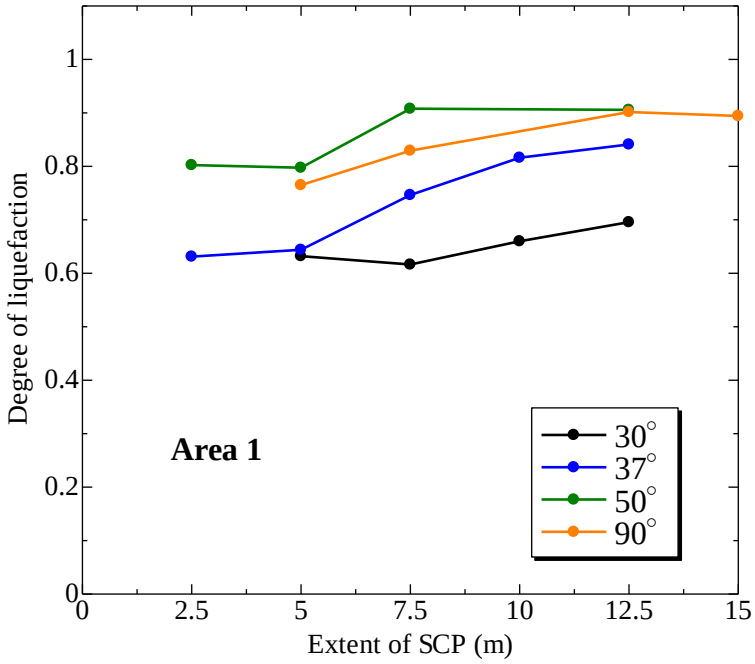

(a) Under embankment center (Area 1)

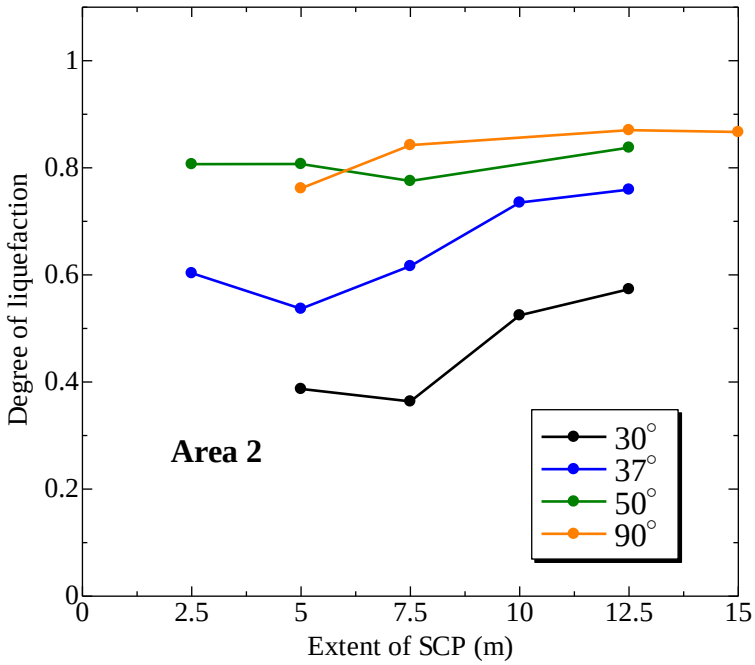

(b) Under top of slope (Area 2)

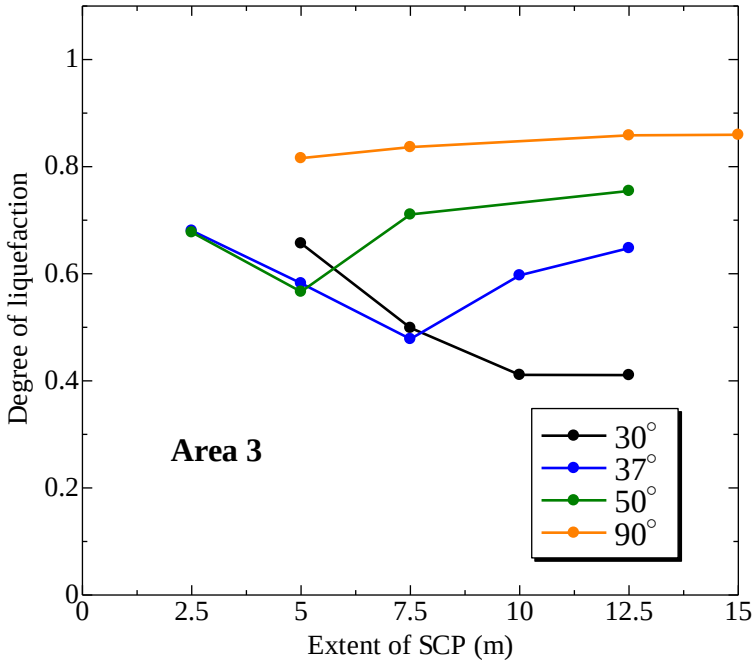

(c) Under embankment toe (Area 3)

Figure 6.3.2 Relation between the extent of SCP and the degree of liquefaction under embankment

From the above results, it is concluded that the degree of liquefaction in the ground under the embankment increases when the extent of the improvement zone exceeds a certain value (5m in this analysis). In addition, when compared in terms of the angle of the improved body, the degree of liquefaction is not significantly affected in the entire improved extent between 90 ° and 50 °, but when the angle of the improved body is smaller than 50 °, it becomes smaller in the entire improved extent. When designing a SCP improved ground, the SCP improvement must be determined to ensure the target safety factor for the embankment and ground. Another purpose of the SCP improvement is to suppress lateral flow deformation of the liquefied ground under the embankment. However, when determining the extent of the improvement zone, it should also be considered that the extent of the improvement zone causes an increase in excess pore water pressure in the ground below the embankment, which may result in reduction of bearing capacity of ground. In addition, it is possible that the amount of settlement due to contractive volume change of the ground due to water pressure dissipation will increase.

6.3.2 Efficiency of SCP improvement extent to mitigate the lateral spreading

Liquefaction-induced permanent seismic deformations experienced by well-constructed and compacted embankments typically arise from a combination of volumetric and shear-type deformations within the liquefiable soil below, as opposed to those caused by global instability within the embankment. The expected effect of the SCP improvement constructed below embankment toe is to mitigate the lateral spreading of the loose sandy soil below the embankment. It is expected that the mitigation of the lateral spreading can reduce the settlement of the embankment associated with the lateral spreading of foundation ground and embankment.

In order to examine the effect of the extent of the improvement zone on the horizontal deformation of the ground below the embankment, Figure 6.3.3 shows the horizontal displacement of the ground improved by 50°. When the extent of the improvement zone is 2.5 m, because of the build-up of excess pore water pressure below the embankment and liquefaction occurred in the free field, a certain deformation of the ground takes place. However, the stiff SCP improvement zone can constrain the liquefied soil in the loose later and make the distribution of the horizontal displacement rather straight compared to the case without SCP improvement. As a result, the ground deformation in the improved cases is significantly smaller than the ground deformation in the unimproved case. It is clearly shown that as the SCP improvement increases, the horizontal displacement become smaller at all depths. Therefore, the graphs clearly illustrate the efficiency of the SCP improvement zone to mitigate the lateral spreading.

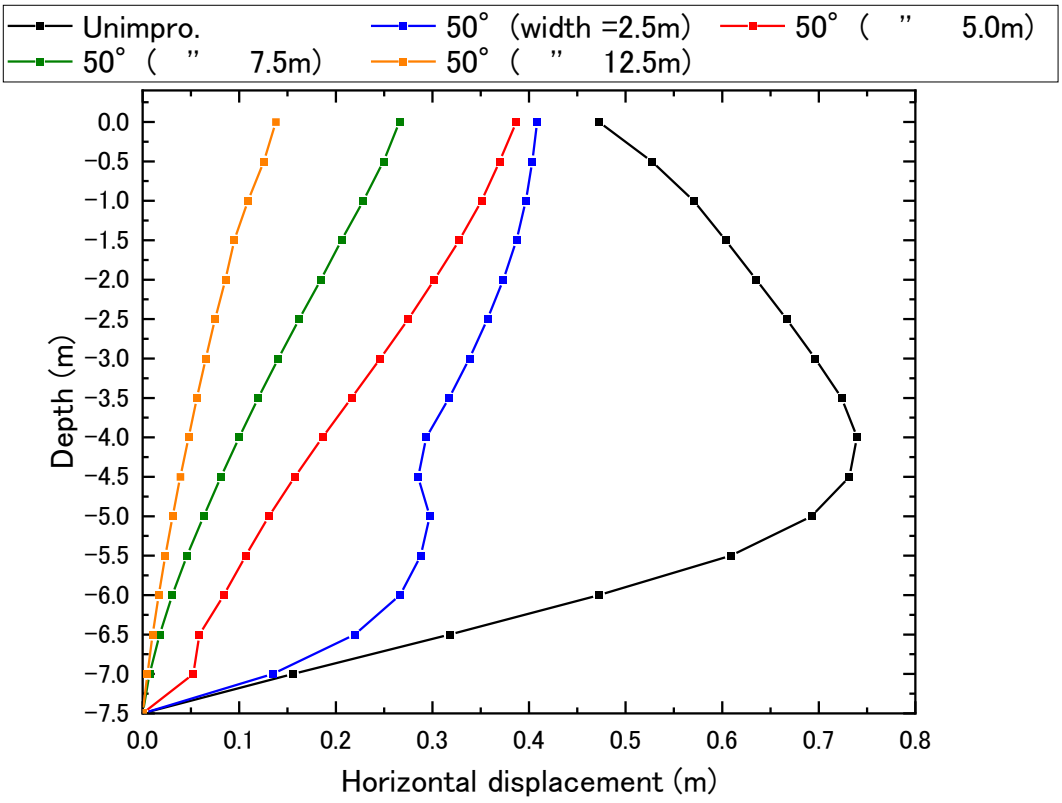

Figure 6.3.3 Distribution of horizontal displacement under the embankment toe

Figure 6.3.4 shows the relationship between the SCP improvement and the area of horizontal displacement at the bottom of the buttock at the end of vibration. In addition, in order to examine the effect of the difference in the angle of the improved body together, the improved ground with improved angles of 30 °, 37 °, 50 ° and 90 ° is taken up and compared. In all cases, it is clear that as the extent of the improvement zone increases, the amount of horizontal displacement under the embankment toe decreases. Among them, the 30 ° improved ground has the effectiveness in mitigating the horizontal displacement even if the extent of the improvement zone is relatively smaller than in other cases. The 37 ° and 50 ° improved ground has almost the same effect of mitigating the horizontal displacement as the 30 ° improved ground when the improved extent is 7.5 m or more. It can be seen that the 90 ° improved ground has a smaller effect of mitigating horizontal displacement than the diagonally improved ground in all the improved extents.

Figure 6.3.5 shows the relationship between the amount of horizontal displacement and the SCP improvement at the embankment method. When the SCP improvement is 7.5 m or less, the horizontal displacement of the buttock on the 30 ° improved ground is the smallest, and as the improved angle increases from 30 ° to 90 °, the horizontal displacement of the buttock is the smallest. Is clear to be large. On the other hand, when

the SCP improvement is larger than 7.5 m, the horizontal displacement of the 30 °, 37 ° and 50 ° improved ground is almost the same, but the 90 ° improved ground is larger than 7.5 m. However, the effect of mitigating the amount of horizontal displacement under the embankment is weaker than that of the diagonally improved ground.

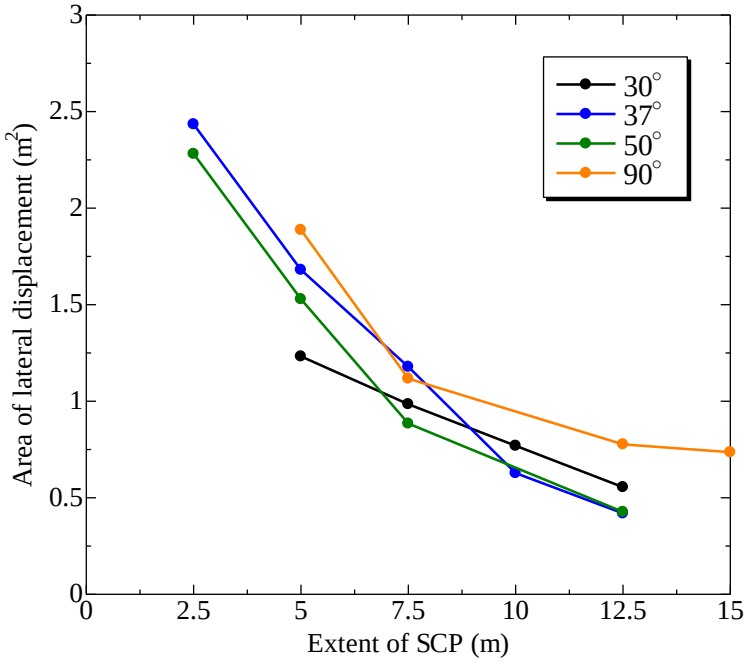

Figure 6.3.4 Relation between extent of SCP and Area of lateral displacement

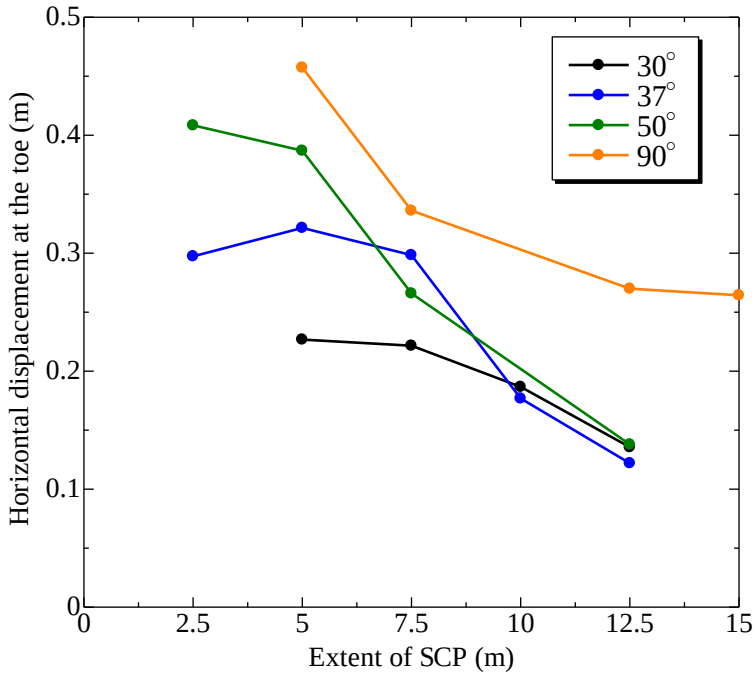

Figure 6.3.5 Horizontal displacement at the embankment toe

6.3.3 Liquefied soil pressures under embankment

In the case of creating a SCP improvement zone under an embankment toe, it was expected that the SCP improvement zone would resist the earth pressure exerted by liquefied subsoil under the embankment and, accordingly, reduce the magnitude of subsoil movement. The deformation of the SCP improvement zone was generated by the difference of earth pressures between two sides of the SCP improvement zone, including both static and dynamic water and soil pressures. The SCP improvement zone as a countermeasure against the lateral spreading of the ground and embankment carries a large amount of kinematic load imposed by the laterally spreading soil and the embankment. The water and soil pressures acting under the embankment toe provide the information regarding contribution of the SCP improvement zone to carrying the load imposed by lateral spreading.

In the free field, in all cases, it liquefied during the shaking (at about 12s), regardless of the conditions of the SCP improvement zone. Therefore, it is considered that the soil water pressures from the free field side will be the same in all cases. In herein, only the embankment side is compared here. Figure 6.3.6 - Figure 6.3.9 indicate the relationships of earth and water pressure and area of lateral displacement for 90, 50, 37 and 30° improvement cases as well as that for unimprovement case from the start to the end of shaking (during 0-50s). In 90° improvement cases as show in Figure 6.3.6, when the extent of SCP improvement is 5m (indicated by blue line), the earth and water pressure generated higher compared to unimprovement case, and then after reaching the maximum value, the earth and water pressure decreased and the lateral displacement increased. When the extent of SCP improvement changed from 5m to 12.5m, the behavior is almost same in each case until reach the maximum earth and water pressure value, however, the area of lateral displacement is smaller at the end of shaking. It is considered that this is the result of the high stiffness mobilized by the SCP improvement with a larger extent after the maximum earth and water pressures reach the maximum value that is the strength of the soil nearby the embankment toe. In cases where the SCP improvement angle smaller than 50° (Figure 6.3.7 - Figure 6.3.9), the maximum earth and water pressures acting on the vertical plane under the embankment toe is the same when the extent of the SCP improvement is in the range of 5-12.5m.

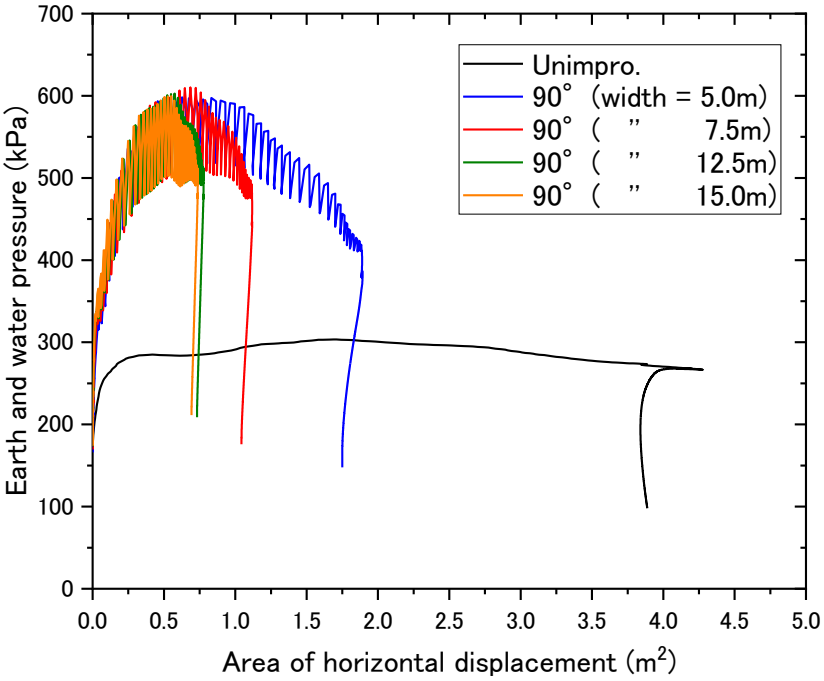

Figure 6.3.6 Relationship of earth and water pressure and area of lateral displacement for 90° improvement case

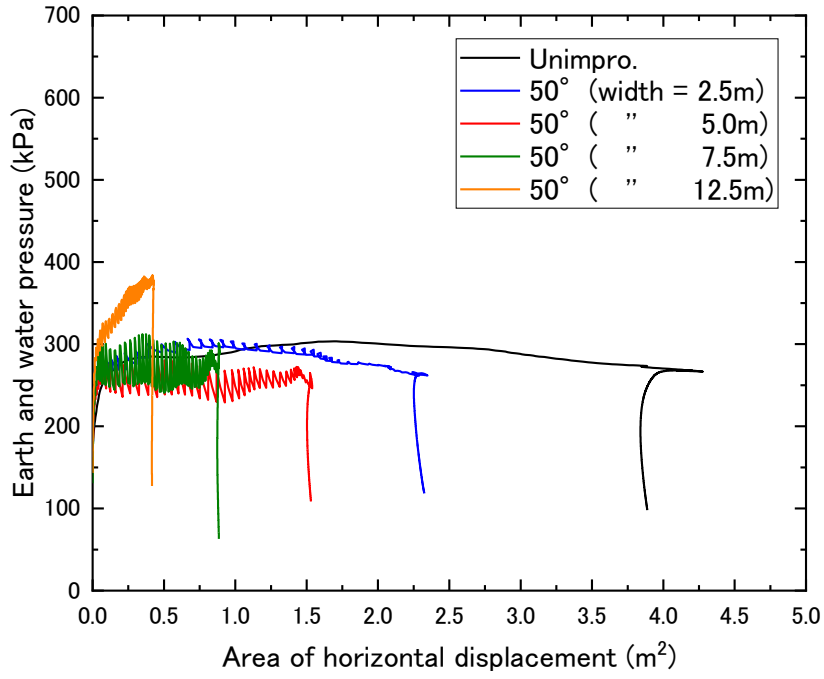

Figure 6.3.7 Relationship of earth and water pressure and area of lateral displacement for 50° improvement case

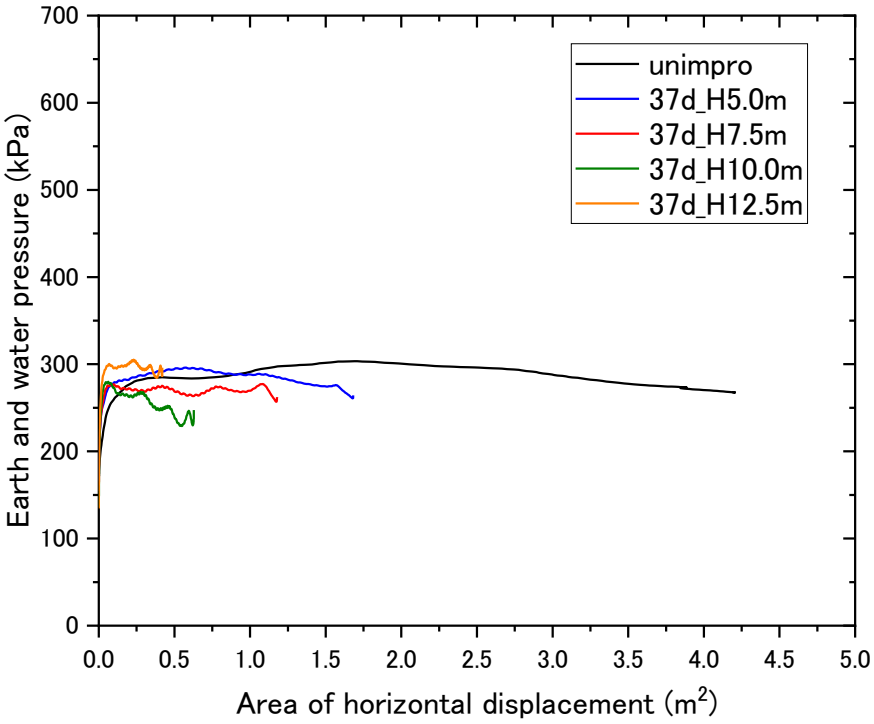

Figure 6.3.8 Relationship of earth and water pressure and area of lateral displacement for 37° improvement case

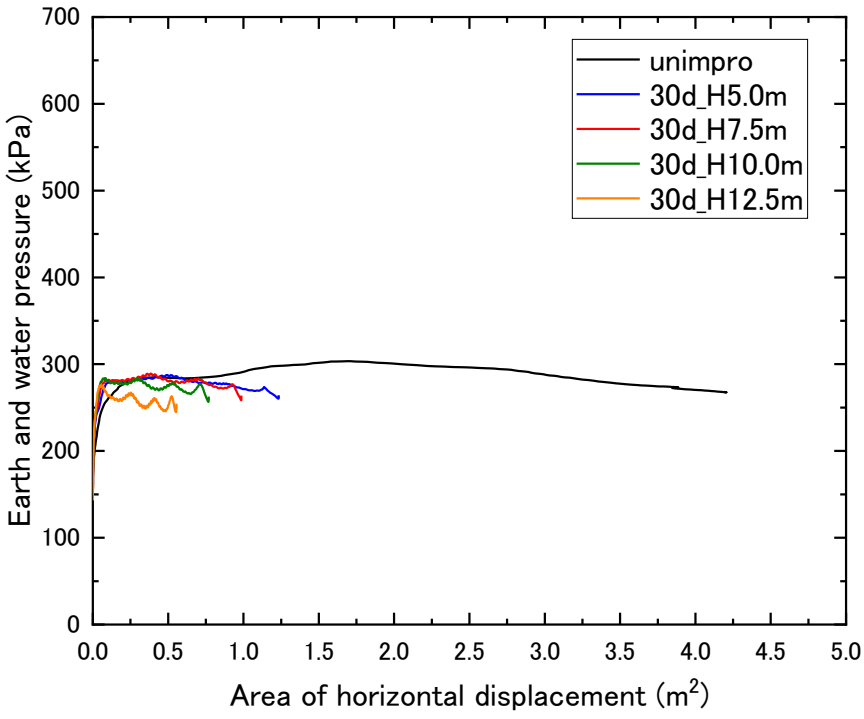

Figure 6.3.9 Relationship of earth and water pressure and area of lateral displacement for 30° improvement case

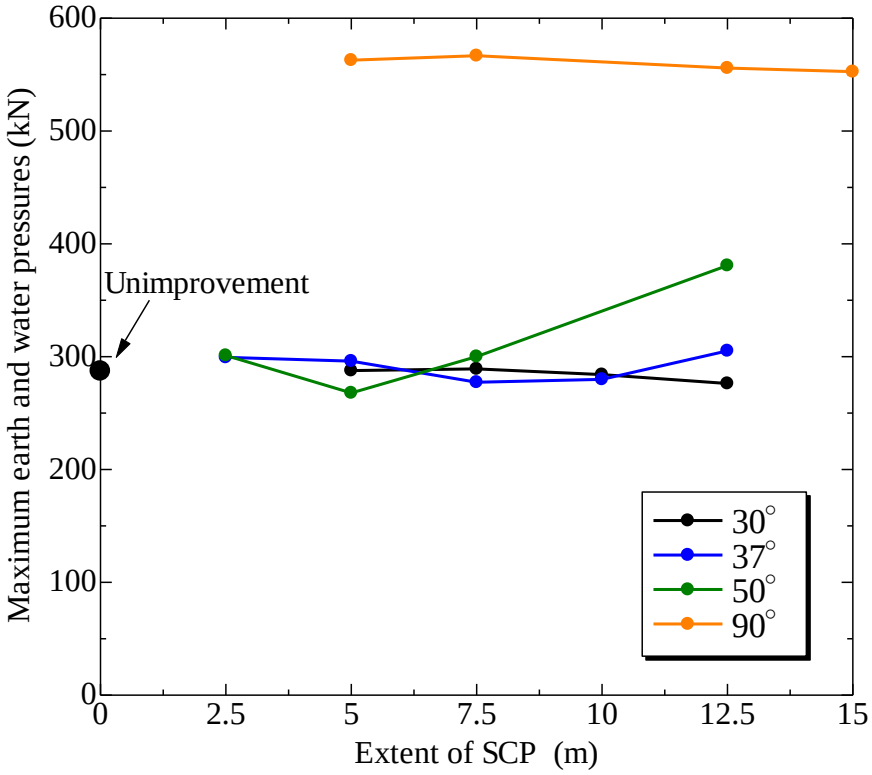

Figure 6.3.10 maximum earth and water pressure acting below embankment toe

6.3.4 Main factors on embankment settlement

Several researchers have previously used experimental and numerical methods to study the seismic behavior of earth embankments on liquefiable soil deposits. Some of these studies have focused on the performance of unmitigated embankments (Matsuo et al. 2000; Pagano et al. 2009; Aydingun and Adalier 2003; Maharjan and Takahashi 2014), whereas others have analyzed the influence of liquefaction mitigation strategies such as compaction, preloading, and sheet pile enclosures on the overall response of the embankment (Adalier and Aydingun 2003; Elgamal et al. 2002; Bhatnagar et al. 2015; Lopez-Caballero et al. 2016). These studies have generally identified the embankment crest settlement, arising from a combination of volumetric and shear-type deformations in the embankment and the liquefiable soil below, as the main predictor of performance. An attempt is made to quantify the settlement of the embankment induced by each fact. From the previous studies that mentioned above, it appeared that the following three major factors contributed the embankment settlement; (i) shear deformation of the embankment caused by horizontal deformation of the underlying liquefied ground, which is dominated by the horizontal displacement at the ground surface, (ii) lateral deformation

of the liquefied loose sand layer below the embankment and (iii) contractive volume change of the liquefied loose sand below the embankment. These factors are schematically illustrated in Figure 6.3.11. the factors (ii) and (iii) are associated with settlement of the embankment base, while factor (i) is associated with a decrease in the embankment height. Generally, a change in volume of embankment during an earthquake is expected to be very small.

Assuming uniform settlement along the embankment base as well as uniform shear deformation of the embankment, the embankment settlement, S, due to shear deformation of embankment, S1, due to lateral deformation of soil below embankment, S2, and the contractive volume change of soil below embankment, S3, can be written as,

$$S = S1 + S2 + S3$$

$$S1 = \frac{2dH_e}{B}$$

$$S2 = \frac{2A}{B}$$

$$S3 = \varepsilon_v H_t$$

Where A=area of the later displacement under embankment toe, ε_v=volumetric stain of the liquefied soil beneath the embankment, Ht=thickness of the soil layer, dt=horizontal displacement at embankment toe, B=width of the embankment base and He=embankment height.

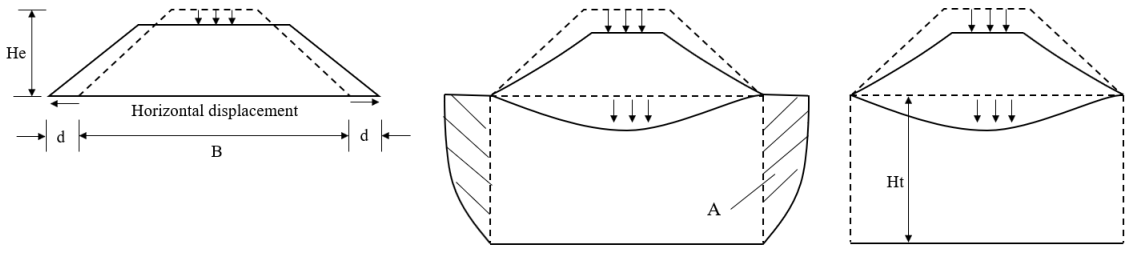

Factor (i) :
Shear deformation of embankment

Factor (ii) :
Lateral deformation of soil below embankment

Factor (iii) :
Contractive volume change of soil below embankment

Figure 6.3.11 Three major factors contributing embankment settlement

Embankment settlements from each factor for each cases are presented in Figure 6.3.12. For the ground improved by each angle of improvement, when the extent of the improvement zone become larger, settlement due to the lateral deformation of soil below embankment and the shear deformation of embankment are reduced above 50%. However, the embankment settlement due to the volume change of the soil under the embankment increased when the extent of the improvement zone increases. In 30° improved case, the settlement due to the volume change of the soil increased from 2% to 15%, in 37° improved case, that increased from 3% to 34%, in 50° improved case, that increased from 4% to 44% and that increased from 12% to 38% in 90° improved case. It indicates that the 90° improvement case, even though the settlement due to the lateral deformation of soil below embankment and the shear deformation of embankment are mitigated significantly, the large amount of contractive volume change will lead to a large embankment settlement. The improvement under the embankment (such as 30° improvement case) is more effective in mitigating the embankment settlement.

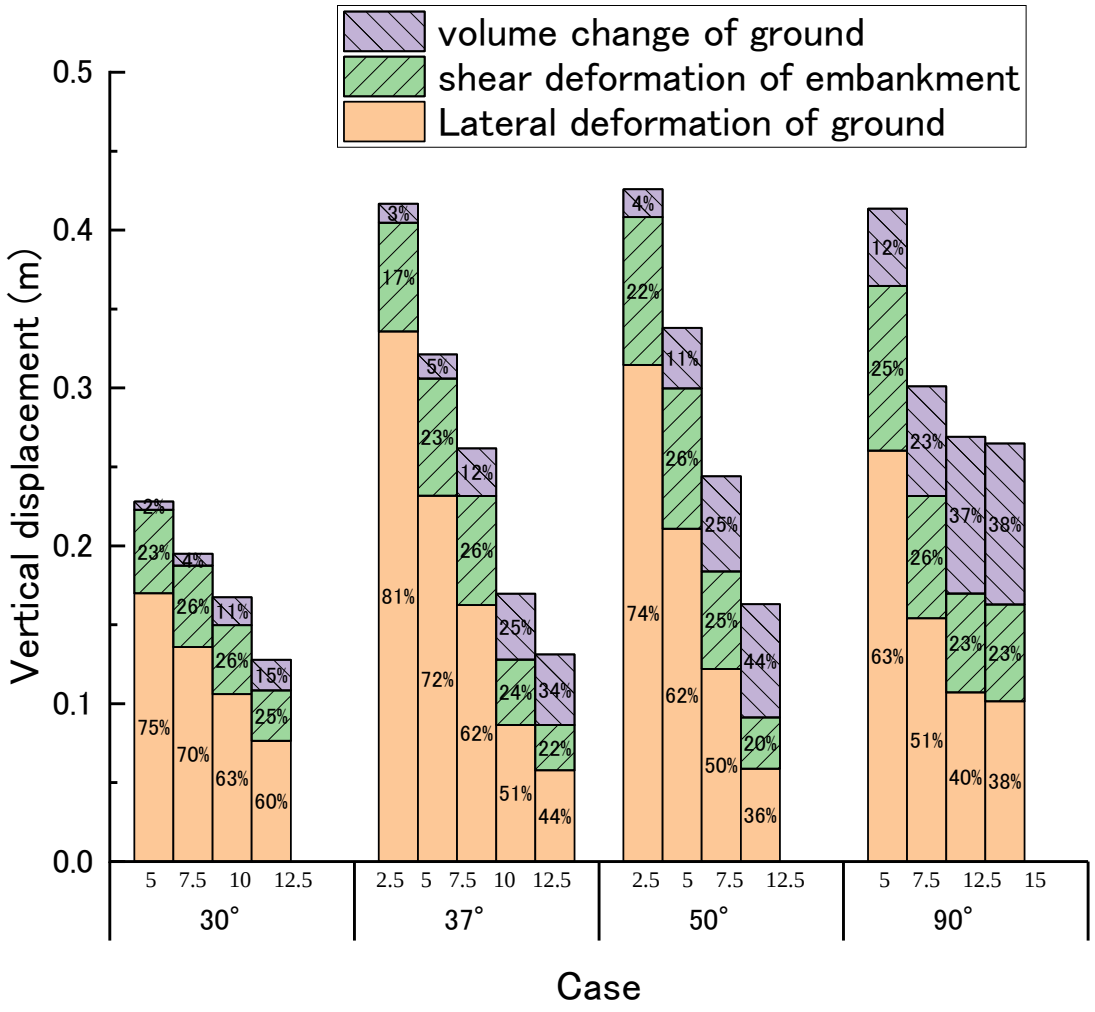

Figure 6.3.12 Major factors of embankment settlement

6.4 Summary

In this chapter, two-dimensional finite element analysis was carried out to investigate the effect of the extent of SCP improvement on the deformation of ground and settlement of the embankment. It was found from the numerical analyses results that as the extent of the SCP improvement increases, the excess pore water pressure in the unimproved ground below the embankment also increases. Nevertheless, it was confirmed that increasing the extent of the SCP improvement is effective in suppressing the lateral deformation of the ground below the embankment. For the area of lateral displacement, there is no significant difference between the different SCP improvement angles. However, for the horizontal displacement at the embankment toe, the effect of the extent of SCP improvement differs depending on the angle of the SCP improvement. The case of diagonal improvement is more effective than the case of 90° improvement. By increasing the extent of the SCP improvement, the amount of settlement of the embankment due to lateral deformation of the ground decreases, but the amount of settlement due to volume change of ground increases, especially in the 90° improvement case.

Chapter 7

Conclusions and recommendations

Liquefaction has usually caused severe damage to embankment structures. There are two main types of factors that are lateral deformation and seismic failure, regarding the embankment damages. The lateral deformation of the foundation ground is typically responsible for damage of the embankment. As a densification method, the sand compaction pile (SCP) method is widely used as a countermeasure against liquefaction and associated ground deformation. However, the conventional SCP method is difficult to apply for existing embankment. A new type of SCP method was developed. The sand piles can be constructed in any direction from the toe of embankment. So, the soil under embankment can be improved. This study focuses on the effect of the various geometric forms of SCP on seismic performance of embankment. To this end, a series of dynamic centrifuge experiments were carried out on embankment ground improved with different angle of SCP. Numerical analyses were also conducted to simulate the experimentally observed behavior and to conduct parametric studies.

In conventional SCP improvement case, where the SCP are constructed vertically under embankment toes, the lateral deformation of the ground can be reduced by about 50%. However, the settlement of the embankment crest is only about 10% smaller. It is probable that this is because the liquefaction of the ground below the embankment cannot be suppressed in this case, and the ground below the embankment deformed toward the embankment toe. On the other hand, in the diagonal improvement ground, the ground under the embankment can be improved. When the improvement rate is 20% or more, the degree of liquefaction is reduced and the deformation of the soil in the area is reduced. If the mitigation effect on lateral deformation is the same, the smaller the uplift deformation under the embankment slope, the smaller the settlement of the embankment crest. By improving the deep layer below the embankment crest, the deformation of the deep portion of the ground is suppressed, and the settlement at the bottom of the embankment becomes flatter. In addition, in vertical improvement case, the settlement of embankment cannot be reduced so much even if the extent of the improvement zone is increased. This is because the deformation of the ground under the embankment slope cannot be suppressed.

7.1 Conclusions

Chapter 3: Centrifuge study on the effect of SCP improvement geometry on mitigation of liquefaction-induced embankment settlement

A series of dynamic centrifuge tests are carried out to investigate the effects of the angle of SCP improvement zone on mitigating liquefaction-induced settlement of embankment crest. The following major conclusions are drawn from the test results:

(1) The excess pore water pressure (EPWP) responses in the ground are influenced by the angle of the improvement zone. During the small shaking (150gal), the maximum EPWP under the embankment center and near the toe in case of 60° and 50° improvement zones is less in comparison with the unimprovement case and 90° improvement case. During the larger shaking (220gal), the maximum EPWP under the embankment center at deep layer tends to become higher values in cases of 60° and 50° improvement zones in comparison with the unimprovement case and 90° improvement case. At a shallower portion of the foundation ground under the embankment center, the trend of the maximum EPWP is similar to that during the small shaking, but there is a marginal difference between cases under the toe.

(2) It is confirmed that the lateral displacement beneath the embankment toes is mitigated by the presence of the improvement zone installed in the foundation ground. Especially, the case with 50° improvement zone is the most effective and contributes to the less settlement of the embankment.

(3) The deformation pattern of the soil below the embankment toe is also important for the mitigation of crest settlement. In the case with 90° improvement zone, relatively larger heave is observed beneath the embankment toe, whereas in the 60° and 50° improvement cases, such heave deformation near the toe is suppressed. Since this heave deformation beneath the toe makes the crest settlement larger, it is suggested that in addition to lateral displacement beneath the embankment toe, the deformability of the soil under the embankment toe is also important for mitigating the crest settlement of embankment.

Chapter 4: Numerical analyses on behavior of SCP improved ground with various geometry

After the validation of the numerical tool, the numerical model was applied to simulate the centrifuge experiments to study the effects of the SCP improvement angle on the seismic performance. By comparing the experimental and analytical results, it can be said

that the numerical tool has confidence in ability of simulation for the realistic behavior on embankments and saturated soils during dynamic loading events.

It is found from the results that the shear deformation of the foundation ground under the embankment is a major factor in settlement. In the improved cases, the lateral deformation of the foundation ground under the embankment can be significantly reduced, while the settlement due to contractive volume change is observed larger in improved cases because the larger excess pore water pressure occurred. The total average vertical displacements in the 90° improvement case (Model-2) and the 50° improvement case (Model-3) are about 65% and 50%, respectively, compared to the unimprovement case (Model-1).

Chapter 5: Effect of angle of SCP improvement on the mitigation of embankment settlement

In this chapter, two-dimensional finite element analysis was used to widely change the angle of the improved body in the range of 90 ° to 30 °, and the effect of the improved angle on the deformation and settlement of the embankment on the liquefied ground was examined.

From the results of the analysis, it was found that the angle of the improved body affects the magnitude of excess pore water pressure in the ground and its distribution in the ground during the earthquake. In the ground improved by 90 ° to 60 °, the excess pore water pressure in the ground below the embankment tends to rise more easily than in the ground without improvement. The degree of liquefaction in each region in the foundation ground can be reduced by making the improvement angle smaller than 60 °. As a result, it is considered that the soil water pressure from the embankment side becomes small and the horizontal displacement under the embankment toe becomes small. Since the deformation of the ground during shaking is almost under undrained condition, it is expected that the amount of settlement of the embankment will be smaller if the horizontal displacement is suppressed. However, even if the horizontal displacement is suppressed, the shape of the settlement distribution at the bottom of the embankment differs due to the difference in the improvement angle. It was confirmed that by making the improvement angle smaller than 60 °, the excess pore water pressure in the foundation ground is suppressed, and the amount of settlement due to drainage after the end of vibration is also reduced.

Chapter 6: Effect of extent of SCP improvement on the performance of embankment

In this chapter, two-dimensional finite element analysis was carried out to investigate the effect of the extent of SCP improvement on the deformation of ground and settlement of the embankment. It was found from the numerical analyses results that as the extent of the SCP improvement increases, the excess pore water pressure in the unimproved ground below the embankment also increases. Nevertheless, it was confirmed that increasing the extent of the SCP improvement is effective in suppressing the lateral deformation of the ground below the embankment. For the area of lateral displacement, there is no significant difference between the different SCP improvement angles. However, for the horizontal displacement at the embankment toe, the effect of the extent of SCP improvement differs depending on the angle of the SCP improvement. The case of diagonal improvement is more effective than the case of 90° improvement. By increasing the extent of the SCP improvement, the amount of settlement of the embankment due to lateral deformation of the ground decreases, but the amount of settlement due to volume change of ground increases, especially in the 90° improvement case.

7.2 Recommendations

In practice, the shape of embankments varies and the natural soil profile of foundation ground is more complex. It is clearly that the conditions of the embankment and foundation ground have a great influence on the effect of the improvement ground, which affects the performance of the embankment. In this study, the shape of the embankment is constant and the foundation ground is modeled as a uniform sand layer. To be more generalized about the effects of SCP improvement with various geometries on the embankment performance, following are some additional recommendations for further studies.

(1) The shape of embankment (i.e., the height, the slope angle of embankment) and the thickness of liquefiable layer might influence the performance of the SCP improvement. Further study is necessary on changing those conditions.

(2) A prediction method should be developed for assess settlement of embankments improved with various geometric improvement.

Reference

Abe, H. (1996) ‘Liquefaction shaking table tests for sandy ground with embankment’, *Japan society of civil engineers*, 554(III–37), pp. 1–17.

Adalier, K. and Aydingun, O. (2003) ‘Numerical analysis of seismically induced liquefaction in earth embankment foundations. Part II. Application of remedial measures’, *Canadian Geotechnical Journal*, 40, pp. 766–779. doi: 10.1139/t03-026.

Adalier, K., Elgamal, A.-W. and Martin, G. R. (1998) ‘Foundation liquefaction countermeasures for earth embankments’, *Journal of Geotechnical and Geoenvironmental Engineering*, 124(6), pp. 500–517.

Adalier, K. and Elgamal, A. (2004) ‘Mitigation of liquefaction and associated ground deformations by stone columns’, *Engineering Geology*, 72, pp. 275–291. doi: 10.1016/j.enggeo.2003.11.001.

Adamidis, O. and Madabhushi, S. P. G. (2017) ‘Deformation mechanisms under shallow foundations on liquefiable layers of varying thickness’, *Géotechnique*, pp. 1–12. doi: 10.1680/jgeot.17.P.067.

Alarcon-Guzman, A., Leonards, G. A. and Chameau, J. L. (1988) ‘Undrained monotonic and cyclic strength of sands’, *Journal of Geotechnical Engineering*, 114(10), pp. 1089–1109.

Bhatnagar, S., Kumari, S. and Sawant, V. A. (2016) ‘Numerical Analysis of Earth Embankment Resting on Liquefiable Soil and Remedial Measures’, *International Journal of Geomechanics*, 16(1), p. 04015029. doi: 10.1061/(ASCE)GM.1943-5622.0000501.

Dashti, S. *et al.* (2010) ‘Centrifuge Testing to Evaluate and Mitigate Liquefaction-Induced Building Settlement Mechanisms’, *Journal of Geotechnical and Geoenvironment Engineering*, 136(7), pp. 918–929. doi: 10.1061/ASCEGT.1943-5606.0000306.

Dobry, R. and Liu, L. (1994) ‘Centrifuge modelling of soil liquefaction’, in *Earthquake Engineering, Tenth World Conference*. Balkema, Rotterdam, pp. 6801–6809.

Elgamal, A. *et al.* (2002) ‘Numerical analysis of embankment foundation liquefaction countermeasures’, *Journal of Earthquake Engineering*, 6(4), pp. 447–471.

Finn, W. D. L. (1998) ‘Postliquefaction deformation of embankment and effects on restraining piles’, *Transportation research record*, (1633), pp. 19–25.

Fukushima, S. and Tatsuoka, F. (1984) ‘Strength and deformation characteristics of saturated sand at extremely low pressures’, *Soils and Foundations*, 24, pp. 30–48. doi: 10.3208/sandf1972.24.4_30.

Ghafghazi, M., Dejong, J. T. and Wilson, D. W. (2017) ‘Evaluation of Becker penetration test interpretation methods for liquefaction assessment in gravelly soils’, 1283(April), pp. 1272–1283.

Ghosh, B. (2003) ‘Behaviour of Rigid Foundation in Layered Soils During Seismic Liquefaction’, *PhD thesis, Department of Engineering, University of Cambridge*.

Ghosh, B. and Madabhushi, S. P. G. (2007) ‘Centrifuge modelling of seismic soil structure interaction effects’, *Nuclear Engineering and Design*, 237(8), pp. 887–896. doi: 10.1016/j.nucengdes.2006.09.027.

Hamada, M. *et al.* (1986) ‘Study on liquefaction-induced permanent ground displacements and earthquake damage’, *JSCE*, III–6(376), pp. 221–229. doi: 10.2208/jscej.1986.376_221.

Harada, K. and Ohbayashi, J. (2017) ‘Development and improvement effectiveness of sand compaction pile method as a countermeasure against liquefaction’, *Soils and Foundations*, 57(6), pp. 980–987. doi: 10.1016/j.sandf.2017.08.025.

Hashiguchi, K. and Chen, Z. P. (1998) ‘Elastoplastic constitutive equation of soils with the subloading surface and the rotational hardening’, *International Journal for Numerical and Analytical Methods in Geomechanics*, 22(3), pp. 197–227.

Hatanaka, M. *et al.* (1987) ‘Some factors affecting the settlement of structures due to sand liquefaction in shaking table tests’, *soils and foundations*, 27(1), pp. 94–101.

Hausler, E. A. (2002) *Influence of ground improvement on settlement and liquefaction: A study based on field history evidence and dynamic geotechnical centrifuge tests*.

Hiro-oka, A. *et al.* (1995) ‘Dynamic Behaviors of Compacted Sands Surrounded by Liquefied Loose Sands’, in *Proc., IS-Tokyo ’95, The First International Conference on Earthquake Geotechnical Engineering*, pp. 681–686.

Idriss, I. M. and Boulanger, R. W. (2006) ‘Semi-empirical procedures for evaluating liquefaction potential during earthquakes’, *Soil Dynamics and Earthquake Engineering*, 26, pp. 115–130. doi: 10.1016/j.soildyn.2004.11.023.

Ishihara, K., Kawase, Y. and Nakajima, M. (1980) ‘Liquefaction characteristics of sand deposits at an oil tank site during the 1978 Miyagiken-oki earthquake’, *Soils and Foundations*, 20(2), pp. 97–111.

Ishihara, K., Tatsuoka, F. and Yasuda, S. (1975) ‘Undrained deformation and liquefaction of sand under cyclic stresses.’, *Soils and Foundations*, 15(1), pp. 29–44. doi: 10.3208/sandf1972.15.29.

Ishihara, K. and Yoshimine, M. (1992) ‘evaluation of settlements in sand deposits following liquefaction during earthquakes’, *soils and foundations*, 32(1), pp. 173–188.

Kaneko, M. *et al.* (1995) ‘River dike failure in Japan by earthquakes in 1993’, in *3rd International Conferense on Recent Advances in Geotedhnical Earthquake Engineering and Soil Dynamics*, pp. 495–498.

Kawakami, F. and Asada, A. (1966) ‘Damage to the ground and earth structures by the Niigata earthquake of June 16, 1964’, *soils and foundations*, 6(1), pp. 14–30. doi: 10.1248/cpb.37.3229.

Kawasaki, K. *et al.* (1998) ‘Earthquake-induced settlement of an isolated footing for power transmission tower’, in *Centrifuge 98*, pp. 271–276.

Kitazume, M. (2005) *The Sand Compaction Pile Method*. doi: 10.1201/9781439824696.

Kitazume, M. *et al.* (2016) ‘New type sand compaction pile method for densification of liquefiable ground underneath existing structure’, *Journal of Geo-Engineering Sciences 3*, pp. 1–13. doi: 10.3233/JGS-150032.

Kitazume, M. and Okamura, M. (2010) ‘Contributions To “Soils and Foundations’’’: Ground Improvement”’, *Soils and Foundations*, 50(6), pp. 965–975. doi: 10.3208/sandf.50.965.

Koga, Y. and Matsuo, O. (1990) ‘Shaking table tests of embankments resting on liquefiable sandy ground’, *Soils and Foundations*, 30(4), pp. 162–174.

Kogai, Y. *et al.* (2000) ‘Use of embedded walls for mitigation of liquefaction-induced displacement in slopes and embankments’, *Soils and Foundations*, 40(4), pp. 75–93.

Li, Y. *et al.* (2019) ‘Dynamic FEM analyses on behavior of SCP improved ground with various geometry’, *Japanese Getechnical Journal*, 14(2), pp. 161–178.

López-querol, S. and Blázquez, R. (2006) ‘Identification of failure mechanisms of road embankments due to liquefaction : optimal corrective measures at seismic sites’, *Canadian Geotechnical Journal*, 43, pp. 889–902. doi: 10.1139/T06-051.

Madabhushi, G. (2014) *Centrifuge modelling for civil engineering*. CRC Press.

Marcuson, W. L. and Silver, M. L. (1987) ‘Shake-Proof Dams.pdf’, *Civil Engineering - ASCE*, 57(12), pp. 44–47.

Martin, G. R. and Finn, W. D. L. (1975) ‘Fundamentals of liquefaction under cyclic loading’, *Journal of the Geotechnical Engineering Division, ASCE*, 101(GT5), pp. 423–438.

Matsuo, O. (1996) ‘Damage to river dikes’, *soils and foundations*, Special, pp. 235–240.

Matsuo, O. *et al.* (2000) ‘Numerical analysis of seismic behavior of embankments founded on liquefiable soils’, *Soils and Foundations*, 40(2), pp. 21–39.

McCulloch, D. and Bonilla, M. (1967) ‘Railroad damage in the Alaska Earthquake’, *Journal of Soil Mechanics and Foundations Division*, 93(SM5), pp. 89–100. Available at: http://trid.trb.org/view.aspx?id=126871.

Mehrzad, B. *et al.* (2018) ‘Centrifuge study into the effect of liquefaction extent on permanent settlement and seismic response of shallow foundations’, *Soils and Foundations*, 58(1), pp. 228–240. doi: 10.1016/j.sandf.2017.12.006.

Mitrani, H. and Madabhushi, S. P. G. (2010) ‘Cementation liquefaction remediation for existing buildings’, *Ground Improvement*, 163(2), pp. 81–94. doi: 10.1680/grim.2010.163.2.81.

Montassar, S. and de Buhan, P. (2013) ‘Numerical prediction of liquefied ground characteristics from back-analysis of lateral spreading centrifuge experiments’, *Computers and Geotechnics*, 52, pp. 7–15. doi: 10.1016/j.compgeo.2013.01.010.

Nasu, M., Fujisawa, H. and Hikimoto, K. (1987) ‘An experimental study on prevention of embankment deformation due to liquefaction of sandy ground’, *Quarterly report of railway technical research institute*, 28(1), pp. 5–6.

Oka, F. *et al.* (2012) ‘Damage patterns of river embankments due to the 2011 off the Pacific Coast of Tohoku Earthquake and a numerical modeling of the deformation of river embankments with a clayey subsoil layer’, *Soils and Foundations*, 52(5), pp. 890–909. doi: 10.1016/j.sandf.2012.11.010.

Okamura, M., Ishihara, M. and Tamura, K. (2006) ‘Liquefied soil pressures on vertical walls with adjacent embankments’, *Soil Dynamics and Earthquake Engineering*, 26, pp. 265–274. doi: 10.1016/j.soildyn.2005.02.017.

Okamura, M. and Matsuo, O. (2002) ‘Effects of remedial measures for mitigating embankment settlement due to foundation liquefaction’, *IJPMG-International Journal of Physical Modelling in Geotechnics*, 2, pp. 1–12.

Okamura, M. and Tamura, K. (2004) ‘Prediction method for liquefaction-induced settlement of embankment with remedial measure by deep mixing method’, *soils and foundations*, 44(4), pp. 53–65.

Olarte, J. *et al.* (2017) ‘Centrifuge modeling of mitigation-soil-foundation-structure interaction on liquefiable ground’, *Soil Dynamics and Earthquake Engineering*. doi: 10.1016/j.soildyn.2017.03.014.

Osterberg, J. (1957) ‘Influence values for vertical stresses in semi-infinite mass due to embankment loading’, in *Proceedings of the 4th international conference on soil mechanics and foundation engineering*, pp. 393–396.

PHRI (1997) *Handbook on Liquefaction Remediation of Reclaimed Land*.

PWRI (2016) *Design manual of liquefaction countermeasures for river embankment. Public Works Research Institute, Ministry of Construction, Japan. (In Janpanese).*

Rasouli, R. *et al.* (2018) 'Mitigation of Nonuniform Settlement of Structures due to Seismic Liquefaction', *Journal of Geotechnical and Geoenvironmental Engineering*, 144(11), p. 04018079. doi: 10.1061/(ASCE)GT.1943-5606.0001974.

Rasouli, R., Towhata, I. and Akima, T. (2016) 'Experimental Evaluation of Drainage Pipes as a Mitigation against Liquefaction-Induced Settlement of Structures', *Journal of Geotechnical and Geoenvironmental Engineering*, 142(9), p. 04016041. doi: 10.1016/j.jclinane.2008.08.024.

Robertson, P. K. and Wride, C. E. (1997) 'Cyclic liquefaction and its evaluation based on SPT and CPT', in *Proceedings of the NCEER workshop on evaluation of liquefaction resistance of soils*, pp. 41–88.

Sasaki, Y. *et al.* (1992) 'Mechanism of permanent displacement of ground caused by seismic liquefaction', *soils and foundations*, 32(3), pp. 79–96.

Sasaki, Y., Moriwaki, T. and Ohbayashi, J. (1997) 'Deformation process of an embankment resting on a liquefiable soil layer', in *Proceedings of Deformation and Progressive failure in Geomechanics, IS-Nagoya'97*, pp. 553–558.

Sasaki, Y. and Tamura, K. (2007) 'Failure mode of embankments due to recent earthquakes in Japan', in *4th International Conference on Earthquake Geotechnical Engineering*, pp. 1–12.

Seed, H. B. (1968) 'Landslides during earthquakes due to soil liquefaction', *Journal of Geotechnical Engineering*, 94, pp. 1055–1123.

Seed, H. B. and Idriss, I. M. (1971) 'Simplified procedure for evaluating soil liquefaction potential', *Journal of Geotechnical Engineering Division , ASCE*, (97), pp. 1249–1273.

Seed, H. B. and Lee, K. L. (1966) 'Liquefaction of Saturated Sands during Cyclic Loading', *Journal of Soil Mechanics and Foundation Division , ASCE*, 92(SM6), pp. 105–134.

Shahir, H. *et al.* (2012) 'Evaluation of variation of permeability in liquefiable soil under earthquake loading', *Computers and Geotechnics*, 40, pp. 74–88. doi: 10.1016/j.compgeo.2011.10.003.

Sharp, M. K., Dobry, R. and Phillips, R. (2010) 'CPT-Based Evaluation of Liquefaction and Lateral Spreading in Centrifuge', *Journal of Geotechnical and Geoenvironmental Engineering*, 136(October), pp. 1334–1346. doi: 10.1061/(ASCE)GT.1943-5606.0000338.

Takahashi, A. (2002) *Soil-pile interaction in liquefaction-induced lateral spreading of soils*.

Takemura, J. *et al.* (1999) ‘Centrifuge model tests on double propped wall excavation in soft clay’, *soils and foundations*, 39(3), pp. 75–87.

Tani, S. (1991) ‘Consideration of Earthquake Damage to Earth Dam for Irrigation in Japan’, in *Proceedings of the 2nd International Conference on Recent Advances in Geotechnical Earthquake Engineering and Soil Dynamics*, pp. 1137–1142.

Tani, S. (1996) ‘Damage to earth dams’, *Soils and Foundations*, Special, pp. 263–272.

Toki, S. *et al.* (1986) ‘Cyclic undrained triaxial strength of sand by a cooperative test program.’, *Soils and Foundations*, 26(3), pp. 117–128. doi: 10.3208/sandf1972.26.3_117.

Towhata, I. *et al.* (1992) ‘Prediction of permanent displacement of liquefied ground by means of minimum energy principle’, *Soils and Foundations*, 32(3), pp. 97–116. doi: 10.1248/cpb.37.3229.

Towhata, I., Orense, R. P. and Toyota, H. (1999) ‘Mathematical principles in prediction of lateral ground displacement induced by seismic liquefaction’, *Soils and Foundations*, 39(2), pp. 1–19.

Wang, G., Wei, X. and Liu, H. (2015) ‘Liquefaction evaluation of dam foundation soils considering overlying structure’, *Journal of Rock Mechanics and Geotechnical Engineering*, 7(2), pp. 226–232. doi: 10.1016/j.jrmge.2015.02.005.

Xia, Z. *et al.* (2010) ‘Fully coupled numerical analysis of repeated shake-consolidation process of earth embankment on liquefiable foundation’, *Soil Dynamics and Earthquake Engineering*, 30(11), pp. 1309–1318. doi: 10.1016/j.soildyn.2010.06.003.

Yamada, G. (1966) ‘Damage to earth structures and foundations by the Niigata earthquake, June 16, 1964.’, *Soils and Foundations*, 6(1), pp. 1–13. doi: 10.1248/cpb.37.3229.

Yoshida, M., Miyajima, M. and Numata, A. (2012) ‘Experimental Study on Liquefaction Countermeasure Technique by Log Piling for Residential Houses’, in *15th World Conference on Earthquake Engineering*.

Zhang, L. (1999) ‘Settlement patterns of soft soil foundations under embankments’, *Canadian Geotechnical Journal*, 36, pp. 774–781.